ANALYSIS OF DEFORMATION BEHAVIOR OF C15000 DURING MULTI-PROFILE DIE EXTRUSION AND OPTIMIZATION OF PROCESS PARAMETERS

Elias Dessie Assena

A Thesis submitted to the Department of Mechanical Engineering
School of Mechanical, Chemical, and Materials Engineering

Presented in Partial Fulfillment of the Requirement for the degree of
Master of Science in Manufacturing Engineering

Office of Graduate Studies

ADAMA SCIENCE AND TECHNOLOGY UNIVERSITY

November 2022 G.C

Adama, Ethiopia

ANALYSIS OF DEFORMATION BEHAVIOR OF C15000 DURING MULTI-PROFILE DIE EXTRUSION AND OPTIMIZATION OF PROCESS PARAMETERS

Elias Dessie Assena

Advisor: -Dr. Guteta Kabeta

A Thesis submitted to the Department of Mechanical Engineering
School of Mechanical, Chemical, and Material Engineering

Presented in Partial Fulfillment of the Requirement for the degree of
Master of Science in Manufacturing Engineering

Office of Graduate Studies
ADAMA SCIENCE AND TECHNOLOGY UNIVERSITY

November 2022 G.C
Adama, Ethiopia

CANDIDATE'S DECLARATION

I hereby declare that this master's thesis entitled **"Analysis of Deformation Behavior of C15000 during Multi Profile Die Extrusion and Optimization of Process Parameters"** is my original work. That is, it has not been submitted for the award of any academic degree, diploma, or certificate in any other university. All sources of materials that are used for this thesis have been duly acknowledged through citation.

Elias Dessie Assena

Signature: ____________ Date: _________

RECOMMENDATION OF ADVISOR

We, the advisors of this thesis, hereby certify that we have read the revised version of the thesis entitled **"Analysis of Deformation Behavior of C15000 during Multi Profile Die Extrusion and Optimization of Process Parameters"** prepared under our guidance by Elias Dessie Assena submitted in partial fulfillment of the requirements for the degree of Masters of Science in Manufacturing Engineering. Therefore, we recommend the submission of a revised version of the thesis to the department following the applicable procedures.

Advisor: Dr. Guteta Kabeta ______________________ ____________________

Signature Date

APPROVAL OF ADVISOR

We, the advisor of the thesis entitled **"Analysis of Deformation Behavior of C15000 during Multi Profile Die Extrusion and Optimization of Process Parameters"** developed by Elias Dessie Assena, hereby certify that the recommendation and suggestions made by the board of examiners are appropriately incorporated into the final version of the thesis.

Advisor: Dr. Guteta Kabeta ______________________ ____________________

Signature Date

APPROVAL BY THE BOARD OF EXAMINERS

We, the undersigned, members of the Board of Examiners of the thesis Elias Dessie Assena have read and evaluated the thesis entitled "Analysis of Deformation Behavior of C15000 during Multi Profile Die Extrusion and Optimization of Process Parameters" and examined the candidate during the open defense. This is, therefore, to certify that the thesis is accepted for partial fulfillment of the requirement of the degree of Master of Science in Manufacturing Engineering.

Chairperson	Signature	Date
Internal examiner	Signature	Date
Desalegn Wogaso (PhD)		12/12/2022
External examiner	Signature	Date

Final approval and acceptance of the thesis are contingent upon the submission of its final copy to the Office of Postgraduate Studies (OPGS) through the Department Graduate Council (DGC) and School Graduate Committee (SGC).

Department Head	Signature	Date
School Dean	Signature	Date
Office of Postgraduate Studies	Signature	Date

ACKNOWLEDGEMENT

First of all, I must thank the invisible force which we define as the almighty God for giving me patience and driving me toward a never-ending process of learning.

The journey of reaching any milestone is never easy without a determined ambition, sincere dedication, and a perfect person who can torch your path of ignorance. I am obliged to Dr. Guteta Kabeta for being an embodiment of the constant source of inspiration and knowledge. Under his guidance, I learned the art of doing research.

I am thankful to Dr. Moera Gutu for his support and cooperation in the fulfillment of the work and motivational speeches at regular intervals during my tenure.

And also, I am thankful to Dr. Devendra Kumar Sinha for their kind support and cooperation in the fulfillment of the work.

At the same time, I am thankful to the teaching staff of the department, whose valuable suggestions at the right time helped me reach my goal.

I sincerely acknowledge the helping hand of the laboratory staff and other nonteaching staff of ASTU, for their timely help and support. My friends, whose consolation during the bad days and encouraging words, helped me maintain the equilibrium during fulfilling my ambition.

After all, the love of family and relatives whose blessings are like the rays of sunshine helps me see strength and march towards the goal.

Table of Contents

LIST OF TABLES

LIST OF FIGURES

Nomenclature

D	Product diameter
L	Length of the die
m	Shear friction coefficient
R	Radius of the billet
T	Temperature
V	Ram velocity
σ	The flow stress of the billet material
$\bar{\varepsilon}$	Effective strain
$\dot{\bar{\varepsilon}}$	Effective strain rate
ρ	Density
c	Specific heat
RPM	Revolution per minute
LC	Linear converging
F	Test force
d	Surface area indentation

ABSTRACT

Copper alloy is one of the most versatile engineering materials. Among various grades of copper, C15000 is getting much more attention in various electrical and optical applications. But as far as the formability and strength of these particular grades are concerned, there is a lack of necessary data and research. Much research has been carried out on aluminum alloy multi-profile die extrusion while there is a shortage of research on copper alloy C15000 extrusion. Therefore, the present thesis aims to enhance the capability of C15000 through a multi-profile extrusion process and further evaluation of formability process parameters optimization. Numerical analysis was carried out by finite element analysis tool (DEFORM- 3D). The mathematical modeling and multi-objective optimization of the process parameters for the optimal value of output were carried out through Multi response surface methodology. The fabrication of the extrusion die and container was carried out as per the results of the numerical simulation. At optimized process parameters; Z-load of 31370N, 33860 N, and 34940 N. whereas; the effective stresses of 55.7 MPa, 55.7MPa, and 55.2 MPa while damage of the billet were 0.425 for cosine, 0.4435 for streamline and 0.498 LC die profiles. The experimental investigation (extrusion of billet material of C15000 grade) was carried out on a hydraulic press machine. Testing and characterization of both commercial and extruded products have been done using mechanical and metallurgical testing machines. The compression strength of the linear convergent die extruded sample is slightly lower than that of the cosine die extruded sample but much higher than that of the commercially available sample. The hardness of the commercially available specimen is 133.9HV. The hardness increases to 161.6HV and 162.8HV, respectively as the specimen is extruded in linear convergent and cosine die profiles, and microstructural analysis shows the microstructures of the extruded products are obviously refined and evenly distributed in the deformed products.

Keywords: *Multi response surface Methodology, Finite element analysis, Extrusion, Die-profile, Optimization*

CHAPTER ONE

INTRODUCTION

1.1 Background of the study

Pure copper has a high thermal conductivity however it loses strength while exposed to high temperatures. Because of their high strength and electrical conductivity, distinctive copper-based alloys have been developed and widely used in industrial applications where there are various electrical connections between cables, circuit breaker parts, wires, and electrical outlets such as high-speed rail contact lines, buses, lead frame structures, heat exchangers, and nuclear reactor components Guo et al., [2017].

Research by Canadinc et al., [2011] on an FCC Cu–Zr alloy showed that a higher proportion of high-angle grain boundaries resulted in a higher resistance of the microstructure to cyclic deformation during fatigue tests, while a high temperature, low strain rate, and large strain amplitude promoted grain growth and disrupted the cycle stability of the material. Singh et al., [1997] argued that Zr in solid solution should contribute significantly to observations of increased microstructural and thermal stability, as well as non-equilibrium conditions caused by rapid melting and solidification, hence expanding Zr's solid solubility.

Zirconium is a typical alloy addition that improves the heat resistance, mechanical characteristics, and exploitation of properties of copper. Zhao et al., [2018] Furthermore, adding Zr in the amount of 0.1–0.2 wt percent increases heat resistance while having no significant effect on electrical characteristics, which is difficult to achieve with other alloying elements like Cr, Mg, Ag, Ni, or Ti. These alloys have good formability when cold worked, such as in open die forging, extrusion, or rolling. Cu–Zr alloys with 0.05–0.15 wt% Zr are mostly employed in the automotive sector as switches and relays, contacts, connectors, terminals, and hybrid car parts. In addition, electronic circuits, electrical connections, lead frames, switches, switchblade jaws, commentators for power, transmitters, and buses for power transmitters, rectifiers, soldering and welding tips, circuit breakers, and high-temperature applications are all frequent uses for zirconium copper in the electromechanical sector. CuZr0.15 is one of the most widely utilized commercial alloys for the uses indicated above. Functional qualities vary depending on the structural state connected with the production process, such as UTS 255–490 MPa, YS 60–

455 MPa, elongation 35–2%, hardness 70–110 HV10, and electrical conductivity of approximately 55 MS/m. As well has better wear characteristics as seen in Tu et al., [2001] also has a strong heat resistance of up to 500 degrees Celsius SARIN VK & GRANT NJ, [1972].

In a NaCl solution environment, the corrosion behavior of CuCr, CuZr, and CuCrZr alloys was researched, and it was shown that over a lengthy moment of practice, the corrosion resistance of CuCr alloy is somewhat better than that of pure copper, resulting in enhanced rust-resistant behavior. Zhang et al., [2011] Owing to high ductility, DeGroh et al., [2008] increased resilience to rupture creep and fatigue Deguchi et al., [2018] The electrical conductivity of this group of alloys is around 50 MS/m and lower, which necessitates increasing the cross-section of the end products in their electrical applications due to the concentration of alloy additive over 1 wt%. In Tian et al., [2018] and Huang et al., [2019], The authors demonstrated that thermal and thermo-mechanical treatments of Cu–Cr–Zr alloys may improve both electrical and mechanical characteristics.

1.1.1 Strengthening mechanism of copper alloy

Copper alloys have recently attracted a lot of interest. The finished performance is directly influenced by their composing design, preparing, and processing. Copper alloys made using various strengthening techniques, on the other hand, have great thermal and electrical conductivity, as well as high strength and plasticity, as well as excellent processing properties. Solution strengthening, aging precipitation strengthening, and dispersion strengthening are all ways for strengthening copper alloys. Certain alloying elements are dissolved in the copper matrix for solution strengthening, which causes lattice distortion and improves the alloy's strength by preventing dislocation migration. The electrical conductivity of the alloy can be considerably diminished due to the scattering impact of electrons on the solute atoms, hence solution strengthening is frequently utilized in conjunction with other strengthening procedures Wang et al., [2018]. The inclusion of metals in the copper matrix whose solid solubility varies substantially at high and low temperatures, such as Cr, is known as aging strengthening. Gao et al., [2019]. In Peng et al., [2017] In the Cu-0.71 wt% Cr alloy illustrated, the precipitate Orowan process is responsible for the considerable increase in strength. The presence of fine precipitates in the matrix, according to the Orowan strengthening mechanism, prevents dislocation motion and results in a strengthening effect, which is primarily dependent on the size, volume fraction, and distribution of the precipitates. We can compute the contribution of precipitation strengthening to strength development using this information Hatakeyama et al., [2008]. The secondary phase is created post-solution and aging treatment, which improves strength by reducing dislocations and grain boundary movement. Hot processing is commonly used to enhance the characteristics of copper alloys in the past.

Many researchers are now working to improve the microstructure of CuZr alloys to improve the alloy's overall performance. for example Equal channel angular pressing (ECAP) Morozova et al., [2017], high-pressure torsion (HPT) Wongsa-Ngam et al., [2012], and multidirectional forging Shakhova et al., [2014] have been implemented to produce the ultrafine-grained structure. According to the other researcher, Feng et al., [2013], the precipitates retain a fine size and dispersion distribution during the extrusion process, which inhibits dynamic recrystallization and assists the alloy to achieve a high degree of strength.

1.1.2 Extrusion process

Traditional plastic deformation approaches such as extrusion and rolling are very easy and effective ways for increasing alloy strength but owing to the work hardening effect, ductility is compromised to some extent. Furthermore, during hot deformation and post-heat treatment, the alloy normally experiences a recrystallization process, which improves ductility but reduces strength Fang et al., [2015]. Grain refinement is considered to be the sole method for an attractive combination of high strength and good ductility shown by Zhao et al., [2006].

Extrusion is a process of a metal product that is commonly used in industry and everyday life equipment. It is another type of manufacturing process, which involves cutting and squeezing. Rahul et al., [2018] Extruded products can be trimmed to the necessary length and then separated into distinct pieces such as brackets, gears, and coat hangers, according to this statement. The process of creating or shaping the desired result involves using a circular die or a variety of forms. A circular billet is inserted in the chamber and pushed or forced through the die cavity by a hydraulically operated ram. Axisymmetric dies are frequently used in this procedure. Extrusion pressure is affected by die angle, node reduction, acceleration, billet temperature, and lubrication.

Extrusion may be divided into four categories. Direct extrusion, indirect extrusion, impact extrusion, and hydrostatic extrusion are the four methods. There are four types of expulsion in general. Direct extrusion, indirect extrusion, impact extrusion, and hydrostatic extrusion are the four methods. When it comes to direct extrusion, a powerful ram forces the entire billet to its die, and more power is required to overcome frictional resistance between the flowing bill and the shield.

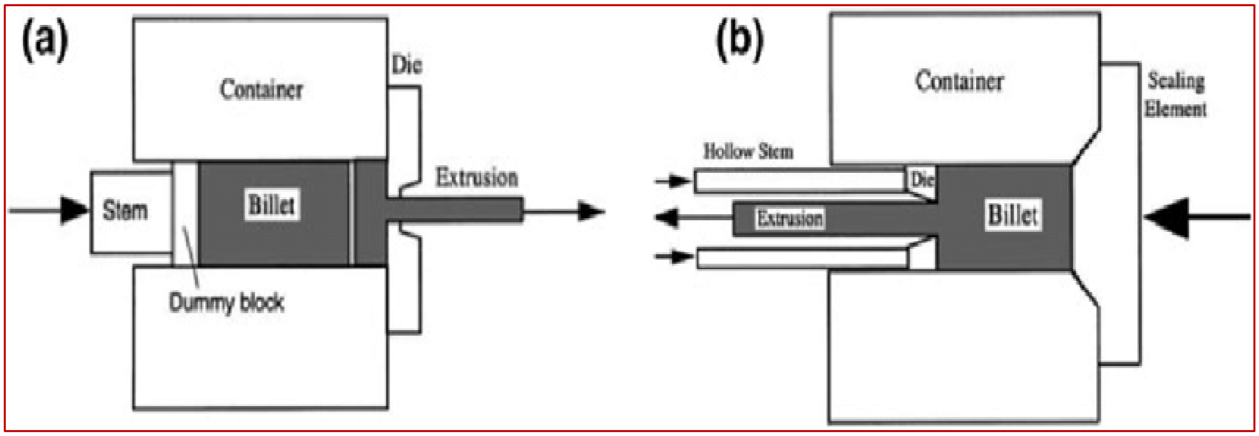

Figure 1. 1 Direct extrusion (a) Indirect extrusion (b) Wagstaff, [2020]

The hollow ram is forced back through a stationary, restricted billet in an indirect operation. The conflict between the billet and the container is removed since there is no relative movement, and the needed power is low. Because the extruded object adheres to the punch during impact extrusion, it is removed with a stripper plate.

A high-pressure fluid is delivered to the workpiece through a die in hydrostatic extrusion. The loaded fluid acts as a lubricant between the billet and the die, preventing the billet chamber from colliding.

Extrusion's Benefits

- Low per-part cost.
- Operational flexibility.
- Because the product is still hot, post-processing modifications are simple in hot extrusion.
- Ongoing operation.
- Large-scale production
- A wide range of raw materials can be utilized.
- Excellent mixing (compounding)

- Excellent surface finish

1.1.3 Die profile design and optimization

In extrusion, the mechanical properties of the material, friction conditions on the device workpiece interface, extrusion ratio, and die profile are some of the important parameters that have a significant impact on the desired product characteristics. Optimizing these parameters is one of the most important tasks that many researchers focus on. The extrusion dies profile can be conical or curved. In the past, due to the problem of producing non-conical die, most of the research has focused on the optimization of rod extrusion die geometry, focusing on conical dies, e.g. that performed by Avitzur et al., [1982] The upper limit method used on the optimization of die angle. Currently, a lot of research has been done on computerized numerical control (CNC) machines and the process of producing complex die shapes and optimizing distorted die profiles. Chen and Ling, [1968] provided upper-bound solutions for axisymmetric extrusion problems. They used three basic axisymmetric curve dyes: cosine, elliptical, and hyperbolic, and transformation techniques to obtain a mathematical consistency. Ghaemi et al., [2013] studied an excellent extrusion die profile by the implementation of slap analysis in a computational algorithm. In addition, the extraction process through both the best conical and the curved die was performed experimentally and with a finite element method. Material strength and friction conditions have been shown to have a dramatic effect on the optimum streamlined die profile. The results show that the advanced streamlined die profile, designed based on the process, is superior to conventional conical die in both metallurgical and manufacturing views. Therefore, the proposed method can be considered an efficient and reliable tool for designing streamlined die profiles. Therefore, this method can be used to produce the desired conditions in terms of extrusion power, deformational homogeneity, and die wear. Gunasekera and Hoshino, [1985] used an upper-bound solution to extrude the multi-sided parts to the bounded billet through converging and curved dies.

1.1.4 Process control

The involvement of various operational variables needs to be restrained within the optimal range during operations to have better control over the process. To find the optimal range, the effect of the particular variable needs to be investigated substantially. As the change in metal during forming operation is concealed by the tooling setup or machinery, it's hard to know the effects of the variable parameters by experimental investigations. So, most of the research in previous work is based on computerized finite elements and analytical investigations.

1.1.4.1 Die length and extrusion ratio

The two-hole die extrusion was carried out with a different die land length by Keife, [1993], and it was observed that the length of the die land affected the shape of the product's straight or curved profile. Chen et al., [2007] studied the influence of state variables like die semi-angle, extrusion ratio, and friction factor for plastic deformation of AA-6062. The extrusion force increases with the increase of the die semi-angle (10° 5 a 5 35°) for a reduction of 1.562 and a minimum shear friction coefficient of 0.1. But in a practical approach with larger frictional resistances, lesser semi-angle dies with larger die lengths need more power to overcome frictional resistances. The optimum die length in terms of relative die length (UR) remains under 0.5 to 1 for a round-to-square bar extrusion studied by Karami & Abrinia, [2014]. And also shows higher reductions cause higher pressures and it is clearly shown, strain values have a more homogenous distribution at lower reductions. They found a good agreement between the analytical, experimental, and FEM results.

1.1.4.2 Friction condition

Most of the FEM tools require friction as input variables whereas in the experimental process the frictional value is not known incisively. So, the friction value needs to be determined by some different procedures at the interface boundary. Frictional resistance depends on several factors like local temperature, relative velocity, geometry and tooling surface, and contact pressure. Numerous research works were there to estimate and model the frictional parameter Ma et al., [2010]. Different techniques like the ring compression test Wang et al., [2012] the most popular one, the T-shaped compression test Zhang et al., [2009] and the barreling curvature of the compression test Chen et al., [2008], double backward extrusion process Buschhausen et al., [1992] backward extrusion type forging Shen et al., [1992] can be employed for the successful determination of friction condition. A quantitative value of the coefficient of friction is desired for the process. The friction model is either the Coulomb friction model or the Tresca friction model depending on the process conditions. If the mean normal stress component is smaller than the flow stress of the material or for low contact pressure conditions like in rolling, sheet metal operations, and wire drawing then the Coulombs friction model is applied. On the other hand where the mean contact pressure is much higher than the normal stress there Tresca's friction model remains suitable. A slightly more complex model i.e Wanheim and Bay's model which smoothens the curve of Coulomb's model and Tresca's model curve is less applied in forming investigations.

1.1.4.3 Temperature and ram velocity

Temperature management is the key factor in aluminum extrusion which decides product quality and the life of the die. During extrusion, the temperature at the die exit is high which decides the microstructure and surface property of the product and improves the die abrasion that causes the error in shape and dimensional tolerances of the extrudate. Higher metal temperature improves the metal flow, but too high temperature induces over-burning phenomena. With the increase of extrusion speed maximum temperature generation increases and the time duration to dissipate the heat decreases accordingly.

1.2 Statement of the problem

Copper is widely used in the aerospace and electronics industries, including high-speed rail contact wires, Circuit breaker parts, buses, and electrical contact materials. Therefore, it can be said that copper alloy is one of the most versatile engineering materials. The strength of pure copper is low at room and high temperatures which are major limitations when it is used in several applications like in bus bars. Among the various grades of copper, C15000 is getting much more attention in various electrical and optical applications due to its superiority in characteristics over pure copper Zhilyaev et al., [2016]. But as far as the formability and strength of these particular grades are concerned still there is need for enhancement of various strengths. Also, there is a lack of necessary data and research on these grades. Therefore, there is a need for high-strength and high-conductivity copper alloys which is a burning issue in the recent past and these days. Due to this, the present thesis aims the analysis of the deformation behavior of grades of copper C15000 for various applications in electrical, electronic, and optical fields.

1.3 Objective

1.3.1 General Objectives

The general objective was to analysis of deformation behavior and evaluate the mechanical metallurgical characteristics of copper zirconium through a multi-profile die extrusion process.

1.3.2 Specific Objectives

The specific objectives are as follows:

1. Numerical simulation of using DEFORM 3D tool as per the experimental design to determine the effective stresses, damage, and Z-load required for extrusion.
2. Optimize multi-profile die extrusion process parameters using response surface methodology
3. Experimental investigations of multi-profile die extrusion of C15000
4. Perform compression, hardness, and microstructure test for commercial and extruded products.

1.5 Scope of the study

The scope of the present thesis mainly focused on Numerical Analysis using the FEM tool called DEFORM-3D and experimental investigation of the multi-profile extrusion process. The study establishes the numerical approach and experimental validations. The present thesis also aimed at compression and hardness test and characterization of solid circular section extrudates used to study the metallurgical and mechanical properties of the samples. Furthermore, optimize multi-profile die extrusion process parameters using response surface methodology.

1.6 Significance of the study

Among the various grades of copper, C15000 is getting much more attention in various electrical and optical applications due to its superiority in characteristics over pure copper. The present thesis is expected to analyze the deformation behavior of grades of copper C15000 through a multi-profile die extrusion process that is in use for various applications in electrical, electronics, and optical fields.

1.7 Limitations of the study

This study is limited to experimental and numerical analysis, and they are not compared due to the time and cost of doing an experimental trial for each. The study can be improved by adding theoretical analysis such as the upper bound theorem and comparing it with numerical analysis and experimental analysis. Wear tests can also be included in the experimental analysis to evaluate tribological change.

1.8 Organization of the study

This thesis paper consists of five chapters. Chapter one briefly explains the background study of the application of C15000 as well as the Strengthening mechanism specifically the extrusion process. This chapter includes problem statements, the scope of the study, general and specific objectives of the study along with thesis structures. Chapter two presents the efforts of researchers from old to recent ones which are related to this study. Chapter three explains about varieties of materials, which are used in the study and methods that are applied during the analysis to achieve the goal of the study. This chapter includes the material used, model approach, experimental plan and design, finite element formulation, numerical simulation data, experimental analysis, material characterization, and analysis of the optimization process. Chapter four explains the results and discussions from the numerical analysis part, experimental analysis parts, and optimization process. Chapter five highlights the conclusion and recommendations. In this chapter, the output /final results of the study are elaborated.

CHAPTER TWO

LITERATURE REVIEW

2.1 Introduction to Extrusion of Copper Alloys

Due to the increasing demand for extruded products in many sectors such as Electrical and electronics an emerging direction to contribute research has been opened to improve the process efficiency as well as product quality. Extrusion is a very easy and effective way for increasing alloy strength grain refinement is considered to be the sole method for an attractive combination of high strength and good ductility and extrusion is the only economical way of manufacturing such long straight complex cross-sectioned products Harničárová et al., [2022]. Copper alloys have recently attracted a lot of interest. The finished performance is directly influenced by their composing design, preparation, and processing. Copper alloys made using various strengthening techniques, on the other hand, have great thermal and electrical conductivity, as well as high strength and plasticity, as well as excellent processing properties Wu et al., [2019]. The process that involves many state variables which improve the complexity of the process is to be considered for better production. The effect of the variables like ram velocity, die length, die profile, operating temperature, and friction condition for both cold and hot extrusion processes have been studied and reported in past research works. The effect of the die profile is mainly responsible for the formation of the dead metal zone and redundant work by controlling the flow of material Venkatesh & Venkatesan, [2015]. The numerical simulation method has been widely used in flow analysis, temperature field simulation, die strength calculation, and friction and lubrication analysis of the extrusion process. Numerical simulation methods are mainly divided into the finite element method, finite difference method, and finite volume method. Hence, it is the most critical area of consideration from the tooling design point of view Conte, [1966]. Apart from this to satisfy the requirements with better product quality, the billet material compositions and type are a new focus in this decade. Based on these requirements an exhaustive literature review has been carried out in different areas that only focusing the primary objective described in this chapter. To fulfill the objective of the total research, it is classified into three categories focusing on different zones such as:

1. Strengthening of copper alloy

2. Finite element method and Process Control

3. Optimization of die extrusion parameters

2.1.1. Strengthening of Copper Alloy

Correia et al., [1997] This research provides a more complete report on the experimental results of mechanical properties and the combined and thermal treatment of Cu-Cr and Cu-Cr-Zr alloy powders and compares their mechanical properties with those that are conventionally processed and rapidly quenched. With the choice of the appropriate two parameters, it has been shown that for coherency strengthening and dispersal strengthening regime, the maximum strengthening can be successfully recorded in the Cu-Cr system at room temperature and relative precipitate size. High-concentrated Cr precipitation is related to the peak hardness of the composite powders.

Feng et al., [2013] in this study, CuCrZr rods are continuously extruded on TLJ400 devices. The micro-structures, mechanical properties, and electrical properties produced by the CEF process were compared with conventional processes. Cu-0.16Cr-0.12Zr alloy with continuous extrusion formation process reaches a maximum strength of 590 MPa and an elongation of 17.2%, which is 1.5% higher than the alloy traditional hot working process of 40 MPa. Meanwhile, the electrical condition has a significant reduction from 78.7% to 77.6% IACS.

Zhang et al., [2017] hot deformation behavior of the Cu–Zr and Cu–Zr–Y alloys was studied by using a thermo-mechanical simulator under diverse deformation conditions. According to the experimental results, during hot deformation, the flow stress of the Cu–Zr and Cu–Zr–Y alloys is sensitive to temperature and strain rate. Flow stress can be increased by deformation temperature and reduced by strain rate.

2.1.2 Finite Element Method and Process Control

Ebrahimi and Najafizadeh, [2004] studied heat generating is caused by a high friction situation, and heat generation promotes friction and flow characteristics. The ram velocity, extrusion ratio, and starting billet temperature all affect frictional heat generation. The friction state at the interfacial boundary was determined using a relatively simple and sensitive barrel compressive test.

Chen et al., [2008] The influence of the process variable on the multi-hole extrusion of aluminum A7075 tube using the indirect extrusion method was studied using both an experimental method and a finite element analysis. The finite element model is already well known for only one-hole extrusion and genuine extrusion processes in this study. The final pieces were used to investigate the influence of process factors on the product form of extruded tubes. An outstanding two-hole extrusion procedure was created based on the FEA, which delivers sound products with no curves. The finite element study confirms that the friction of indirect extrusion does not influence the extrusion load. The major flaw in the process of extruding a curved shape in multi-hole extrusion is the extruded tube.

Meng-jun et al., [2010] mainly focus on to use of thermal simulation and numerical simulation technologies to analyze the deformation behavior of 6063 Al alloy at low-temperature high-speed extrusion utilizing the DEFORM 2-D program. During the operation, a greater dead metal zone is induced, and a larger strain value is detected at the die entry, making low-temperature high-speed extrusion feasible to reduce energy consumption.

Orangi et al., [2011] used ABAQUS/explicit finite element software to explore the influence of frictional coefficients and reduction area on extrusion pressure and product velocity for internally circular and elliptical, and externally polygonal, rectangular, and elliptical sections. Because the amount of power needed to overcome friction in extrusion is directly related to the area of contact, the billet and die lengths are restricted depending on the situation.

Ketabchi et al., [2012] the influence of temperature and punch speed on effective stress, effective strain, and force estimate in a backward extrusion of Al-7075 alloy was investigated using a three-dimensional finite-element code and the DEFORM-3D program, and the backward extrusion process was studied using data from uniaxial compression experiments. Exploring the reaction of metals to deformation and extrusion is critical because it influences the tooling life (die, container, and punch), production efficiency, and product quality. During the forming process, the effects of varied punch speeds on the effective stress/strain distribution and forming load were examined. The modeling findings revealed that during the process, the effective stress/strain distributions in the billet were inhomogeneous. The forming load could be predicted using a 3D FEM simulation during the forming process.

Syahrullail et al., [2013] the effects of the die half angle of the taper die during the cold extrusion process on the effective strain distributions of billet extruded with varied die half angles were explored using cold-work plane strain extrusion equipment. Extruded billet with a bigger die half angle exhibits lower extrusion force, lower surface roughness, and higher relative sliding velocity. The effective strains were condensed at the taper die area for all experimental conditions (deformation area).

Syahrullail et al., [2013] in this study to optimize the die length a modification of frictional resistances with the participation of users is essential this is examined. The effective strain distributions of billet extruded with a taper die which has variable die half angles were explored and reveal the impacts of the die half angle of the taper die during the cold extrusion process were investigated using cold-work plane strain extrusion equipment. Billet extruded with a greater die half angle demonstrates a decrease in extrusion force, reduced surface roughness value, and rise in relative sliding velocity. For all experimental settings, the effective strains were condensed at the taper die area (deformation area).

Das et al., [2014] This research analyzes the influence of the zone of pores on the die, die pockets, and the extrusion velocity on the extrusion load, effective strain, and the extruded product dimension. Extrusion load is seen to rise with a rise in extrusion speed and is carried out using finite element analysis. The die pockets aid in lowering the extrusion load. The extruded product lengths become much more regular when pockets die formed. The choice of process parameter is dependent upon the needed quality of the product.

Chen et al., [2015] the extrusion experiment and finite element simulation were carried out and compared to ensure that the modeled constitutive equation was accurate. The primary goal of this research is to better understand the flow behavior of homogenized 7005 aluminum alloy throughout a broad range of temperatures and strain rates, as well as to offer fundamental data for extrusion modeling. The temperature distribution in the billet throughout the die is heavily influenced by the strain rate. A metal's flow stress is affected by temperature and strain rate. Flow stress rises as the temperature drops and the strain rate rises. Extrusion velocity increases strain rate and maximum extrusion temperature, both of which have a direct impact on the mechanical qualities of the product.

Oyinbo et al., [2015] For the extrusion of triangular, square, hexagonal, heptagonal, and octagonal sections from round billets, the die profile function has been devised using a mathematically contoured die profile. For extrusion of triangular, square, hexagonal, heptagonal, octagonal, T, L, and H sections from round billet, FEM modeling was carried out using DEFORM-3D software and aluminum alloy AA6063 as stiff plastic material. FEM modeling was used to establish load prediction, effective stress, effective strain, effective strain rate, and temperature distribution during deformation. And it was discovered that when the reduction, friction factor, and die length rise, so does the extrusion pressure. The forecast loads for axisymmetric forms do not vary much. Predictive loads for non-axisymmetric forms are also shown to be greater than for axisymmetric shapes.

Venkatesh & Venkatesan, [2015] After a thorough investigation of SiC-reinforced Al composites using the UB, FEM, and experiment methods for six different die profiles, it was discovered that the cosine profile die has been the most optimized die profile for extrusion of SiC DRMM Al 6061 composites with the above-mentioned volume fraction and particle size, because results obtained using the upper bound technique, finite element technique, and experimental methods have not borne any significant diffraction.

Ab Rahim et al., [2016] the main focus of this research was to investigate whether the upgraded Deform 3D software could be used to mimic the aluminum extrusion process in a steady state using a Lagrangian method. The extrudate temperature is the most essential process parameter in aluminum extrusion since it impacts product quality and indicates whether or not the extrusion speed may be increased. Also, when the ram goes farther, the temperature increases at first and then stabilizes. Extrusion forces and surface quality may be projected using simulation models.

Sathishkumar et al., [2017] The influence of extrusion process parameters, namely three distinct extrusion ratios at varying billet temperatures, on the plastic strain and strain rate of aluminum matrix composite during hot extrusion has been studied using finite element (FE) analysis. For simulation, the dynamic explicit FE code in ANSYS 15.0 workbench was utilized. For all billet temperatures, both plastic strain and strain rate increase with the extrusion ratio. Furthermore, increased plastic strain and strain rate were shown to occur at the maximum extrusion ratio at a higher billet temperature. Higher extrusion ratios, on the other hand, have led to hot shortness and surface fractures. It was also shown that the extrusion ratio has the greatest impact on the onset of surface fractures.

Farzad & Ebrahimi, [2017] A novel approach for obtaining a kinematically permissible velocity field for randomly generated profiles has been presented. Then, utilizing upper boundary analysis and the Bezier curve (SA) technique, an optimal plane strain extrusion dies profile was proposed to decrease the repeat of the operation and the load demand. The extrusion process characteristics of an ideal curved die profile and an optimum fixed angle are compared using FMM analysis. The result of modeling the finite element revealed that it is preferable to utilize an optimal curved die rather than a constant angle die when the maximum needed power reduction is 10.5 percent and the product inhomogeneity factor is reduced by 50%. The comparison of the optimum curved and constant angle dies profiles in terms of normal stress operating on the die along the tool-workpiece interface in FEM analysis indicates that the stress at the interface in the case of the ideal curved die is extremely low. As a result, the ideal die life curve should be longer than the optimal constant angle dies life curve. Furthermore, the material's work-hardening characteristics were shown to not affect the optimal curved die profile.

Wang et al., [2017] Researchers were able to obtain deformation information on magnesium alloy in the die cavity, which included the distribution of the stress field, strain field, and temperature field, as well as the influence of different process parameters on extrusion pressure, using Deform-3D finite element simulation software in this paper. The deformation temperature of the AZ31 magnesium alloy is a significant component determining deformation resistance; as the temperature rises, the quantity of deformation increases, and deformation resistance falls. The speed of flowing metal is changed in the contact area between the edge of the male die head and the blank, in the area of cylinder wall deformation, in the contact area between the bottom of the blank and female die, and in the area of deformation of the lug, its stress is higher, and if the lubrication is poor, it is easy to produce crack.

Sahu et al., [2018] A finite element analysis and trials of multi-hole forward, backward, and combination forward and backward extrusion were carried out in this research. With a rise in extrusion ratio, die land length, and extrusion speed, the extrusion load increases. Extrusion ratio and die length were shown to have a greater impact on extrusion load than extrusion speed.

Lower die land length and lower extrusion speed reduce the coefficient of variation of extruded parts. A good selection of die land length and extrusion speed for a certain extrusion ratio is critical for producing more consistent products in a multi-hole extrusion process.

Banerjee et al., [2018] the current study used both the experimental technique and finite element analysis to assess the effects of process factors on the extrusion of aluminum-alloy AA 7178 rods. Aluminum alloy AA 7178 comprises alloying components like Zn, Mg, Cu, etc. The practical methods to reliably detect stress, strain, and temperature are currently relatively restricted. In the current study, 2D FEM modeling of the aluminum extrusion process was done to identify the status of stress, load, and billet dimensions before and after. The mechanical characteristics are utilized to carry out the FEM analysis. Finite element simulation is done by utilizing ANSYS-LS-DYNA software. Both the state of stress and the load are complicatedly connected to the extrusion parameters, including starting billet temperature, ram speed, reduction ratio, friction at the surfaces, and die shape.

Bhavani, [2019] Experimental and theoretical studies were carried out in the available environment to get the most ideal forming system in terms of lowest load requirements and equipment-like shape. This was done for two forming processes: lateral extrusion and forward extrusion, which were simulated using DEFORM-3-d and compared to one another. Furthermore, polynomial and Bezier die profiles outperform cosine, circular, elliptic, and hyperbolic die profiles. The cosine dies, on the other hand, is proven to be the best at extremely low friction. Friction at the die-billet contact does not affect the internal work of deformation.

Engelhardt et al., [2019] this research discussed two FEA software packages for extrusion industrial applications that might aid in material flow prediction and hence ease the tool design process. In the first study, simulation approaches were employed to visualize and optimize material flow during the extrusion of a heat sink profile with complicated geometry that included waviness and profile displacement. The findings revealed that viscoplastic friction conditions alone are insufficient for predicting material flow, particularly when bearing lengths seem to have a greater impact.

Rajabzadeh Gatabi et al., [2020] This work built a three-dimensional nonlinear dynamic finite element model to investigate the influence of various factors on void development in cold rod extrusion. When friction was low, it was discovered that the shrinkage of off-center voids in the circular direction was larger than that in the radial direction. In the high friction condition, however, void contraction in the radial direction outweighs void contraction in the hoop direction, particularly in dies with bigger semi-angles.

Ranjan Yadav et al., [2020] The influence of process factors such as coefficient of friction, semi-die-angle, and die profile radius is investigated in this article utilizing finite element modeling of an axisymmetric extrusion process employing aluminum alloy. And it was established that deformation homogeneity rises significantly by decreasing the semi-die-angle with the vertical axis or increasing the semi-die-angle with the horizontal axis. The coefficient of friction has minimal impact on the deformation homogeneity of billet material and it decreases with an increased coefficient of friction. A nearly pure homogenous flow of material with little mesh distortion is produced by increasing the coefficient of friction. It suggests using a greater die profile radius to decrease maximum contact pressure.

Hotea & Juhasz, [2020] Extrusion ratio, operating temperature, and the rate of breakdown of the aluminum alloy are some of the most critical characteristics that determine the extrusion process and the quality of the material withdrawing from the die in this article. Temperature and extrusion speed are the two most critical process factors that determine both the quality of the extruded product and the process productivity. Temperature is by far the most significant of the numerous process factors discovered in aluminum extrusion since it impacts product quality and indicates the potential for enhanced release rate. Temperature and velocity, as well as stress conditions in the deformation zone, particularly in the mold area, all play a role in a high-strength aluminum alloy's extrudability.

Shukur & Jaber, [2020] the influence of die geometry and extrusion velocity on the forming load were investigated experimentally and numerically in this work. The extrusion process is simulated and analyzed using Ansys 16, which is based on FEM. The research found that the forming load rises as the die angle and ram speed increase, that small die angles are more impacted by ram speed than large die angles, and that the maximum forming load for all die angles occurs towards the mid-travel of the ram stroke.

Workie & Tesfaye, [2021] to extrude the square part from the circular billet with cosine and the 3rd order polynomial die profile, FEM modeling was done using DEFORM-3D software. The upper limit theorem was used to explore hypothetical extrusion. The conclusions of a minimum extrusion load are obtained by comparing cosine dies from the third polynomial dies for both analytical and numerical analysis. Optimal extrudate dies Al6063/SiC composite material. Extrusion Load in the form of a variable percent reduction in the area of a square form extruded with a cosine die profile. A 30% drop Cosine die profile, for example, has a lower extrusion load than other Cosine reduction and 3rd-order polynomial die profiles.

Dewang & Sharma, [2021] The purpose of this study is to explore the influence of friction coefficient, die angle, die profile radius, and workpiece preset temperature on the extrusion process using FEM modeling. Maximum heat flux is shown to drop initially with increasing die-angle due to simpler material movement along the profile radius of the die as well as being dependent on maximum nodal temperature, which also drops. Maximum nodal temperature decreases with increasing die profile radius and the higher the friction coefficient, the greater the rise in nodal temperature in the billet.

2.1.3 Optimization of die extrusion parameters

Jurković et al., [2009] multiple optimization strategies are employed in this study to determine the ideal cold forward extrusion parameters, with a focus on the geometrical component of the process, the die angle. The standard Taguchi and genetic algorithms, as well as alternative optimization approaches, have proven features, virtues, and limits. According to the results, classical experimental design approaches are too complicated to utilize. Experiments must be undertaken in huge numbers, particularly as the number of process components expands. To overcome this problem, the Taguchi technique employs a unique design of orthogonal arrays to analyze the complete parameter space with the fewest feasible tests. On the other hand, using typical experimental design processes, a mathematical model may be developed that is a strong tool for anticipating response for any input parameter value within the experiment domain, and optimum values may be any of the parameter points.

Zhang et al., [2012] Based on Taguchi's design of experiments, 32 variations of process parameters were created in this article to simulate the extrusion process for a hollow aluminum profile using HyperXtrude. S/N ratio analysis and ANOVA were utilized to investigate the effects of process variables (such as billet diameter, ram speed, billet preheated temperature, die temperature, and container temperature) on VRD and extrusion force. The extent of the impact of process parameters on VRD was determined using ANOVA, and the results of the analysis revealed that billet diameter (or extrusion ratio) had the greatest influence, followed by die temperature, ram speed, and container temperature, with billet preheated temperature having a minor influence. The aforementioned conclusion was completely consistent with real observation. The optimal combination of process parameters for minimum VRD was determined using S/N analysis. When compared to the baseline process parameters, VRD is reduced by half after optimization.

Sadollah & Bahreininejad, [2012] The application of several optimization algorithms for identifying the optimal cold forward extrusion parameters was examined in this study, with an emphasis on the geometrical aspect of the process (half-die angle). The least extrusion force may be achieved with low strain and a low coefficient of friction. As a consequence, the reduction in extrusion force will be proportional to the half-die angle. As compared to traditional optimization approaches, genetic algorithms (GA) and simulated annealing (SA) have effectively provided the optimum point to identify optimal input parameters for fitness functions in the cold forward extrusion process. During the optimization process, metaheuristic methods reduce extrusion load more than typical optimization approaches like the Taguchi method.

Rao & Krishna, [2012] the work focus on a Finite Element Analysis-based technique for predicting the optimum process variables of the AL6061 alloy extrusion process by adjusting the die angle, ram speed, and coefficient of friction. For the experimental runs, the author used Taguchi's L9 design, and simulations were performed using DEFORM-3D software with die angles, COF, and ram speeds. The relevance of input variables on output responses was determined using an ANOVA, as was the percentage contribution of each variable. According to the literature, the best process variables will substantially assist in extruding the provided material with the least amount of extrusion load and die exit temperature.

Sharififar & Akbari Mousavi, [2015] examine the connection between relevant factors and optimize the extrusion force, the Taguchi technique, artificial neural networks, and genetic algorithm are utilized in this article. The extrusion force is affected by the diameter of the billet opening and the length of the die. The length of the die has an opposing influence on the extrusion force. The force is minimized when the die length is optimal. Extrusion force is inversely proportional to the diameter of the billet hole.

K et al., [2016] article's work was a finite element study of extrusion load and stress during the extrusion of aluminum 6061 alloys. The best collection of extrusion variables for the selected replies was found. The trial runs were carried out using Taguchi's L16 design matrix. An ANOVA is used to determine the impact of factors on responses. In addition, the percentage contribution of each variable to each answer was visually depicted. The Taguchi optimization approach was used to generate the set of optimum process variables based on the greatest S/N ratio. The Taguchi approach is also used to discover the optimal model for a square shape in MINI TAB software.

Ong et al., [2018] because the cost is sensitive to the forming condition, the optimal forming parameters are crucial in forming technologies. Different optimization techniques, including the traditional mathematical approach, PSO, FPA, and CSA, are used in the extrusion process to discover process parameters and get the best forming parameters. The results show that the PSO, FPA, and CSA optimization methods are quick and easy to use, and they produce promising results in determining the best process parameters for the lowest extrusion force. The obtained half-die angle paths also show that low strain and low coefficient of friction lead to lower extrusion force. As a result, in this example, the half-die angle is the only parameter that has to be improved.

Jajimoggala et al., [2019] this study verified the procedure of hot extrusion for AA6061. The influence on process parameters and design of extrusion load, exit temperature, displacement, and damage was done using the DEFORMTM-3D simulation program based on FEM. The Taguchi Method of Taguchi, simultaneously with GRA (a multi-performance response optimization), was applied for the optimization of process parameters for extrusion load, exit temperature, displacement, and damage. The GRA was created to transform a multi-performance response into a single optimum output designated as the GRG. This calculates the best process parameter level setting to maximize all performance aspects simultaneously. The optimal process parameters were established using the technique of Grey-based-Taguchi to optimize extrusion load, exit temperature, displacement, and damage.

Yang et al., [2019] in this research, by utilizing RSM combination with NSGA-II, the acquisition of the optimum extrusion process parameters obtained the greatest tensile strength and the smallest surface roughness and build time. In addition, the answers are confirmed through experimental verification. Based on the ANOVA and F-value findings, the most effective parameters for tensile strength, surface roughness, and build time is determined to be nozzle diameter and layer thickness. In contrast, liquefier temperature is less effective on surface roughness, and surface roughness is indifferent to the extrusion velocity and tensile strength. Surface roughness rises greatly when employing a bigger nozzle diameter, high extrusion, filling velocity, and thick layers. The increase in the nozzle diameter, filling velocity, and layer thickness lower the build.

Shuqin, [2020] This article begins with decreasing the extrusion torque and extrusion temperature to increase the quality of the extrusion thread and the life of the extrusion tap, using a mix of numerical simulation and experimental design. Then, determine the effect of processing factors on the index value by range analysis. The appropriate combination parameters of extruded internal threads were developed and validated through tests. To get the optimum extrusion effect, orthogonal tests with the bottom hole diameter, extrusion speed, and friction factor as variables are carried out. The impact of these parameters on the extrusion torque and extrusion temperature is evaluated, and the ideal procedure is established.

Namburi et al., [2020] Extrusion force is the most significant aim of the extrusion procedure. Therefore, studies on extrusion forces are necessary. This study focuses on the modeling and simulation of extrusion process parameters on aluminum 1100 alloy and the optimization of the parameters. A Taguchi analysis has been performed to gather the data for different input parameters, and an analysis of variance (ANOVA) has been used to identify the optimal values of the force necessary for the extrusion of various input parameters. The die angle has substantial relevance in lowering the force.

Lechner et al., [2021] To produce an ideal set of process parameters for the indirect extrusion of CCA rods, the process was modeled using the FEM-based program DEFORM 2D and evaluated using the techniques of statistical DoE. Therefore, a CCD with 29 runs was used. Regression models, exhibiting substantial linear and quadratic effects and interactions of the five examined process parameters, formed the foundation for the optimization of the indirect CCA extrusion process. All response variables were largely impacted by the process parameter, Die angle. For a minimal length of full aluminum head, the three process parameters extrusion ratio, ram speed, and die angle as well as the interaction between extrusion ratio and die angle were critical. However, the other response variables sleeve fracture, change in copper volume fraction, and fraction of CCA rod were influenced primarily by ram speed, copper weight percentage, and die angle. Response surface techniques and desire index were utilized to obtain an optimal overall setup of these most impacting process aspects.

Ranjbari et al., [2021] The effects of decreasing the area (RA), twist angle (), and length of twist zone (L) on the strain inhomogeneity and load of the process were evaluated in this study on the AA6061-T6 aluminum alloy treated by vortex extrusion. Using the response surface approach and ANOVA findings, the two factors interaction (2FI) and quadratic polynomial models were constructed to forecast strain inhomogeneity and process load, respectively While twist angle (φ), reduction in area (RA), and the interaction of twist angle and reduction in area (φxRA) are the most effective factors impacting strain inhomogeneity, the load of the process is controlled by the major parameters of φ, RA, and the interactions of (φ*RA),(φ*φ) and (RA*RA).

Liu et al., [2021] in this article, the cold extrusion method of forming a clutch outer gear hub was presented, and the effects of primary process parameters on the forming load and fillet clearance were evaluated using the Deform software. Besides, multi-objective optimization of the cold extrusion process using a combination of response surface technique and two metaheuristic methods, namely MOGA and NSGA-II, was undertaken. Finally, to test the reliability and correctness of optimization findings, the cold extrusion forming process of finite element simulation and experiment was carried out. Forming load is direct whereas fillet clearance is inversely related to the entry angle of the punch and wall thickness of the billet. With high reliability and fitting accuracy, response surface models can better describe objective functions of forming load and fillet clearance to design variables such as punch entrance angle, billet wall thickness, calibration band length, and friction coefficient, which can be used for subsequent multi-objective optimization. A comparison of findings of meta-heuristic techniques demonstrates that the NSGA-II algorithm has a relative advantage over the MOGA algorithm.

Table 2. 1 Literature review summary

Author	Material	Parameters	Die profile used	Remark
Balaji et al. 2016	soft low carbon steel	Reduction ratio, die length	Streamline	The viscoplastic deformation analysis by FEM has been successfully applied to predict the deformation field, die geometry, and plastic

				boundaries during metal extrusion
Fernández et al., [2021]	Bimetallic AZ31B-Ti6Al4V	Die semi-angle, extrusion relation, and friction	Conical	Finally, the most relevant manufacturing parameter to reduce the damage factor in the core is the die semi-angle as well as to obtain minimum values for the extrusion.
Sahu et al., [2019]		semi-cone angle, Pocket Depth, number of holes	Conical multi-hole	The finite element analyses of multi-hole extrusion have been carried out with different die designs. The extrusion load, effective stress, and the bending of the profile are studied.
Venkatesh and Venkatesan, [2015]	Al–SiC DRMM composite	Die profile	fourth-order polynomial, third-order polynomial, cosine, elliptical, hyperbolic and conical	After an exhaustive study of UB, FEM, and experimental methods for six various die profiles. the benefit of the cosine die profile over the rest of the five different profiles is learned.
Workie and Tesfaye, [2021]	Al/SiC composite	Die profile and percentage of area reduction	3rd order polynomial and cosine	The results of minimum extrusion load are developed in cosine die profiles as compared to the 3rd-order polynomial dies for both analytical and numerical analysis.
Namburi et al., [2020]	1100 Aluminum alloy	Die Angle, Coefficient of friction, and Ram Speed	Linear converging	Numerical experimentation has been done by using the finite element method. Taguchi analysis has been employed to obtain the optimum values of the force required for the extrusion.

Research Gap

Many researchers have done multi-profile die extrusion of aluminum alloys but so far only limited work on copper alloys such as C15000 which finds various applications in industries and has also it drawn a lot of attention in place, pure copper. The present thesis aimed at the analysis of the deformation behavior of C15000 through the multi-profile die extrusion process.

CHAPTER THREE

MATERIALS AND METHODS

3.1 MATERIALS

There is a wide range of applications of copper zirconium alloys in aerospace and electronics industries, including high-speed rail contact wires, Circuit breaker parts, buses, and electrical contact materials. Most of the metals are strain-rate sensitive at hot working conditions because of recrystallization and grain growth limitations. The effect of various variable process parameters on maximum extrusion load, effective stress, and damage has been studied with the help of the commercial simulation package DEFORM-3D. Linear converging, streamline and cosine die reduction of the well-deformable material C15000, has been considered and the die material was H13(versatile chromium-molybdenum hot work steel).

Wrought copper alloy C15000 (Zirconium Copper)

Chemical composition: Zr=0.15%, Cu = 99.8%

Table 3. 1 property of C15000 material AZO materials,[2012]

Properties	C15000
Density	8.89 g/cm^3
Melting point	980°C
Tensile strength, ultimate	430 MPa
Tensile strength, yield	415 MPa
Modulus of elasticity	129 GPa
Thermal conductivity	360 W/mK
Electrical Conductivity	65 % IACS
Hardness	HRB 65

For the analysis of numerical simulation results, the plastic deformation of the billet material in an extrusion process.

Flow stress data for Cu-Zr Zhang et al., [2017]:

$$\dot{\varepsilon} = 5.777 * 10^{25} [sinh(0.014\sigma)]^{13.873} exp\left(-\frac{532696}{8.314T}\right) \quad (3.\ 1)$$

3.1.1. Die Material

H13 Tool Steel

H13 Tool Steel is a versatile chromium-molybdenum hot work steel that is widely used in hot work and cold work tooling applications. The hot hardness (hot strength) of H13 resists thermal fatigue cracking which occurs as a result of cyclic heating and cooling cycles in hot work tooling applications. Because of its excellent combination of high toughness and resistance to thermal fatigue cracking (also known as heat checking), H13 is used for more hot work tooling applications than any other tool steel Novotny & Banerjee, [2016].

Applications: Inserts, cores, and cavities for die casting dies, die casting shot sleeves, hot forging dies, extrusion dies, and plastic mold cavities and components that require high toughness and excellent polish ability.

Composition

Table 3. 2 Composition of H13 tool steel AZO materials,[2013]

C	Mn	Si	Cr	Mo	V	Fe
0.40	0.40	1.00	5.25	1.35	1.00	Balance

Physical properties

- Density: 0.280 lb/in^3 (7750 kg/m^3)
- Specific Gravity: 7.75
- Machinability: 65-70% of a 1% carbon steel

3.2. Methods

The methods utilized for this study were literature reviews for data collection about the extrusion concept and DEFORM-3D software, which is a Finite Element Method (FEM) based process simulation system designed to analyze various forming processes used by metal forming and related industries. Initially, the models of the die and the workpiece are generated using SOLIDWORK software. These models were imported into DEFORM-3D software for the extrusion operation to be simulated validating the parameters. Copper alloy C15000 was used to prepare a work billet with a 25mm length and 16mm diameter. Perform experimental investigations for multi-profile die extrusion of copper alloy and plain copper commercially for selected parametric combinations to assess the product capability. Then perform testing and characterization for the extruded product to determine the mechanical properties of the material and metallurgical investigation. The die is made of H13 The die is heat treated to increase hardness and finished.

3.2.1. Finite Element Analysis

The deformation behaviors of the material in the metal forming process are generally explained through rigid viscoplastic formulation Shiro Kobayashi, Soo-Ik Oh, [1989] Differential and integral equations can be resolved by a numerical method called the finite element method. The commercial finite element method code was applied through DEFORM-3D for carrying out numerical simulation analysis of deformation behavior. The basic equations of the rigid-plastic element are as follows:

Equilibrium equation:

$$\frac{\partial \sigma_{ij}}{\partial x_i} = 0, \qquad or \qquad \sigma_{ij,j} = 0 \tag{3.2}$$

Velocity strain-rate relations and incompressibility equations:

$$\dot{\varepsilon}_{ij} = \frac{1}{2}\left(u_{i,j} + u_{j,i}\right) \qquad and \qquad u_{ij} = 0 \tag{3.3}$$

$$yield\ criterion,\ f\left(\sigma_{ij}\right) = 0: \quad \bar{\sigma} = \sqrt{\frac{3}{2}}\left(\sigma_{ij}'\sigma_{ij}'\right)^{1/2} = \bar{\sigma}\left(\bar{\varepsilon}, \bar{\varepsilon}\right) \tag{3.4}$$

Constitutive equations:

$$\dot{\varepsilon}_{ij} = \frac{\partial f\left(\sigma_{ij}\right)}{\partial \sigma_{ij}}\dot{\lambda}: \qquad \dot{\varepsilon}_{ij} = \frac{3}{2}\frac{\dot{\bar{\varepsilon}}}{\bar{\sigma}}\sigma_{ij}' \tag{3.5}$$

$$with \quad \dot{\bar{\varepsilon}} = \sqrt{\frac{2}{3}}\left(\dot{\varepsilon}_{ij}\dot{\varepsilon}_{ij}\right)^{1/2} \tag{3.6}$$

Boundary conditions: $\sigma_{ij} n_i = F_j \ on\, S_F, u_i = U_i \ on\, S_U$ (3.7)

Where σ_{ij} and $\dot{\varepsilon}_{ij}$ are the stress and the strain rate respectively $\bar{\sigma}$ and $\dot{\bar{\varepsilon}}$ are the effective stress and the effective strain rate, respectively, F_j is the force on the boundary surface of S_F and U_i is the deformation velocity on the boundary surface of S_{ij} . The weak form of rigid-plastic FEM can be determined by applying the variation method to Eqs. (3.2) – (3.8), Yang et al., [2008]

$$\delta\pi = \int_V \bar{\sigma}\delta\dot{\bar{\varepsilon}}\,dV + K\int_V \bar{\varepsilon}_v \delta\dot{\varepsilon}_v\,dV - \int_{S_F} F_i \delta u_i\,dS = o \tag{3.8}$$

Where V and S are the volume and the surface area of the material, respectively, and K is the penalty constant. The most crucial part of simulation in software is the selection of an appropriate material model. DEFORM-3D contains various material models (for elastic-plastic, rigid-plastic, and porous material), and each model has different suitability, so the selection of the correct material model as per the requirement is the prime necessity to get accurate results. Most of the material models require detailed material properties such as young's modulus of elasticity, strain hardening exponent, strength coefficient, etc., as input to the preprocessor before running the solver. In addition to material properties, preprocessors also require an input of detailed process parameters such as friction coefficient, extrusion wheel velocity, heat transfer coefficients, etc. The yielding criteria which are used for solving a problem are Von Mises (in the Deform3-D). Eqs. (3.9) and (3.10) show effective strain and effective stress respectively.

$$\bar{\varepsilon} = \frac{\sqrt{2}}{3}\sqrt{(\varepsilon_1 - \varepsilon_2)^2 + (\varepsilon_2 - \varepsilon_3)^2 + (\varepsilon_3 - \varepsilon_1)^2} \tag{3.9}$$

$$\bar{\sigma} = \frac{1}{\sqrt{2}}\sqrt{(\sigma_1 - \sigma_2)^2 + (\sigma_2 - \sigma_3)^2 + (\sigma_3 - \sigma_1)^2} \tag{3.10}$$

Where ε_i and σ_i are principal strain and principal stress in the direction (i) respectively Zhou et al., [2003]

3.2.1.1. Numerical Simulation

DEFORM-3D is a tool based on a three-dimensional finite element simulation system to explore numerous forming and heat treatment conditions in the metal forming industries sectors. Designers and engineers are allowed to reduce material costs during production, shop floor costs, redesign tooling, and improve tool life and also production time of the new product. Mainly there are three major components in the Deform-3D tool system, the preprocessor, the simulation engine, and the postprocessor as shown in Fig. 3.1.

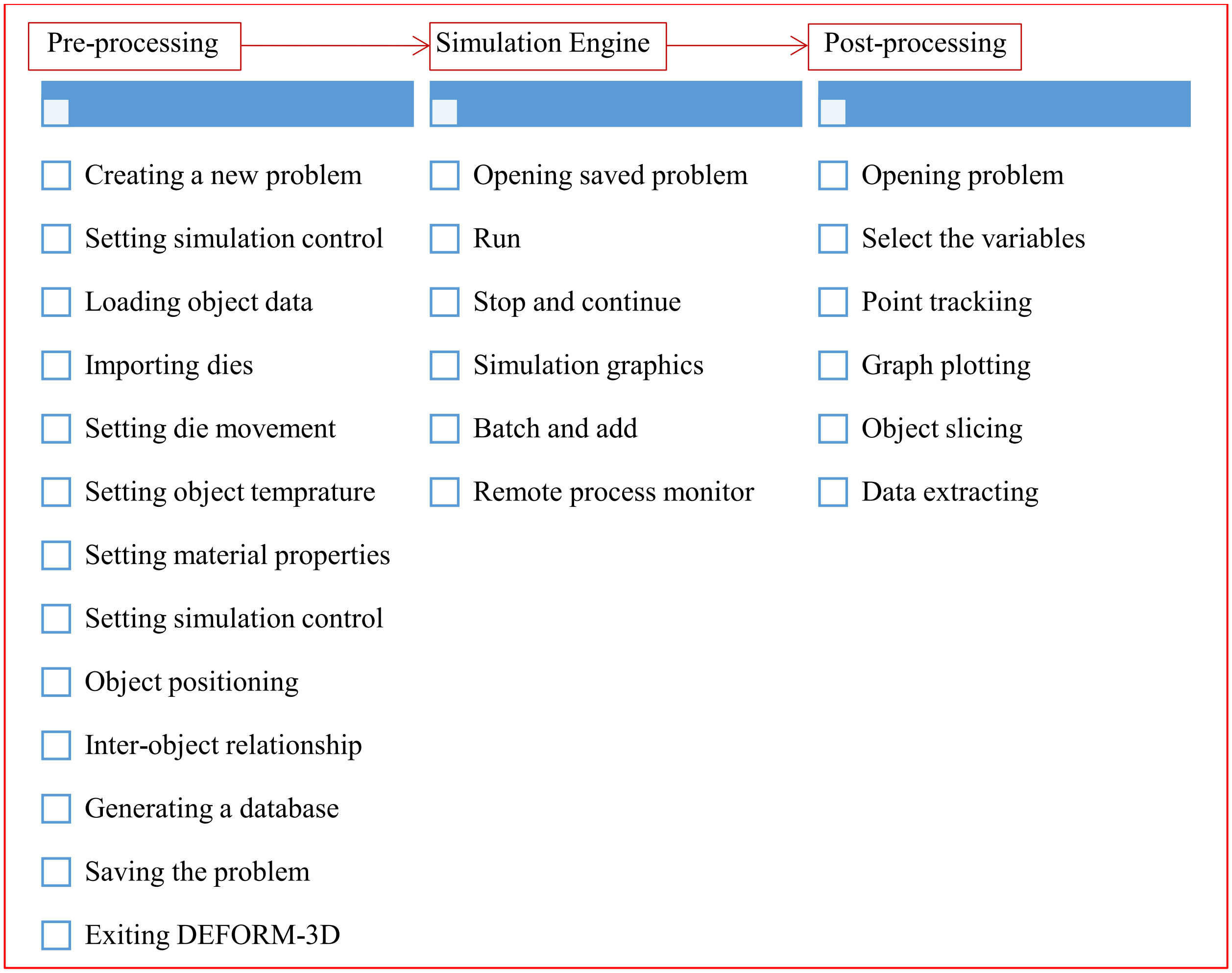

Figure 3. 1 The block diagram of the simulation process in DEFORM-3D software

Pre-processor by Simulation Control

Lagrangian incremental iteration type with deformation mode was activated for the simulation. Mechanical, thermal, and phase transfer problems can be simulated by deform mode. Punch was considered the primary die for which the stepping and stopping criteria were decided. Stepping of the primary die can be controlled by either time or displacement reference. The primary die will move the stroke length per step as specified up to the completion of the total number of steps assigned. The total travel of the primary die is the total step times the primary die velocity (displacement/step). Time and total step selection are crucial parameters. A larger time step causes inaccurate solutions and convergence problems whereas a smaller time step needs unnecessary extra time for the solution. The maximum displacement of a node should not exceed one-third of the edge of an element, so a finer mesh size corresponding smaller step size should be chosen. Coarse meshes cause several problems like mesh degradation, problems in remeshing, and excessive volume loss. The remeshing option will be triggered depending on the time, step, and stroke increment as well as penetration by the master objects. After meshing, the data/information contained by the old mesh can be interpolated into the new mesh.

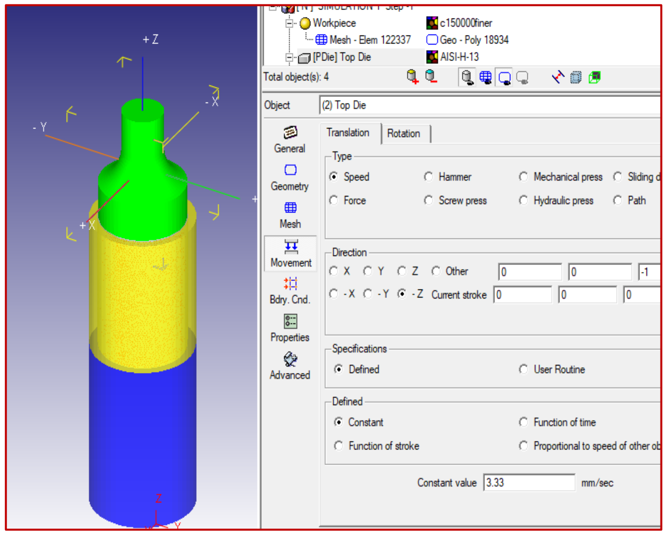

Figure 3.2 Simulation control in DEFORM 3D software

Materials

If an object is defined with mesh, then it must have a material to be assigned. The material data can be allocated by selecting the material icon. The properties of most of the standard materials are available in the software database list. The software also facilitates a generation of a new material model. In this case, the material model selected is an isotropic and rigid visco-plastic model.

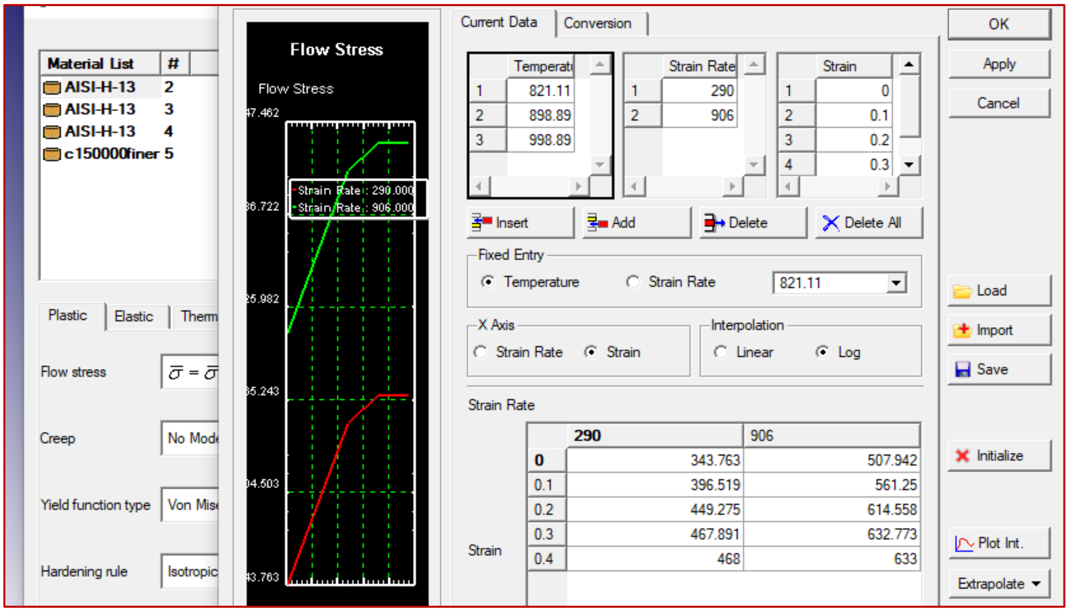

Figure 3.3 materials are available in the software database list and the new material model

Object definition

How the deformation will be modeled for the different objects, need to be defined here. A non-deformable body can be modeled as a rigid body i.e. container, bottom dies, and top die, and represented by only geometric profiles (DIEGO). This kind of object can perform force transmission, velocity and thermal transmission, and diffusion calculations. These types are used for tooling setups. Depending on the characteristics of the material, the billet can be defined as a rigid-plastic as well as a rigid-viscoplastic model. After a particular value of strain rate, the material shows plastic deformation. This material model does not consider the spring back effects. These two material models are utilized for this investigation but other models like elastic, elasto-plastic (does not consider strain rate sensitivity), and porous are also available with this software.

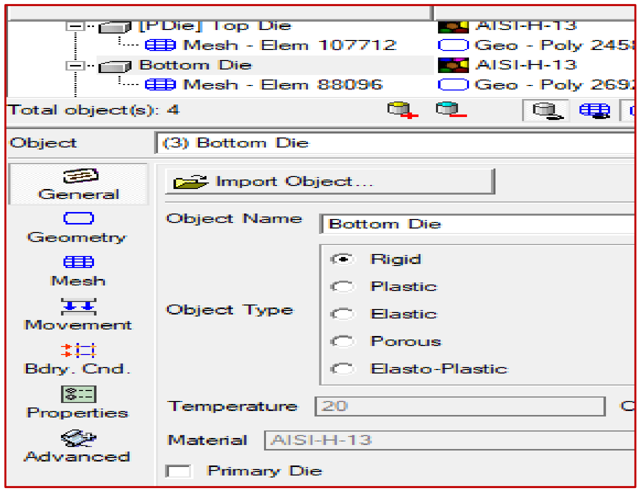

Figure 3. 4 Object definition Rigid for bottom die

Inter-object relation

The master/slave relationship to define inter-object relations between different objects was set. The finer mesh should be assigned to the slave or softer object. In this case, it was not necessary to define a "No contact" relation. The friction value and thermal transfer property are assigned to the inter-object boundary in this step. The activated nodes indicate the contact or assignment between the node and the surface which restricts the penetration of the master object into the slave. The behavior of the contacting object while in contact is defined here. The shear friction coefficient and conduction heat transfer coefficient between the inter-material boundary are assigned in this problem. The frictional resistance was assumed to be of the shear type in this formulation and the friction factor m $\left(0 \le m \le 1\right)$ can be expressed as: $m = \sqrt{3}\frac{\tau}{\sigma}$ in this 0.4 is used.

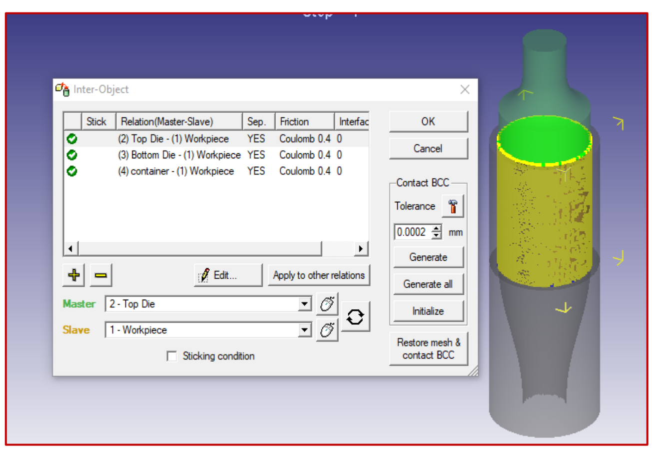

Figure 3. 5 Inter-object relation

Boundary condition

The boundary condition controls, how the boundary of an object will interact with others as well as with the environment. In most cases, the object boundary exchanges heat with the surrounding. The movement boundary condition of the objects is defined in such a way as to satisfy the extrusion condition. The velocity of the die and container is set to zero in all directions whereas the punch is allowed to move in the extruded direction only.

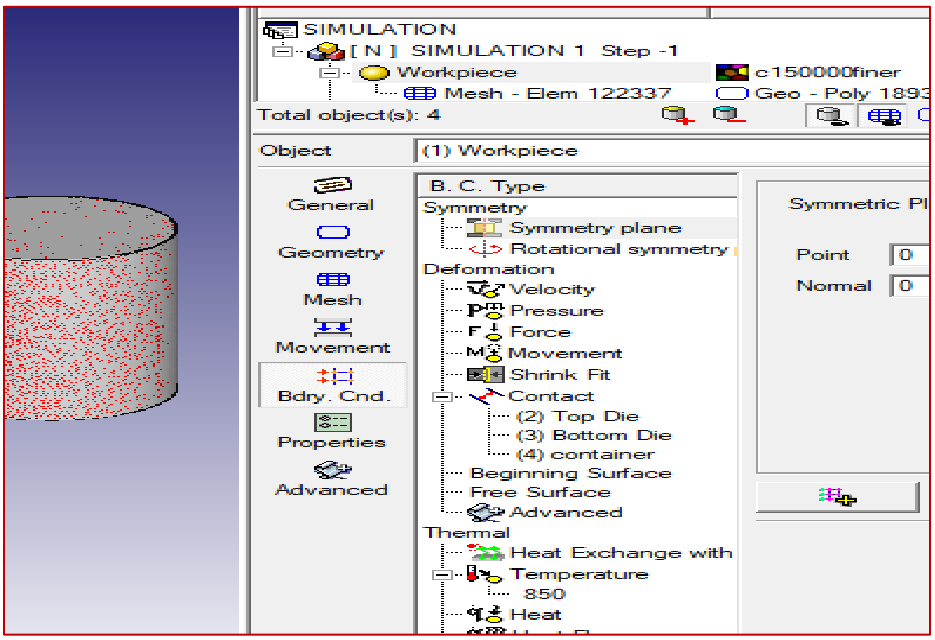

Figure 3. 6 Boundary condition

Simulation Engine

The assigned simulation or numerical work defined in the pre-processor step is further processed by clicking a run icon. For a faster solution with less memory consumption, the conjugate gradient solver was selected. The message window shows the execution information which also includes convergence information. The last most recent step can be visualized from the simulation graphics option while the problem is running. Different effects like effective stress, strain, and temperature distribution can be visualized for that step only. The problem can be aborted by the user in case of any constraint or continued up to the message of completion.

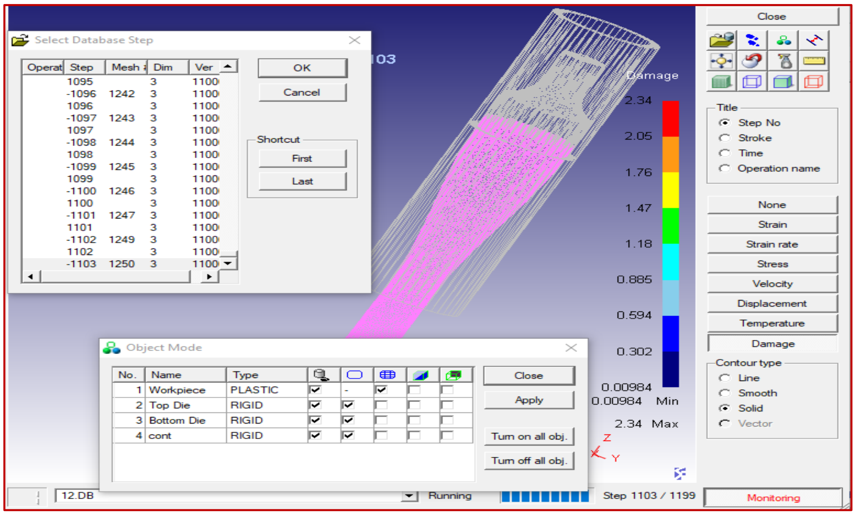

Figure 3. 7 Simulation engine when software running database

Post Processor

In this stage, the outcome results were visualized, and the same can be extracted from the database. The geometry after deformation with tool movement at every step with different views can be collected. The distribution of state variables on the objects in the form of contour plots can be analyzed. Contoured plots are facilitated to vary the distribution style like solid saddling distribution, line distribution, and vector distribution. The graphs between any of the state variables about different abscissa can be plotted and extracted. Point tracking and flow net are the two most important facilities to study the internal behavior of the component at the deformation stage provided in the post-processor. The graphic utility window provides the facility of manipulating the range and vision as per the analysis.

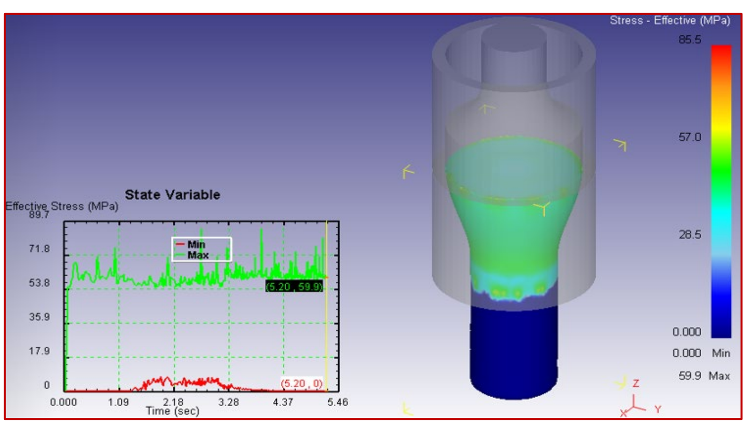

Figure 3. 8 Post-processor extracted data

3.2.2. Optimization by Response Surface Methodology

An essential part of any research is improving the performance of its processes and increasing the yields of the systems. This process is referred to as optimization. A specific variable change in the general application can be determined under optimum conditions while holding the other variables at a constant level. This is often referred to as a one-variable technique. One main disadvantage of using this technique is that it will not contain the interaction effects between the variables and, additionally, it will not fully describe the effects of the variables on the procedure. To solve these problems, optimization studies can be achieved using the technique of response surface methodology (RSM). The RSM process is a group of statistical and mathematical methods used in developing, and optimizing a process, in which a response surface of interest is affected by several variables. RSM is a powerful technique that has important applications in the design of an experiment, the development and design of a new product, and the optimization of existing products and process designs. It defines the effects of the important factors, alone or in combination with the involved processes Olivero et al., [1995].

3.2.2.1 Stages for RSM application

Several different methodologies for the response surface process were first introduced in the 1950s by Box and others Becker et al., [2015]. The term "response surface" comes from a graphical perspective created using a mathematical model. Response surface methodology (RSM) is a collection of statistical and mathematical techniques useful for developing, improving, and optimizing processes. It also has important applications in the design, development, and formulation of new products, as well as in the improvement of existing product designs. The most extensive applications of RSM are in the industrial world, particularly in situations where several input variables potentially influence performance measures or quality characteristics of the product or process. These performance measures or quality characteristics are called the response. They are typically measured on a continuous scale, although attribute responses, ranks, and sensory responses are not unusual. Most real-world applications of RSM will involve more than one response. The input variables are sometimes called independent variables, and they are subject to the control of the engineer or scientist, at least for purposes of a test or an experiment.

Response surface models are techniques that are based on fitting an experimental model to the experimental data obtained regarding an experimental design.

Most applications of RSM for optimization involve the following several stages:

- First, a screening factor is run to reduce the number of factors (independent) variables to a relative few, so the procedure will be more efficient and require a smaller number of runs or tests. Secondly, a determination is made on current levels of the major effect factors resulting in a value for the response that is close to the optimum region. If the current levels of the factors are not consistent with optimum performance, then the experimenter must adjust the process variables that will lead the process toward the optimum level.
- Thirdly, researchers carry out the chosen experimental design according to the selected experimental matrix.
- Next, mathematical/statistical models of the experimental design data are developed by fitting linear or quadratic polynomial functions. The fitness of the models then needs to be evaluated. Lastly, the stationary points (optimum values) are obtained for the variables.

These stages are summarized in the flowchart provided in Figure 3.9

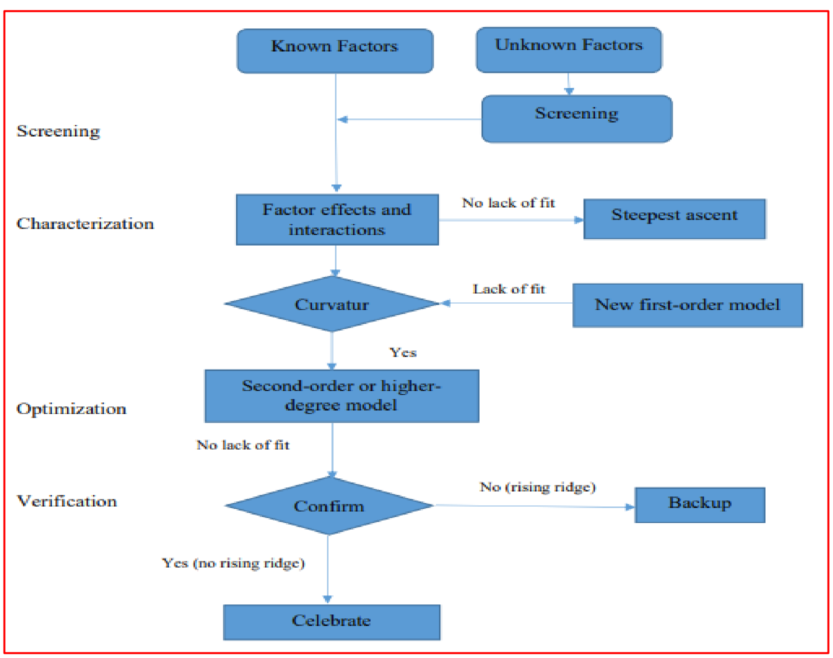

Figure 3. 9 Flow chart of RSM

3.2.2.2 RSM Modeling

A Second-order Experimental Design

A full 3^k factorial design is a design matrix with very limited application in RSM when the number of variables is greater than two. This is due to the large number of experiments required for such a design (calculated by expression $N=3^k$ where N is the total experiment run, and k is the number of variables). Therefore, its efficiency was lost when modeling quadratic functions. Because of this, full three-level factorial designs for more than two factors require more experimental runs than are commonly accommodated in practice. Designs containing a smaller number of design points, such as the Box– Behnken, central composite, and Doehlert designs are more frequently used. For two variables, the efficiency can be compared with designs such as central composite Sarabia & Ortiz, [2009].

In the present work, the Box-Behnken design of experiments is utilized for generating the experiment sequence. As per the design of the Box-Behnken methodology, a total number of twenty-seven trials are undertaken. Out of twenty-seven trials, twenty-four trials are random and the three trials are repetitive per Box-Behnken design methodology.

3.2.3. Experimental Procedures

3.2.3.1. Die Profile Design and Modeling

Die profile plays an important role in guiding the metal flow in extrusion. Metal flow in extrusion is directly influenced by the die profile and friction condition. The load requirement for deformation, by using a cosine die profile is minimum at zero friction conditions due to its geometrical fetcher zero entry and exit angle. But it is a traditional practice to use LC die due to the ease of manufacturing. Streamline, LC, and cosine dies along with the container, punch, and billet geometry were designed and modeled by SolidWorks® software. The die profile functions for streamline, cosine and LC die are as follows Venkatesan & Venkatesh, [2014]:

$$R(z) = R_1 + (R_1 - R_2)\left[2\frac{z^3}{L^3} - 3\frac{z^2}{L^2}\right] \quad (3.11)$$

$$R(z) = R_2 + (R_1 - R_2)\frac{(L-Z)}{L} \quad (3.12)$$

$$R(z) = \frac{R_1 + R_2}{2} + \frac{R_1 - R_2}{2}\cos\left(\frac{\pi z}{L}\right) \quad (3.13)$$

where ‘L’ is the die length and ‘Z’ is the number of steps in between ‘0’ and ‘L’.

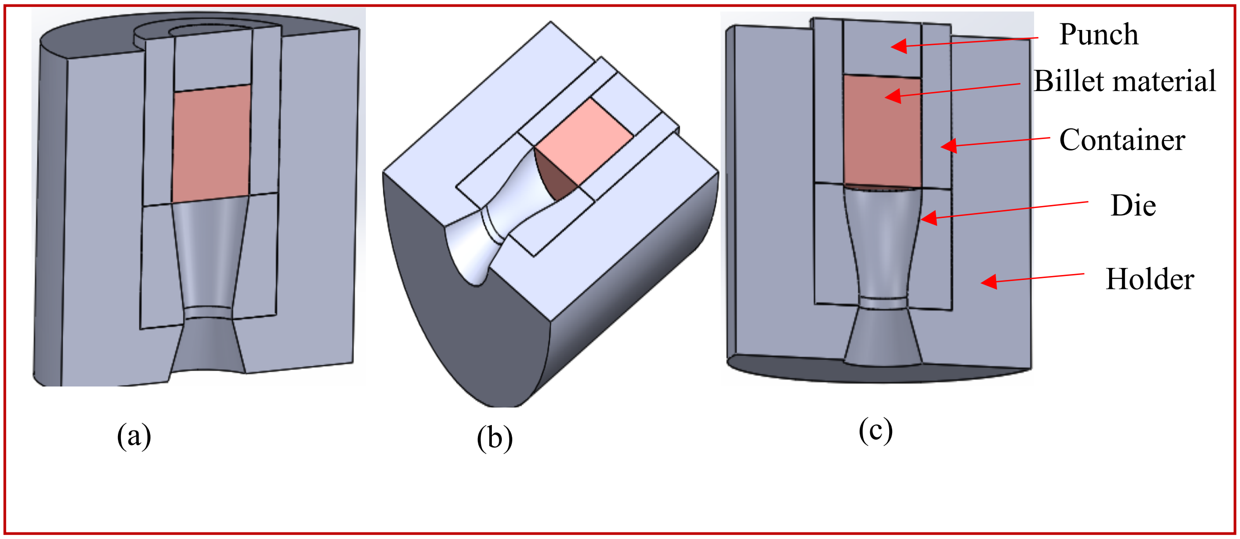

Figure 3. 10 Die profile model (a) Linear convergent (b) Cosine (c) Streamline

Die profiles for the cosine die, streamline die and LC die are shown in Figure 3.10 for a product diameter of 10mm. with a die length of 10mm. Solid models of dies for product diameters 7, 10, and 13mm with different die lengths following streamline profile, LC profile, and cosine law have been developed referring to equations (3.9), (3.10) & (3.11). Finite element methods of computer simulations are capable of predicting the effect of all essential parameters which influence the process. Commercially available DEFORM-3D software (was used for the aforementioned investigation. The solid geometries were imported as a .stl file and simulation of extrusion of C15000 alloy were carried out by lagrangian incremental type rigid-viscoplastic simulation with direct iteration method and conjugate-gradient solver at a normal temperature of 800,850 and 900°C and ram speed of 100, 150, 200mm/min.

3.2.3.2 Die fabrication

Due to the sensitivity of extrusion process parameters and the difficulty of extrusion setup arrangement the sample preparation takes a longer period to accomplish.

Figure 3. 11 Die material selection cut into the piece using a hacksaw

The figure below shows the series of steps that this study follows for sample preparations. The raw material and extrusion components are prepared

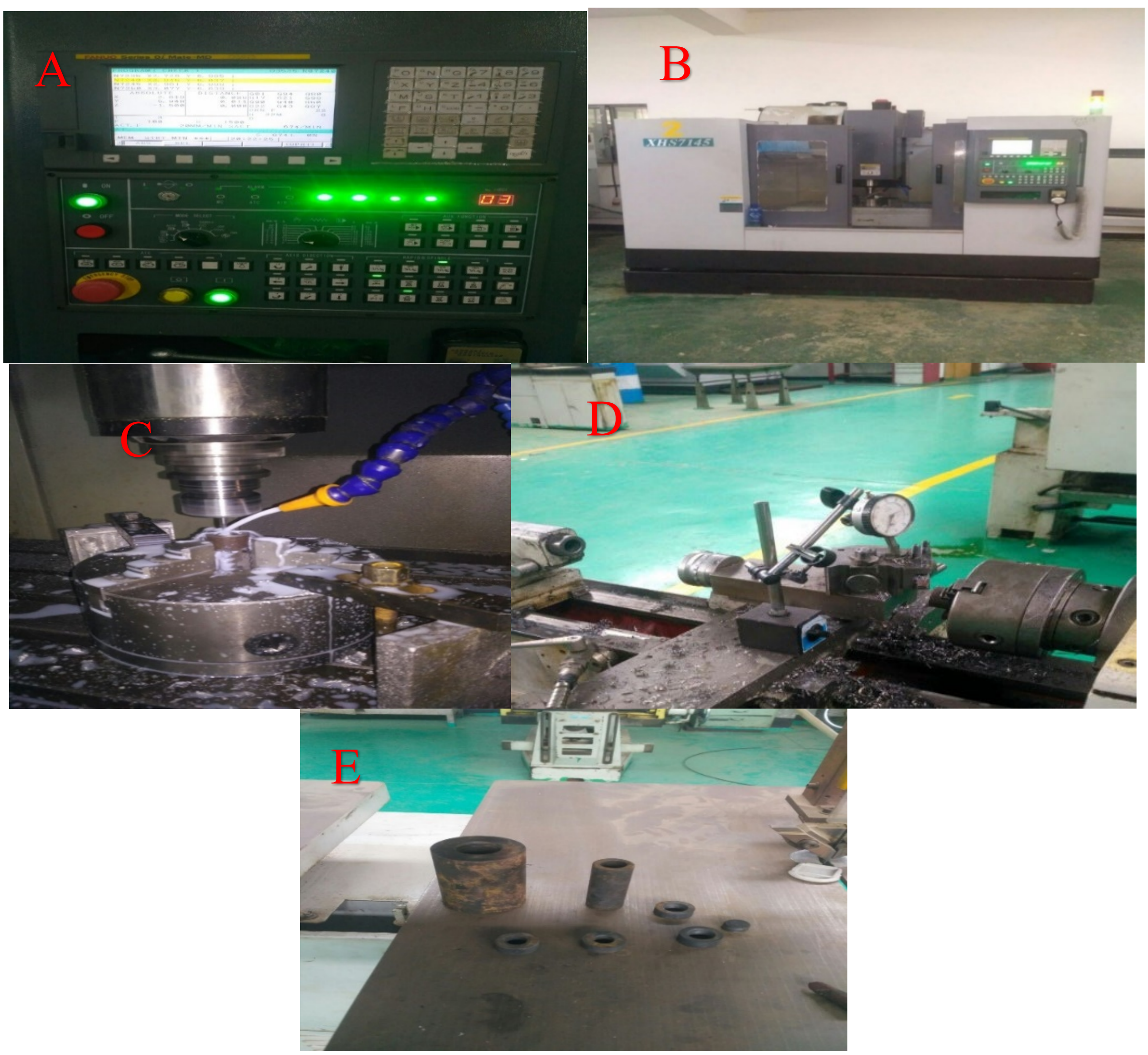

Figure 3. 12 Series of processes during extrusion sample preparation (a-e)

In this study, a direct hot extrusion process is used for sample preparation. The extrusion process was performed on C15000 copper alloy using a 150-ton hydraulic press see Figure 3.14, which is accessible at MIDI (manufacturing industry development institute).

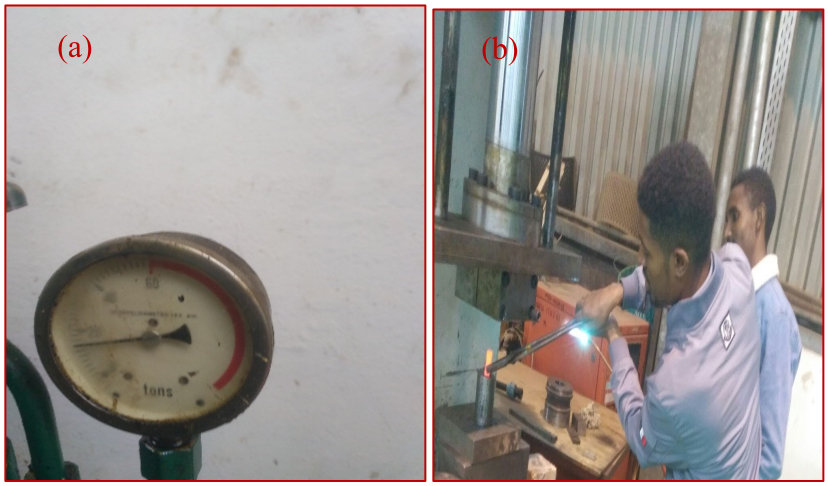

Figure 3. 13 The extrusion process performed on C15000 copper alloy using a 150-ton hydraulic press (a) Ton reading (b) Arranging in press machine

Figure 3.14 shows the hydraulic press which is ready for the extrusion-making process. Then by making extrusion arrangements on the hydraulic press heat is given using oxyAcetylene, until the required temperature is achieved. The ram speed is can be increased as preferred.

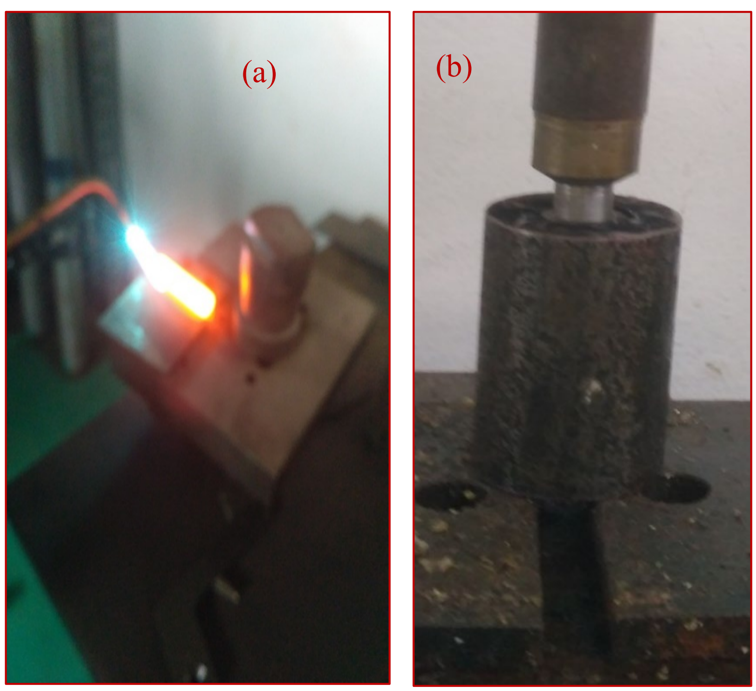

Figure 3. 14 shows extrusion making process of (a) heating (b) pressing in the die

Finally, the required cosine and linear convergent profile die extrusion is performed as shown in the figure below.

Figure 3. 15 Samples and extrusion components after the extrusion process

3.2.3. Material Testing and Characterization

Methodology for experimental investigation in this section the methodology for sample preparation and characterization are presented for sample preparation from process identification to finishing.

The experiments analysis was executed on the commercial copper zirconium (C15000) rods of 16mm diameter, which were prepared by continuous casting. During the forming process, the billet material was firstly cleaned and extruded to Product diameters 13.1mm and 12.18mm and Die lengths 10mm and 10.2mm, on a hydraulic press machine at a ram velocity of 117.2 and 132.3mm/minute and billet temperature 900°C respectively for cosine and LC die profile. It is a key function in assessing and ensuring the quality, properties, and behavior of a material, and is thus an important step in guaranteeing the quality and success of your finished product. Universal testing machines fall within the general class of mechanical-testing devices that were traditionally used to test the tensile and compressive strength of materials. Hardness testing is the most common heat-treatment test performed throughout the industry due in large part to its speed and simplicity. The microscope is to the manufacturing engineer what the hammer is to a carpenter. Their usefulness and versatility in metallurgical investigations are fundamental.

3.2.4 Material Testing and Characterizations

In the present study, material characterization analysis was conducted before and after commercial copper zirconium material was deformed through a hydraulic press machine to understand the improvement that appears on the billet materials after the extrusion process was conducted.

3.3.2.1 Microstructure analysis

The microscope is to the materials that the hammer is to a carpenter. Their usefulness and versatility in metallurgical investigations are fundamental.

Table 3. 3 Resources required during material characterization

s.no	Resources
1	Abrasive cutting machine
2	Sandpapers
3	Polishing machine
4	Diamond suspension liquid
5	Water
6	Dryer (air compressor)
7	Etchants
8	Optical microscopy

A microstructural examination is generally performed using optical microscopes (OM) to magnify features of the material under analysis. Metallurgical examinations may evaluate:

- Intergranular Attack or Corrosion,
- Grain Size
- Extent of Decarburization and Carburization
- Inclusion Rating
- Percent Spheroidization
- Sample Preparation

To identify and evaluate the microstructure of the material, it is very important to prepare the sample carefully and properly. The following steps have been carried out to analyze the microstructural examination of the deformed specimens.

1. Sectioning: specimens are carefully sectioned to avoid altering or destroying the structure of the materials. An abrasive cutting wheel has been used, it's important to keep the specimens cool with coolant to avoid overheating.

2. Mounting: after the specimen is sectioned to a convenient size, it is mounted in a plastic or epoxy material to facilitate handling and the grinding and polishing steps. Mounting media ensured to be compatible with the specimen to hardness and abrasion resistance. Typical mounting materials are thermosetting phenolics such as Bakelite, and thermoplastic materials such as methyl methacrylate (Lucite).

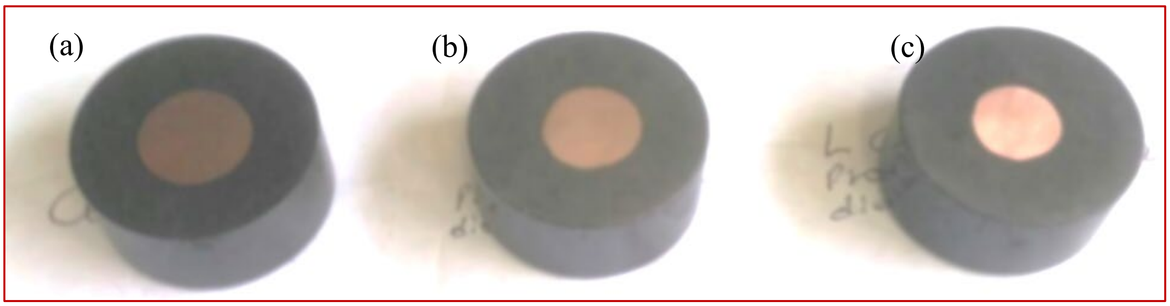

Figure 3. 16 Mounted Process of 16 mm raw material (a) and 13mm cosine (b), 14mm LC (c) of deformed products

3. Grinding: grinding follows mounting to remove the surface damage that occurred during the sectioning step and to provide a flat surface. Grinding involves the use of a series of progressively finer abrasive grits (sandpaper). Four types of grits size abrasives have been used for grinding processes (coarse grinding (240 µm), fine grinding (800 µm), super fine grinding (1200µm), and ultrafine grinding (2000µm)). This procedure provides a flat surface for the specimens.

4. Polishing: the polishing step removes the last thin layer of the metal. It provides a mirror-like surface. The diamond suspension has been used for lubrication during the process.

5. Etching: the final step that might be used is etching to show the microstructure of the test specimens. This step reveals features such as grain boundaries, twins, and second-phase particles not seen in the unetched sample. In this step 50 ml ethanol and 0.5 ml Nitric acid (HNO_3) have been used as etching chemicals. Finally, optical microscopy has been used to see the microstructural surface of the specimens by 200µm.

Figure 3. 17 Microstructural analysis of C15000 material

3.3.2.2 Hardness Test

A hardness test has been conducted to know the resistance of commercial copper zirconium material and which is subjected to plastic deformation under different die profiles induced by an applied force, by using Vickers hardness test (HVS- 50) methods consisting of a diamond indenter in the form of right pyramids with a square base and an angle of 136 degrees between opposite faces subjected to a load of 10kgf and the full load is applied for an average time of 10 to 15 seconds.

$$HV = \frac{cons\tan t \times test\ force}{surface\ area\ of\ indentation} \tag{3.12}$$

$$= 0.102 \times 2F(\sin(\frac{136}{2}))/d^2 \tag{3.13}$$

Where F- is the test force, d- surface area indentation and 136/2 is the angle between the opposite faces subjected to a load of 10kgf Moore & Booth, [2015].

Figure 3. 18 Vickers hardness testing of C15000 material

Hardness testing is the most common heat-treatment test performed throughout the industry due in large part to its speed and simplicity. Vickers is considered the most versatile of microhardness test methods. It can be used for virtually any material, from very soft to very hard.

3.3.2.3 Compression test

It is a key function in assessing and ensuring the quality, properties, and behavior of a material, and is thus an important step in guaranteeing the quality and success of your finished product. Universal testing machines fall within the general class of mechanical-testing devices that were traditionally used to test the tensile and compressive strength of materials.

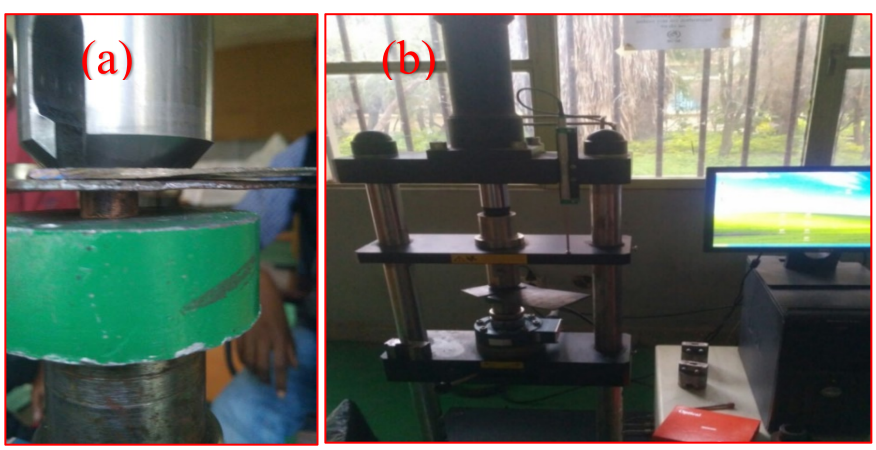

Figure 3. 19 Compression testing of (a) sample and (b) machine

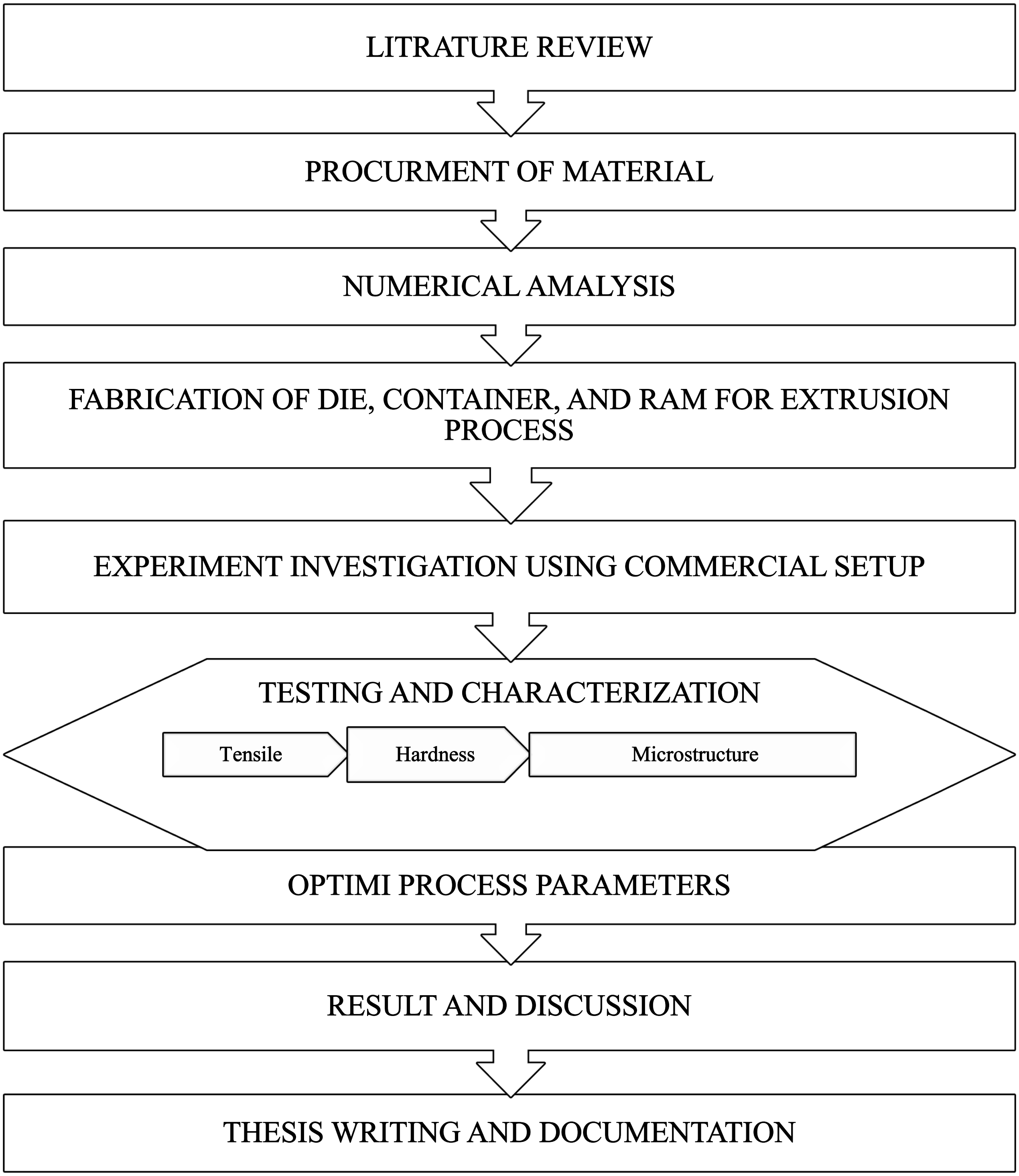

Figure 3. 20 Flow chart of the proposed methodology

CHAPTER FOUR

RESULT AND DISCUSSION

4.1 Numerical Simulations Analysis

The billet is the representation of the collection of subdomains known as finite elements, which are bounded by the set of nodes depending on the type of element selected. All the properties of the body are assigned to the nodes. It is an approximate technique to estimate the target and by increasing the elements the accuracy can be improved.

4.1.1 Establishment of finite element model

The finite element model of the extrusion established by DEFORM 3D software

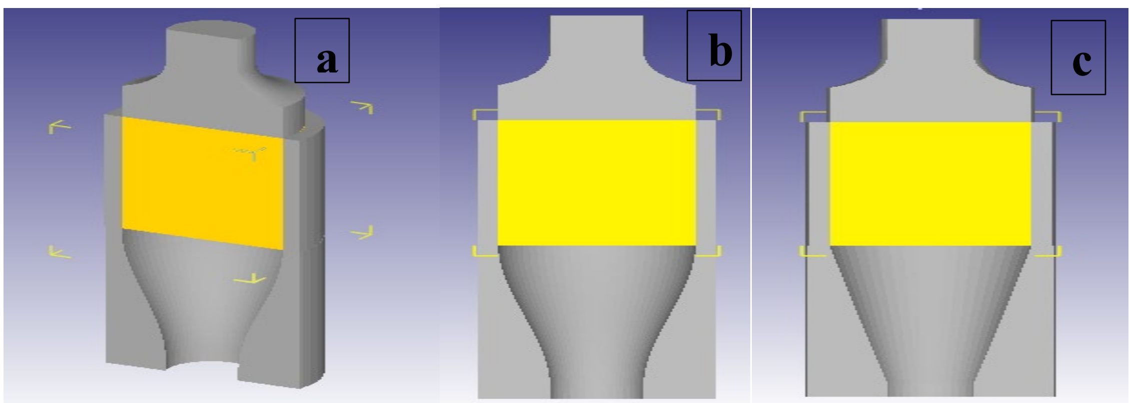

Figure 4. 1 Finite element model a) cosine b)streamline c)linear convergent

In the current research work, a thermo-mechanical analysis of the axisymmetric extrusion process is carried out through the FEM-based software DEFORM-3D. Figure 4.1 shows the FE model of the axisymmetric extrusion process having die and billet. The initial radius of the cylindrical bar is 16 mm and 23 mm in length before extrusion. Cosine, streamline, and linear convergent dies are considered. The billet is considered a deformable entity whereas the die is treated as a rigid body for FEM simulation. The billet and die are discretized with 100000 mesh elements. The behavior of copper zirconium alloy is described through flow-stresses curves according to Flow stress data for Cu-Zr Zhang et al., [2017]. The deformation of the billet within the die is actuated by defining displacement in the downward direction by 23 mm according to three different ram speeds. The coefficient of friction between the interacting surfaces of the die and billet is assumed as 0.4. Thermal and mechanical properties as well as thermal, and mechanical boundary conditions and initial conditions are defined for billet and die along with frictional heat generation for the evolution of temperature in the billet.

4.1.2 Simulation

The finite element simulation of copper zirconium billet material for 16 mm diameter was done at different extrusion ram velocities, preheating temperatures, die profiles (cosine, streamline, linear convergent), extrusion ratio, and die lengths. The following parameters have been studied after a successful run of the finite element simulations for 16 mm diameter copper zirconium billet material:

- The total load required for deformation of the copper zirconium.
- The effective stress distribution.
- Damage distribution

4.1.2.1 Effect of die profile on load

Die profile or die type is an important focus in the case of extrusion as it is responsible for the formation of the dead metal zone and controlling the flow characteristics. By considering the three commonly industrial practiced dies i.e., cosine, LC, and streamlined die energy consumption for the extrusion was investigated. A comparative load versus parameters plot for the different dies is shown in Figure 4.2 at a constant of another parameter. The extrusion load is increased with increased die length and ram speed whereas decreases with increased temperature and product diameter for all three dies as shown in Figure 4.2 and the minimum extrusion load is existed in cosine die profiles. In streamline and LC dies the deformation is higher than the cosine dies and it needed a higher extrusion load to extrude C15000 billet from the initial to the end of the process. It is observed from the below figure that the load required for extrusion is maximum by streamline die. The area in between the plots is indicating the amount of energy loss due to the redundant work. Cosine profiled die geometry has got an initial curvature effect at the die entrance which facilitates the free flow of particles without causing any adhering and scratch.

But the absence of an initial curvature effect on conical and streamlined, die profiles causes the flow particles with adhering behavior and scratch effect on the die entrance and the bearing surfaces. This damage mechanism prevails on these profiles and reserves the negative factor such as higher extrusion load requirement, development of friction, and nonhomogeneous material flow and strain development. The comparative graph plotted for the load cosine profiled die is declared to be an optimal die by encountering a very lesser load than the highest load of the streamline die.

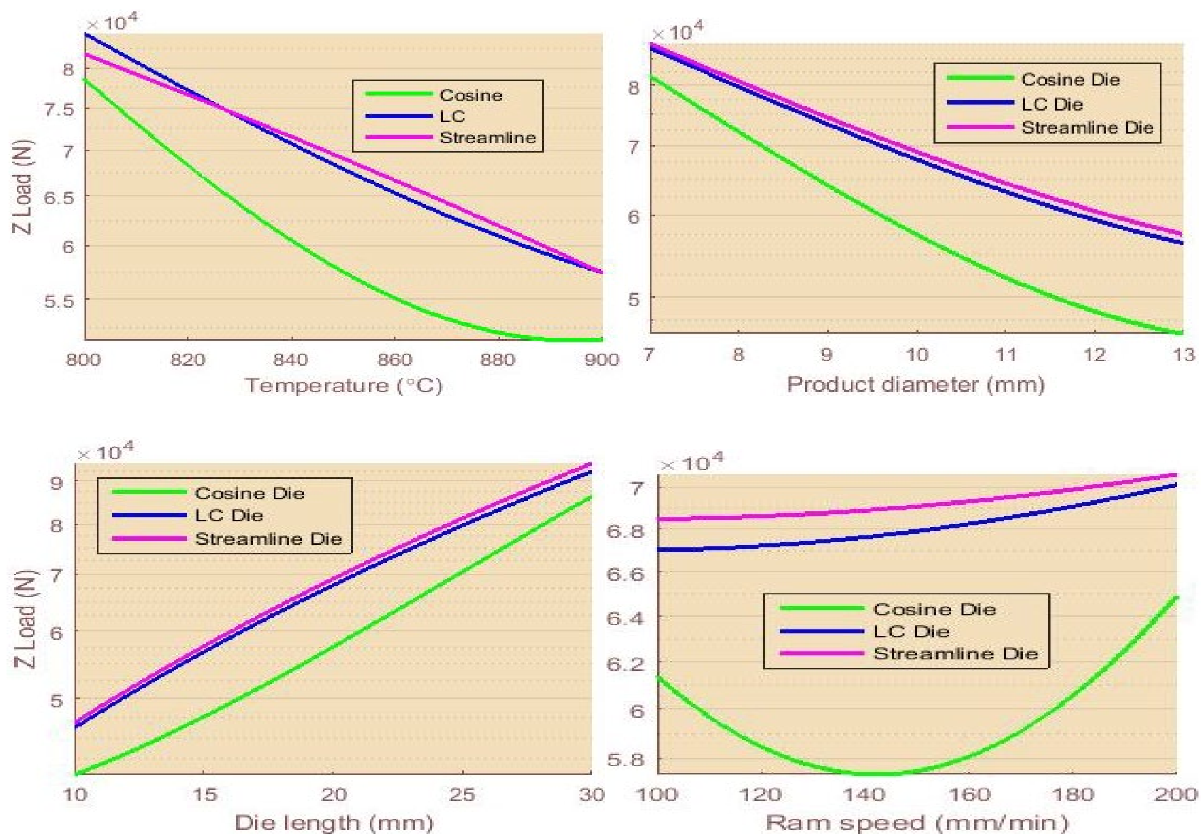

Figure 4. 2 Comparative loads versus parameters plot for the different dies

4.1.2.2 Effect of die profile on effective stress

The peak stresses occur along the contact surface and in the region where the diameter of the workpiece narrows down due to deformation The plastic deformation locates near the surface of the workpiece, where plastic strains are at the maximum. In this regard, the Streamline die results higher slope and maximum compared to other profiles. In the cosine die profile the stress effect is minimum on a minimum die length and ram speed and maximum on a maximum die length and ram speed whereas maximum on a minimum temperature and product diameter and minimum on a maximum temperature and product diameter. For LC and streamline die profile is similar to the cosine die but the values are maximum as compared to the cosine die as shown below in Figure 4.3.

The flow of material in cosine die appears to be gradual. The entry and exit angle of the cosine die profile is zero which causes the complete deformation in the in-between sections of die length. So, the stress-induced for cosine profile extrusion is comparatively lesser.

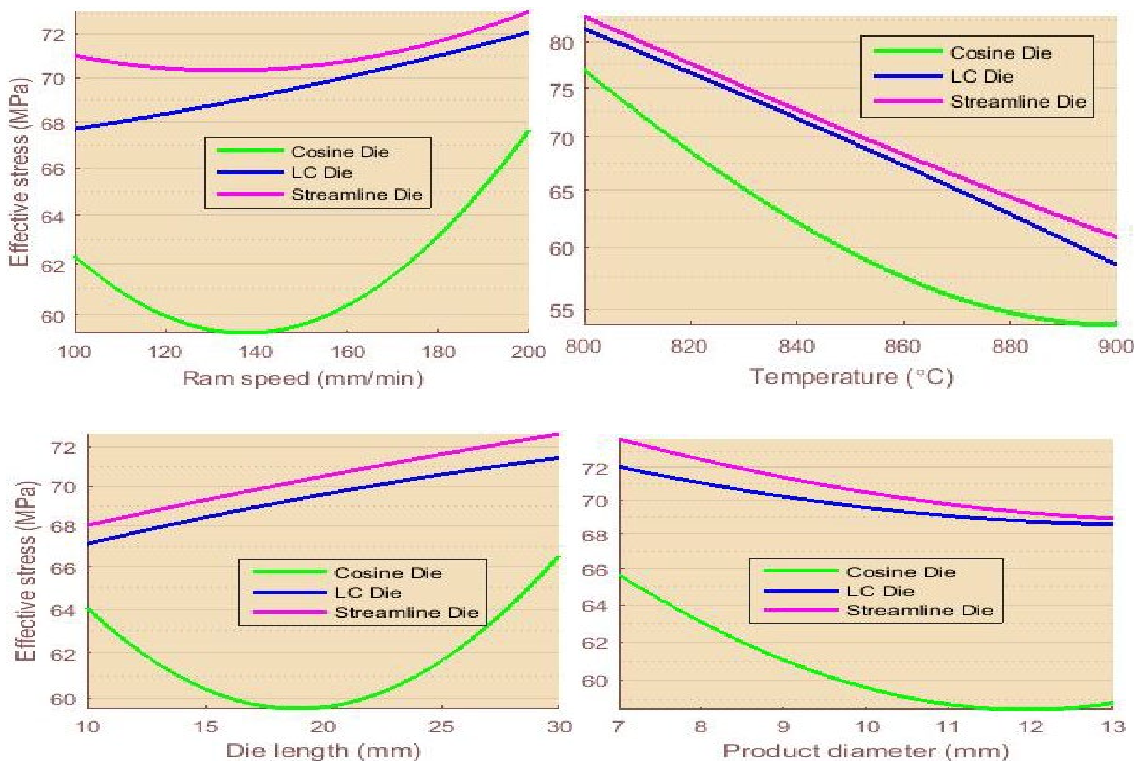

Figure 4. 3 Comparative effective stress versus parameters plots for the different dies

4.1.2.3 Effect of die profile on damage

The influence of the process parameters on the damage factor is quoted in the figure below. Figure 4.4a shows that the value of damage distribution over the surface of the billet is observed for 800°C and 900°C temperatures at the same ram speed, product diameter, and die length. The damage occurs at 800°C temperature for a ram speed of 150 mm/min, 10 mm product diameter and 20 mm die length and no damage is observed for 900°C temperature. It is observed that the maximum damage distribution occurs on the surface of the billet in decreasing temperatures. The property depicted for product diameter. This critical damage occurs because of the maximum tensile stress at a point on the billet surface. The damage value decreases with increasing the product diameter and temperature and maximum stress. In the extrusion process, the conical and streamlined die performs like a stress raiser. As seen in figure 4.4 with increasing die length and ram speed increasing damage, the cosine dies profile has lesser damage depicted than the streamline and linear convergent die. The variation in deformation through three profile dies in comparison can be analyzed from the figure below. At the initial zone and final zone, the deformation is very less in cosine die whereas at the intermediate zone it is severe but in the case of linear converging and streamline dies the slope is uniform.

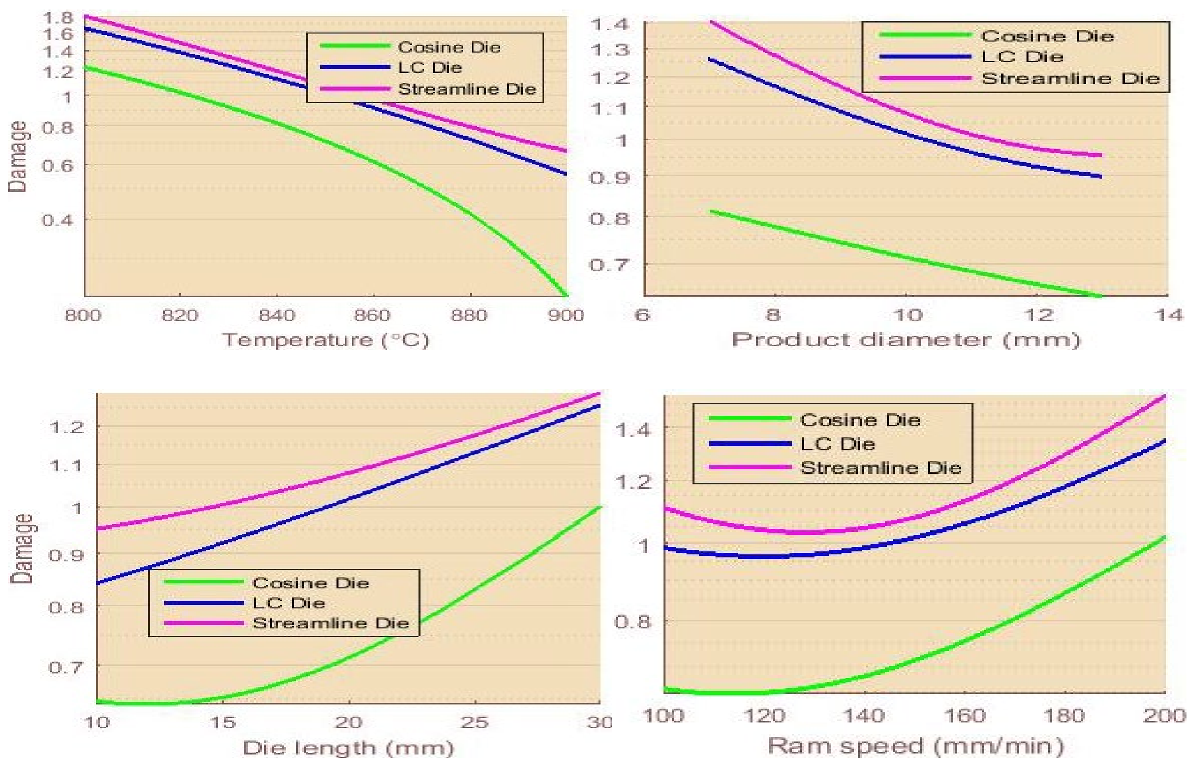

Figure 4. 4 Comparative damage versus parameters plot for the different dies

4.2 Optimization of process parameter

Using MINITAB 20, A statistical software, the significant coefficients are determined and final models are developed incorporating these coefficients to estimate extrusion die force, effective stress, and damage. For four factors and three levels, as per RSM, box-Behnken design 27 experiments need to be performed. Parameters and their levels are presented in Table 4.1 and numerical values are presented in Table 4.2.

Table 4. 1 Process Parameters and their Limits

Factors	Levels		
Ram speed (mm/min)	100	150	200
Product diameter (mm)	7	10	16
Die length (mm)	10	20	30
Billet temperature (°C)	800	850	900

Table 4. 2 FEM analysis Results (for linear convergent, Cosine, and Streamline die)

V	D	L	T	linear convergent die			Cosine die			Streamline die		
				Damage	Stress	Load	damage	stress	Load	damage	Stress	Load
200	7	20	850	1.95248	76.1487	89896	1.63674	72.4309	90781	1.70691	73.7418	91891
150	7	10	850	0.97102	70.2509	64404	0.97481	68.8615	63835	1.11732	68.6396	64263
150	13	20	900	0.56380	58.1443	45433	0.43530	57.9998	44572	0.48308	57.7554	44789
150	10	20	850	0.97627	69.8636	68390	0.96490	59.5775	57387	0.92282	69.4934	69147
150	10	10	900	0.50000	57.2521	40244	0.49828	57.0057	39444	0.42610	57.0381	39114
200	13	20	850	1.05442	73.3004	56445	1.01917	69.9423	55159	1.39941	70.1978	55774
150	10	20	850	0.97627	69.8636	68390	0.96490	59.6631	57694	0.92282	69.4934	69147
150	7	20	800	1.92730	83.8642	108153	1.53137	83.8088	108076	2.01855	85.3416	95997
150	10	30	800	1.97352	83.6493	117549	1.97045	83.6040	111507	1.84442	86.4174	115588
100	10	20	900	0.51599	57.7221	56479	0.48848	57.6380	55705	0.55407	58.0554	55735
150	13	20	800	1.38078	81.2696	66020	1.30285	81.2979	65823	1.61527	80.3029	64752
150	7	30	850	1.36620	74.2546	109227	1.32934	73.6884	108782	1.48658	74.0077	113345
150	10	10	800	1.31049	79.4656	57524	1.28680	79.9130	56102	1.50886	79.6556	55724
100	13	20	850	0.88168	66.4451	53248	0.92783	66.1928	53009	0.91179	67.5806	52081
200	10	20	900	0.67005	60.5636	59647	0.75103	60.7263	57245	0.81610	66.7819	55751
150	13	10	850	0.87631	67.1892	35259	0.78987	67.6354	33914	0.73070	67.4006	34617
200	10	20	800	2.04500	83.8075	85271	1.62527	84.4816	85095	2.19367	83.6835	84667
100	7	20	850	0.99935	69.8406	87685	0.86022	68.9970	85230	1.30005	79.3269	90712
150	10	30	900	0.64186	60.8448	79871	0.75238	61.8533	80132	0.76584	62.9853	80832
150	10	20	850	0.97627	69.8636	68390	0.96490	59.6631	57694	0.92282	69.4934	69147
150	13	30	850	1.01561	70.4592	71767	1.04323	70.6176	72546	1.04892	70.8263	72064
200	10	10	850	0.96805	68.5435	48831	1.10632	77.9047	47978	1.01067	68.8133	47421
150	7	20	900	0.66756	60.5102	75776	0.60002	59.8871	72506	0.76140	61.3163	75872
100	10	10	850	0.83397	65.3779	46719	1.00433	65.4525	45642	1.06782	68.8326	47390
100	10	20	800	1.58200	80.4707	81604	1.45491	80.1709	81106	1.67061	81.0626	80747
200	10	30	850	1.94340	74.5871	96527	1.70670	73.1305	94908	1.85139	74.4350	95867
100	10	30	850	0.95757	69.8115	91554	0.97579	68.3576	90304	0.90429	68.8832	91134

Cosine die profile

$$Z\ load = 2574049 - 427V - 30214D + 6399L - 5361T + 2.266V^2 + 713.7D^2 + 60.32L^2 + 3.024T^2 - 3.18V\cdot D + 1.13V\cdot L - 0.245V\cdot T - 44.5D\cdot L + 13.39D\cdot T - 7.36L\cdot T \quad (4.1)$$

$$Effective\ stress = 2001 - 0.403V - 6.97D - 2.03L - 4.135T + 0.002151V^2 + 0.2921D^2 + 0.05702L^2 + 0.002299T^2 - 0.00085V\cdot D - 0.00384V\cdot L - 0.000122V\cdot T - 0.0044D\cdot L + 0.00024D\cdot T + 0.00058L\cdot T \quad (4.2)$$

$$Damage = 13.6 - 0.0188V - 0.029D + 0.1159L - 0.0200T + 0.000050V^2 + 0.00149D^2 + 0.001110L^2 + 0.000007T^2 - 0.00065V\cdot D + 0.000314V\cdot L + 0.000009V\cdot T - 0.000692D\cdot L + 0.000095D\cdot T - 0.000215L\cdot T \quad (4.3)$$

Linear convergent die profile

$$Z\ load = 1170764 - 41V - 22774D + 10820L - 2303T + 0.265V^2 + 421.5D^2 + 13.59L^2 + 1.248T^2 + 0.66V\cdot D + 1.43V\cdot L - 0.050V\cdot T - 60.0D\cdot L + 12.17D\cdot T - 10.20L\cdot T \quad (4.4)$$

$$Effective\ stress = 389 + 0.012V - 2.38D + 0.523L - 0.515T + 0.000129V^2 + 0.0809D^2 - 0.00295L^2 + 0.000176T^2 + 0.00197V\cdot D + 0.000805V\cdot L - 0.000050V\cdot T - 0.00593D\cdot L + 0.00001D\cdot T - 0.000295L\cdot T \quad (4.5)$$

$$Damage = 32.4 + 0.0109V - 0.485D + 0.184L - 0.0639T + 0.00006V^2 + 0.00709D^2 + 0.000317L^2 + 0.000034T^2 - 0.000748V\cdot D + 0.000426V\cdot L - 0.000031V\cdot T - 0.00180D\cdot L + 0.000507D\cdot T - 0.000261L\cdot T \quad (4.6)$$

Streamline die profile

$$Z\ load = 299081 + 221V - 14532D + 9849L - 397T + 0.193V^2 + 396.4D^2 + 15.1L^2 + 0.213T^2 + 2.72V\cdot D + 2.35V\cdot L - 0.390V\cdot T - 72.1D\cdot L + 3.05D\cdot T - 9.07L\cdot T \quad (4.7)$$

$$Effective\ stress = 785 - 0.799V - 3.98D + 0.32L - 1.280T + 0.000620V^2 + 0.0953D^2 - 0.0013L^2 + 0.000570T^2 + 0.00586V\cdot D + 0.00279V\cdot L + 0.000611V\cdot T - 0.0105D\cdot L + 0.00070D\cdot T - 0.00041L\cdot T \quad (4.8)$$

$$Damage = 58.16 - 0.01405V - 0.4111D - 0.0745L - 0.1141T + 0.000098V^2 + 0.01144D^2 + 0.000425L^2 + 0.000062T^2 + 0.000097V\cdot D + 0.000502V\cdot L - 0.000026V\cdot T - 0.000251D\cdot L + 0.000115D\cdot T + 0.000002L\cdot T \quad (4.9)$$

4.2.1 Checking the Adequacy of the Developed Models

The adequacy of the developed models is tested using ANOVA. The statistical analysis for Z-load, Effective stress, and Damage was performed using the ANOVA. The analysis of variance was performed to find out the adequacy of the model. Table 4.3 to 4.11 shows the ANOVA results of Z-load, effective stress, and damage. The high F value (46.22 45.81 232.51 34.10 143.86 138.68 224.37 23.04 95.51) with a very low P value (0.000) indicates the high significance of the chosen model. As illustrated in table 4.3, the billet temperature creates the prime impact on the total sum of squares through 65.3% as the percentage contribution followed by extrusion ram speed of 9.3%, die length of 9.2%, and 4.1% product diameter percentage contribution followed by interaction effect of ram speed and product diameter of 2.9% percentage contribution in damage. As illustrated in table 4.4, the billet temperature creates the prime impact on the total sum of squares through 76.4% as the percentage contribution followed by a square of billet temperature of 8.4%, die length of 8.3%, ram speed of 7.4% and 6% product diameter percentage contribution followed by of ram speed of 4% percentage contribution in effective stress. As illustrated in table 4.5, the die length creates the prime impact on the total sum of squares through 49.5% as the percentage contribution followed by a product diameter of 28.1%, billet temperature of 16.8% percentage contribution followed by a square of billet temperature of 2.4% and square of product diameter of 2.2% percentage contribution in load.

Based on the results in Table 4.3 to 4.11, the coefficient of determination (R^2), 96.41%, the adjusted coefficient (R^2 adj.), 92.23%, and the predicted coefficient (R^2 pred.), 79.34%, were the least percentage attained. It is suggested that the coefficient of determination and the adjusted coefficient should be at least 0.8 for a good fit of the model. The coefficient of determination for the model's equation indicates the adequacy of the model since only 3.59% of the total variation was unexplained by the model. Therefore, the model can be used for theoretical prediction of the damage, effective stress, and Z-load.

Analysis of Variance damage (cosine)

Table 4. 3 ANOVA Test Results for damage of cosine die profile

Source	DF	Adj SS	Adj MS	F-Value	P-Value
Model	14	3.99498	0.28536	46.22	0.000
Linear	4	3.57629	0.89407	144.81	0.000
V	1	0.37938	0.37938	61.44	0.000
D	1	0.16668	0.16668	26.99	0.000
L	1	0.37364	0.37364	60.52	0.000
T	1	2.65659	2.65659	430.26	0.000
Square	4	0.15061	0.03765	6.10	0.006
V*V	1	0.08445	0.08445	13.68	0.003
D*D	1	0.00082	0.00082	0.13	0.721
L*L	1	0.06574	0.06574	10.65	0.007
T*T	1	0.00180	0.00180	0.29	0.599
2-Way Interaction	6	0.26808	0.04468	7.24	0.002
V*D	1	0.11737	0.11737	19.01	0.001
V*L	1	0.09889	0.09889	16.02	0.002
V*T	1	0.00212	0.00212	0.34	0.568
D*L	1	0.00256	0.00256	0.41	0.532
D*T	1	0.00102	0.00102	0.16	0.692
L*T	1	0.04613	0.04613	7.47	0.018
Error	12	0.07409	0.00617		
Lack-of-Fit	10	0.07409	0.00741	*	*
Pure Error	2	0.00000	0.00000		
Total	26	4.06908			

S	R-sq	R-sq(adj)	R-sq(pred)
0.0785769	98.18%	96.05%	89.51%

Analysis of Variance effective stress

Table 4. 4 ANOVA Test Results for effective stress of cosine die profile

Source	DF	Adj SS	Adj MS	F-Value	P-Value
Model	14	2043.11	145.94	45.81	0.000
Linear	4	1708.90	427.23	134.12	0.000
V	1	84.31	84.31	26.47	0.000
D	1	16.31	16.31	5.12	0.043
L	1	17.47	17.47	5.48	0.037
T	1	1590.82	1590.82	499.39	0.000
Square	4	317.79	79.45	24.94	0.000
V*V	1	154.23	154.23	48.42	0.000
D*D	1	126.46	126.46	39.70	0.000
L*L	1	173.43	173.43	54.44	0.000
T*T	1	176.20	176.20	55.31	0.000
2-Way Interaction	6	16.42	2.74	0.86	0.550
V*D	1	0.02	0.02	0.01	0.931
V*L	1	14.74	14.74	4.63	0.053
V*T	1	0.37	0.37	0.12	0.738
D*L	1	0.85	0.85	0.27	0.615
D*T	1	0.10	0.10	0.03	0.864
L*T	1	0.33	0.33	0.10	0.752
Error	12	38.23	3.19		
Lack-of-Fit	10	38.22	3.82	1564.88	0.001
Pure Error	2	0.00	0.00		
Total	26	2081.34			

S	R-sq	R-sq(adj)	R-sq(pred)
1.78480	98.16%	96.02%	89.42%

Analysis of Variance (Z load)

Table 4. 5 ANOVA Test Results for Zload of cosine die profile

Source	DF	Adj SS	Adj MS	F-Value	P-Value
Model	14	12329813369	880700955	232.51	0.000
Linear	4	11723375716	2930843929	773.77	0.000
V	1	33902408	33902408	8.95	0.011
D	1	3474360914	3474360914	917.27	0.000
L	1	6132013141	6132013141	1618.91	0.000
T	1	2083099252	2083099252	549.96	0.000
Square	4	485384828	121346207	32.04	0.000
V*V	1	171221484	171221484	45.20	0.000
D*D	1	274556956	274556956	72.49	0.000
L*L	1	194088314	194088314	51.24	0.000
T*T	1	304812480	304812480	80.47	0.000
2-Way Interaction	6	121052825	20175471	5.33	0.007
V*D	1	2891700	2891700	0.76	0.399
V*L	1	1285956	1285956	0.34	0.571
V*T	1	1499400	1499400	0.40	0.541
D*L	1	9969806	9969806	2.63	0.131
D*T	1	51258440	51258440	13.53	0.003
L*T	1	54147522	54147522	14.30	0.003
Error	12	45452852	3787738		
Lack-of-Fit	10	45390019	4539002	144.48	0.007
Pure Error	2	62833	31416		
Total	26	12375266221			

S	R-sq	R-sq(adj)	R-sq(pred)
1946.21	99.63%	99.20%	97.89%

Analysis of Variance damage (linear convergent)

Table 4. 6 ANOVA Test Results for damage of LC die profile

Source	DF	Adj SS	Adj MS	F-Value	P-Value
Model	14	5.88986	0.42070	34.10	0.000
Linear	4	5.24602	1.31150	106.30	0.000
V	1	0.68299	0.68299	55.36	0.000
D	1	0.37147	0.37147	30.11	0.000
L	1	0.49545	0.49545	40.16	0.000
T	1	3.69611	3.69611	299.57	0.000
Square	4	0.15307	0.03827	3.10	0.057
V*V	1	0.14071	0.14071	11.40	0.005
D*D	1	0.02539	0.02539	2.06	0.177
L*L	1	0.00535	0.00535	0.43	0.523
T*T	1	0.03783	0.03783	3.07	0.105
2-Way Interaction	6	0.49076	0.08179	6.63	0.003
V*D	1	0.15225	0.15225	12.34	0.004
V*L	1	0.18137	0.18137	14.70	0.002
V*T	1	0.02386	0.02386	1.93	0.190
D*L	1	0.01637	0.01637	1.33	0.272
D*T	1	0.04901	0.04901	3.97	0.069
L*T	1	0.06790	0.06790	5.50	0.037
Error	12	0.14806	0.01234		
Lack-of-Fit	10	0.14806	0.01481	*	*
Pure Error	2	0.00000	0.00000		
Total	26	6.03791			

S	R-sq	R-sq(adj)	R-sq(pred)
0.111077	97.55%	94.69%	85.88%

Analysis of Variance effective stress

Table 4. 7 ANOVA Test Results for effective stress of LC die profile

Source	DF	Adj SS	Adj MS	F-Value	P-Value
Model	14	1727.49	123.39	143.86	0.000
Linear	4	1718.80	429.70	500.97	0.000
V	1	62.03	62.03	72.32	0.000
D	1	27.18	27.18	31.69	0.000
L	1	54.30	54.30	63.31	0.000
T	1	1575.29	1575.29	1836.54	0.000
Square	4	7.66	1.92	2.23	0.126
V*V	1	0.55	0.55	0.64	0.438
D*D	1	4.85	4.85	5.66	0.035
L*L	1	0.46	0.46	0.54	0.476
T*T	1	1.03	1.03	1.20	0.294
2-Way Interaction	6	1.02	0.17	0.20	0.971
V*D	1	0.07	0.07	0.09	0.773
V*L	1	0.65	0.65	0.76	0.402
V*T	1	0.06	0.06	0.07	0.794
D*L	1	0.13	0.13	0.16	0.699
D*T	1	0.01	0.01	0.02	0.904
L*T	1	0.09	0.09	0.10	0.755
Error	12	10.29	0.86		
Lack-of-Fit	10	10.29	1.03	*	*
Pure Error	2	0.00	0.00		
Total	26	1737.78			

S	R-sq	R-sq(adj)	R-sq(pred)
0.926146	99.41%	98.72%	96.59%

Analysis of Variance (Z load)

Table 4. 8 ANOVA Test Results for Zload of LC die profile

Source	DF	Adj SS	Adj MS	F-Value	P-Value
Model	14	12149684960	867834640	138.68	0.000
Linear	4	11933011082	2983252770	476.73	0.000
V	1	31130965	31130965	4.97	0.046
D	1	3569680580	3569680580	570.44	0.000
L	1	6234159016	6234159016	996.23	0.000
T	1	2098040520	2098040520	335.27	0.000
Square	4	58266816	14566704	2.33	0.115
V*V	1	2342306	2342306	0.37	0.552
D*D	1	18028740	18028740	2.88	0.115
L*L	1	9849428	9849428	1.57	0.234
T*T	1	51944537	51944537	8.30	0.014
2-Way Interaction	6	158407062	26401177	4.22	0.016
V*D	1	243049	243049	0.04	0.847
V*L	1	2046330	2046330	0.33	0.578
V*T	1	62250	62250	0.01	0.922
D*L	1	17284806	17284806	2.76	0.122
D*T	1	34751025	34751025	5.55	0.036
L*T	1	104019601	104019601	16.62	0.002
Error	12	75092690	6257724		
Lack-of-Fit	10	75092690	7509269	*	*
Pure Error	2	0	0		
Total	26	12224777650			

S	R-sq	R-sq(adj)	R-sq(pred)
2501.54	99.39%	98.67%	96.46%

Analysis of Variance damage (damage)

Table 4. 9 ANOVA Test Results for damage of streamlined die profile

Source	DF	Adj SS	Adj MS	F-Value	P-Value
Model	14	6.10732	0.43624	224.37	0.000
Linear	4	5.43668	1.35917	699.06	0.000
V	1	0.55020	0.55020	282.98	0.000
D	1	0.40393	0.40393	207.75	0.000
L	1	0.34679	0.34679	178.36	0.000
T	1	4.13576	4.13576	2127.13	0.000
Square	4	0.39529	0.09882	50.83	0.000
V*V	1	0.32152	0.32152	165.36	0.000
D*D	1	0.11164	0.11164	57.42	0.000
L*L	1	0.00965	0.00965	4.97	0.046
T*T	1	0.12719	0.12719	65.42	0.000
2-Way Interaction	6	0.27535	0.04589	23.60	0.000
V*D	1	0.00163	0.00163	0.84	0.378
V*L	1	0.25213	0.25213	129.68	0.000
V*T	1	0.01703	0.01703	8.76	0.012
D*L	1	0.00065	0.00065	0.33	0.573
D*T	1	0.00390	0.00390	2.01	0.182
L*T	1	0.00000	0.00000	0.00	0.963
Error	12	0.02333	0.00194		
Lack-of-Fit	10	0.02333	0.00233	*	*
Pure Error	2	0.00000	0.00000		
Total	26	6.13065			

S	R-sq	R-sq(adj)	R-sq(pred)
0.0440941	99.62%	99.18%	97.81%

Analysis of Variance effective stress

Table 4. 10 ANOVA Test Results for effective stress of streamline die profile

Source	DF	Adj SS	Adj MS	F-Value	P-Value
Model	14	1667.26	119.09	23.04	0.000
Linear	4	1608.17	402.04	77.79	0.000
V	1	16.13	16.13	3.12	0.103
D	1	66.79	66.79	12.92	0.004
L	1	61.54	61.54	11.91	0.005
T	1	1463.71	1463.71	283.21	0.000
Square	4	23.54	5.88	1.14	0.385
V*V	1	12.80	12.80	2.48	0.142
D*D	1	4.61	4.61	0.89	0.364
L*L	1	0.09	0.09	0.02	0.895
T*T	1	10.82	10.82	2.09	0.174
2-Way Interaction	6	35.55	5.93	1.15	0.394
V*D	1	16.82	16.82	3.25	0.096
V*L	1	7.76	7.76	1.50	0.244
V*T	1	9.32	9.32	1.80	0.204
D*L	1	0.94	0.94	0.18	0.677
D*T	1	0.55	0.55	0.11	0.751
L*T	1	0.17	0.17	0.03	0.861
Error	12	62.02	5.17		
Lack-of-Fit	10	62.02	6.20	*	*
Pure Error	2	0.00	0.00		
Total	26	1729.28			

S	R-sq	R-sq(adj)	R-sq(pred)
2.27339	96.41%	92.23%	79.34%

Analysis of Variance (Z load)

Table 4. 11 ANOVA Test Results for Z-load of streamlined die profile

Source	DF	Adj SS	Adj MS	F-Value	P-Value
Model	14	12073566679	862397620	95.51	0.000
Linear	4	11929501976	2982375494	330.28	0.000
V	1	15349932	15349932	1.70	0.217
D	1	3605437334	3605437334	399.28	0.000
L	1	6547387550	6547387550	725.09	0.000
T	1	1761327160	1761327160	195.06	0.000
Square	4	16977953	4244488	0.47	0.757
V*V	1	1250011	1250011	0.14	0.716
D*D	1	9828300	9828300	1.09	0.317
L*L	1	12124320	12124320	1.34	0.269
T*T	1	1520120	1520120	0.17	0.689
2-Way Interaction	6	127086750	21181125	2.35	0.098
V*D	1	1580049	1580049	0.17	0.683
V*L	1	5527201	5527201	0.61	0.449
V*T	1	3810304	3810304	0.42	0.528
D*L	1	33843306	33843306	3.75	0.077
D*T	1	6561	6561	0.00	0.979
L*T	1	82319329	82319329	9.12	0.011
Error	12	108357011	9029751		
Lack-of-Fit	10	108357011	10835701	*	*
Pure Error	2	0	0		
Total	26	12181923691			

S	R-sq	R-sq(adj)	R-sq(pred)
3004.95	99.11%	98.07%	94.88%

Where SS = Sum of Squares, MS = Mean Squares, DF = Degree of Freedom, F = Fisher's ratio, and P = probability ratio.

4.2.2 Main Effect Plot of Output Responses

4.2.2.1 Effect of extrusion parameter on load

Effect die length on load

Of the few important state variables die length is the one that controls friction loss, formation of the dead metal zone, and flow characteristics. An optimum die length to reduce tool and production cost are necessary for minimizing the power consumption by internal shear deformation. Total Z-load for LC dies increases from 57524 N to 117549 N, for cosine die increases from 56102 N to 111507 N and for streamline die increases from 55724 N to 115588 N from this result we can conclude that as the die length increases, the force required to extrude the part increases. This result can be explained because as the length of the die increases, the contact area of the billet with the die increases too; as a consequence, this causes an increase in the energy consumption due to friction, total force required increases too. Figure 4.5 shows the load versus time graph of die length 10mm (A) and 30mm (B) at the constant parameter of ram speed 150mm/min, temperature 800°C, and product diameter of 10mm.

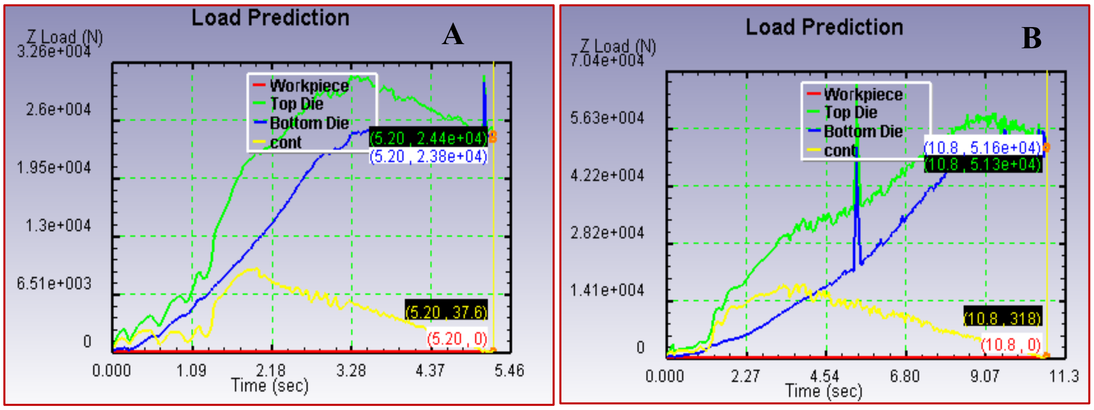

Figure 4. 5 loads versus time image of die length 10mm (A) and 30mm (B)

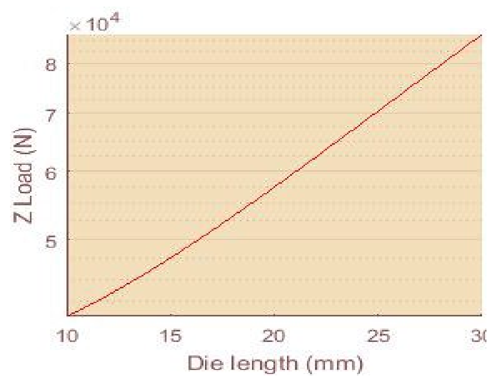

Figure 4. 6 Load versus die length graph

Effect of ram velocity on load

The ram speed is linked to the deformation speed that will be imposed on the part during the process and it is the factor that has the least relevance in the extrusion force. As ram speed decreases from 200 mm/min to 100 mm/min the total Zload also decreases from 48831 N to 46719 N for LC die profile, 47978 to 45642 for the cosine die profile, and 47421 to 47390 for the streamline die profile from this we can state that with the increasing speed of extrusion stem, required extrusion force increases. This is because the larger ram speed causes a higher strain rate and greater flow stress. Although the increased plastic deformation heat in the extrusion process will make the material soften, it could not compromise the flow stress increase. Therefore, the required extrusion force increases with the increasing ram speed. The variation of load with respect to time at different ram velocities is plotted in Figure 4.7 for cosine, LC, and streamline die, to examine the minimal effects on the process. As the ram speed raises extrusion load rises. Figure 4.7 shows the load versus time graph of ram speed 200mm/min (A) and 100mm/min (B) at the constant parameter of die length of 10mm, temperature 850°C, and product diameter of 10mm.

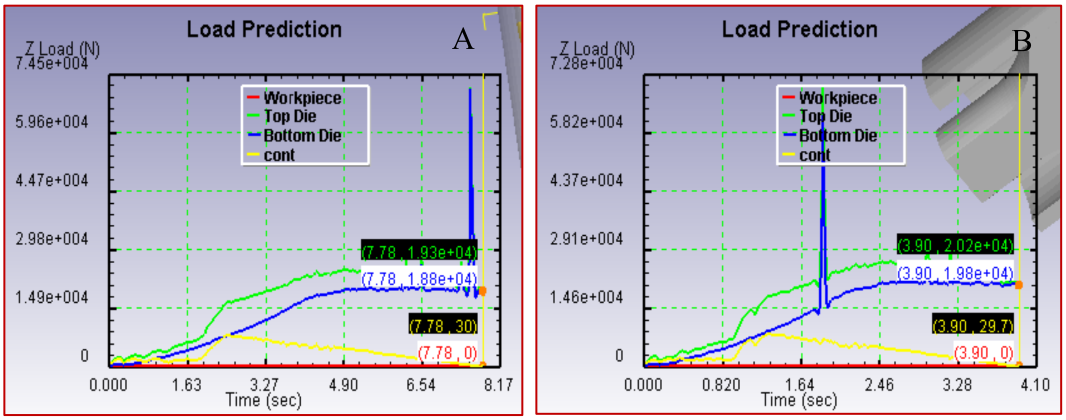

Figure 4. 7 Loads versus time graph of ram speed 200mm/min (A) and 100mm/min (B)

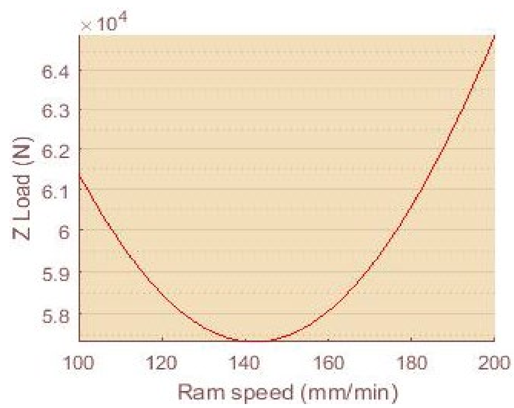

Figure 4. 8 Load versus Ram speed graph

Effect of product diameter on load

As product diameter increases from 7 mm to 13 mm, the total Zload decreases from 64404 N to 35259 N for LC die profile, 63835 N to 33914 N for the cosine die profile, and 64263 N to 34617 N for the streamline die profile. The influence of the product diameter is inversely proportional to the necessary extrusion force. As the diameter increases, the necessary force decreases. Product diameter plays a dominant role in the hot extrusion process. As the die surface area was large for a higher product diameter the friction rises at the consolidation of the billet die. Concurrently lesser product diameter creates more metal flow so more extrusion load was required. For a large volume of production in industries or for longer products, it is highly essential to improve lesser product diameter. Load gradually increases with an increase in reduction and then becomes steady. It is also clear that initially, the load is almost the same for all Reduction. Figure 4.9 shows the load versus time graph of product diameter 7mm (A) and 13mm (B) at a constant parameter of die length of 10mm, temperature 850°C, and ram speed of 150mm/min.

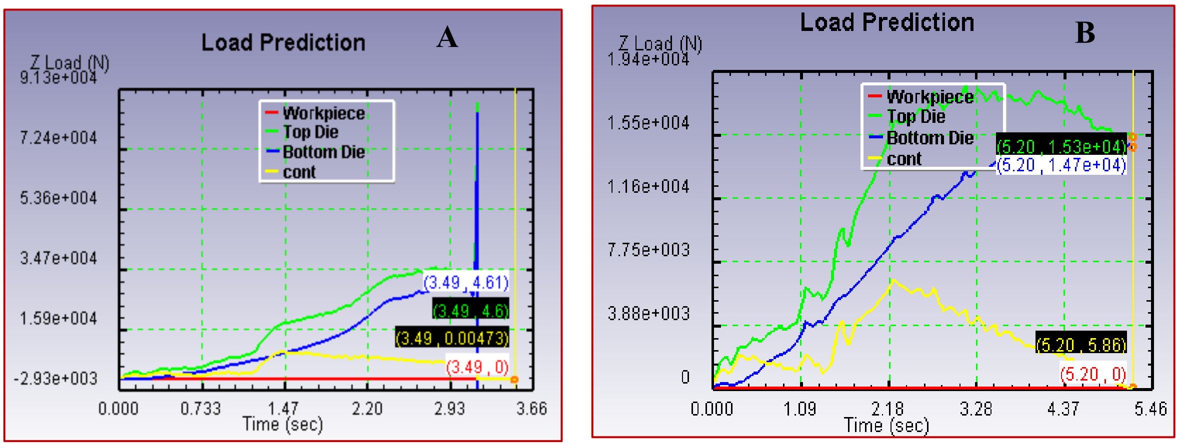

Figure 4. 9 Shows the load versus time graph of product diameters 7mm (A) and 13mm (B)

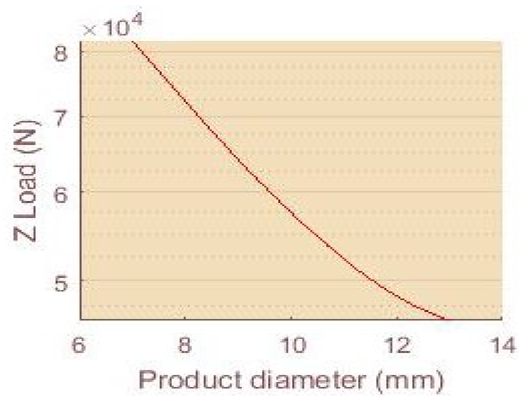

Figure 4. 10 Load versus product diameter graph

Effect of Temperature on load

At elevated temperatures, the molecular bonding between inter molecules becomes distorted thereby allowing faster deformation or higher strain gradient by consuming lesser extrusion force than at cold conditions. Product diameter increases from 800 °C to 900 °C the total Zload decreases from 81604 N to 56479 N for LC die profile, 81106 N to 55705 N for the cosine die profile, and 80747 N to 55735 N for the streamline die profile. Normally, as the temperature increases, the stress necessary to deform a part is lower in line with material flow stresses. This effect can be observed in Figure 4.11, an increase in temperature reduces the stress necessary to deform the billet and, thus, the extrusion force is lower. Because the temperature decreases the flow stress of metallic materials, and it is typically used to increase the formability of these materials. Temperature is the second parameter with the least influence on the extrusion force of the process. Figure 4.11 shows the load versus time graph of temperature 800°C (A) and 900°C (B) at a constant parameter of die length of 20mm, ram speed of 100mm/min, and product diameter of 10mm.

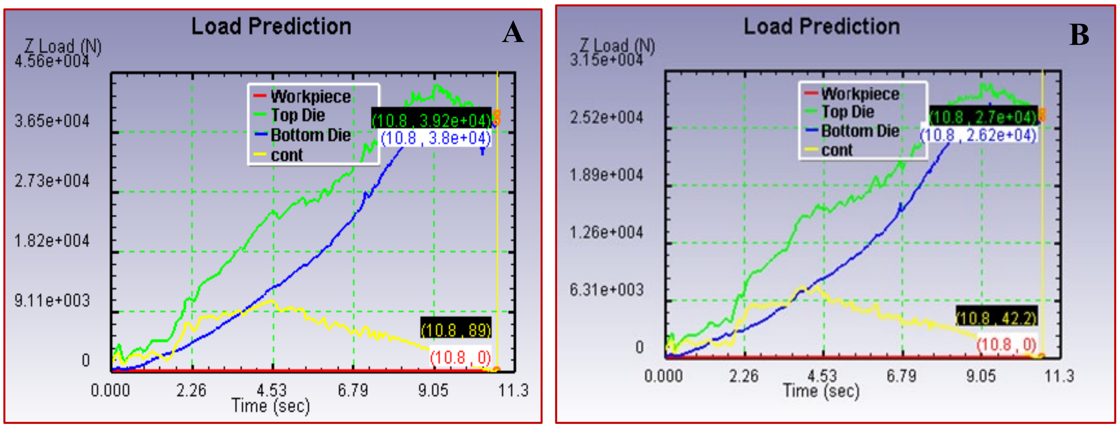

Figure 4. 11 Shows the load versus time graph of temperatures 800°C (A) and 900°C (B)

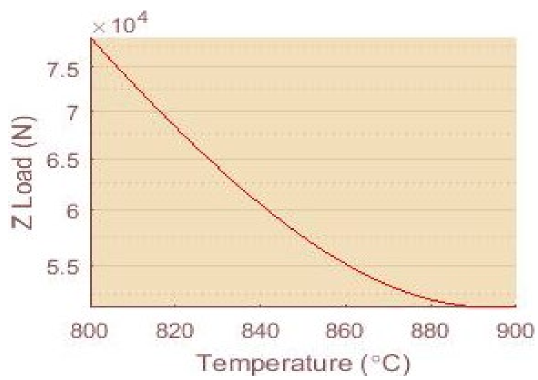

Figure 4. 12 Load versus temperature graph

Main plots are drawn for each output response, it is understood in the figure below that Force required for extrusion increases with the increase in ram speed, and die length whereas decreases with increasing product diameter and temperature.

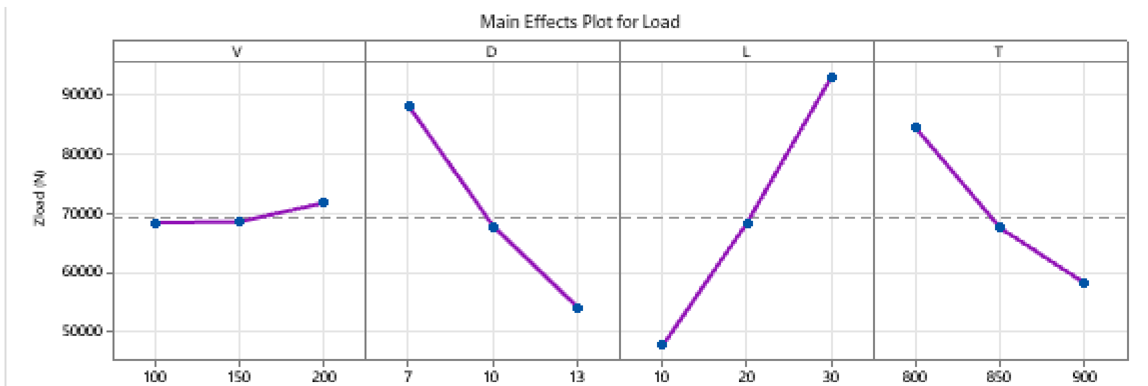

Figure 4. 13 Main plots are drawn for the Zload output response of cosine die

4.2.2.2 Effect of extrusion parameter on effective stress

Effect of die length on effective stress

Die length increases from 10 mm to 30 mm the total effective stress increases from 68.5435 MPa to 83.6493 MPa for LC die profile, 77.9047 MPa to 83.604 MPa for the cosine die profile, and 68.8133 MPa to 86.4174 MPa for streamline die profile. The increase in die length increases the effective stress. This results because it is associated with frictional work. The higher stress is observed for the maximum die length which depicts more energy consumption.

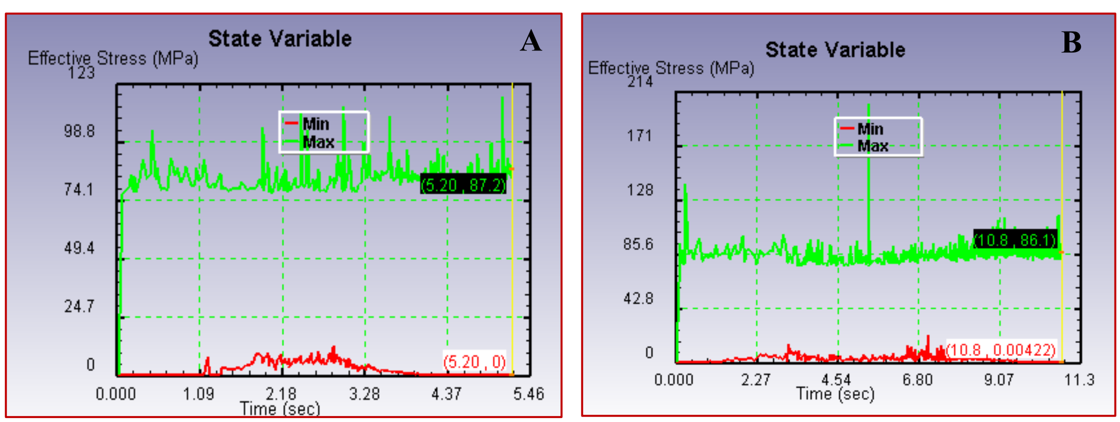

Figure 4. 14 Effective stress versus time graph of die length 10mm (A) and 30mm (B)

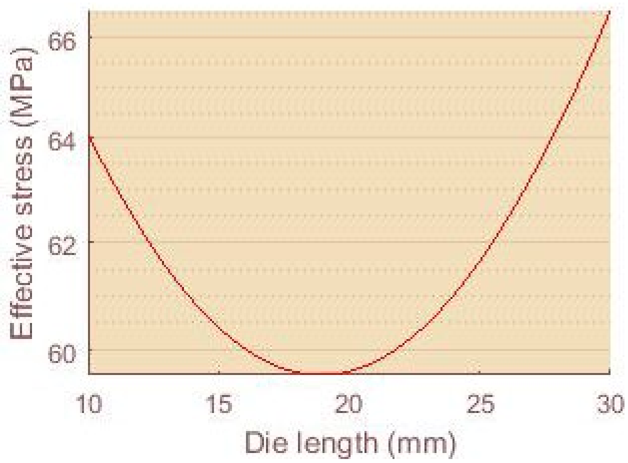

Figure 4. 15 Effective stress versus die length graph

Effect of ram speed on effective stress

Ram speed decreases from 200mm/min and 100mm/min the total effective stress decreases from 68.5435 MPa to 65.3779 MPa for LC die profile, 77.9047 MPa to 65.4525 MPa for the cosine die profile, and 68.8133 MPa to 66.8326 MPa for streamline die profile. Ram speed is another major contributing factor required to achieve a high production rate. High ram speed reduces the contact area leading to a reduction in friction between the die and the billet and ultimately reducing the temperature variation due to friction. Thus, the uniform temperature reduces the defects in the final product. Though the impact of ram speed influences the response, higher ram speed would impart a higher strain rate followed by higher flow stress which naturally increases the energy required to extrude. To study the effect of ram velocity on the process, the parameter was varied from 100m/min-200m/min by considering other parameters constant.

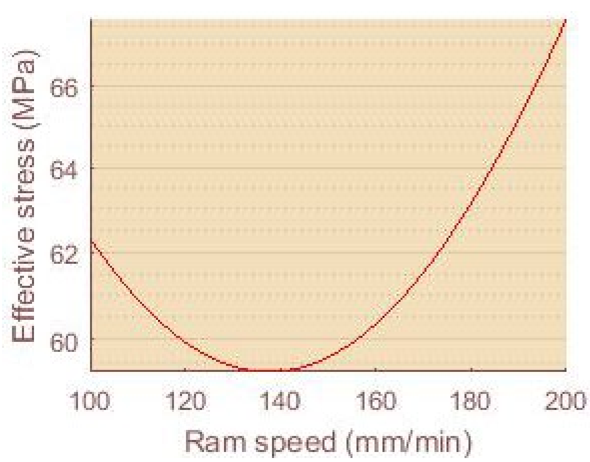

Figure 4. 16 Effective stress versus die length graph

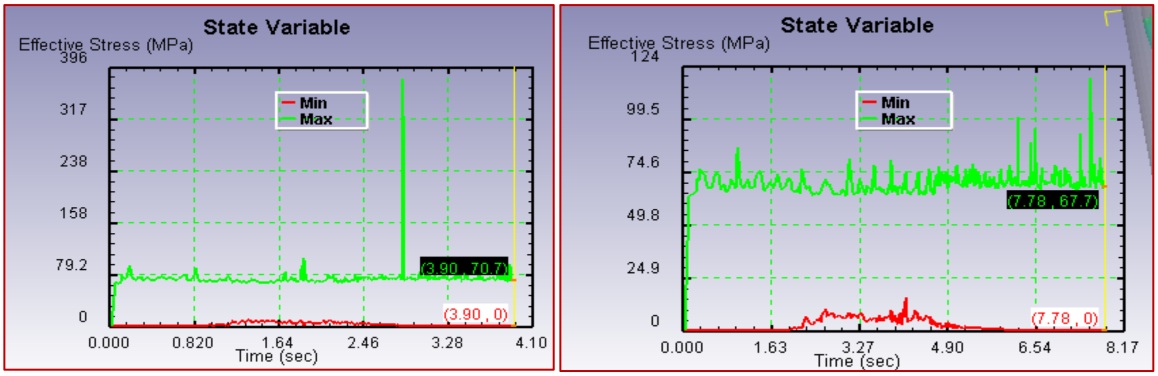

Figure 4. 17 effective stress versus time graph of ram speed 200mm/min (A) and 100mm/min (B)

Effect of product diameter on effective stress

Product diameter increases from 7 mm and 13 mm the total effective stress decreases from 70.2509 MPa to 67.1892 MPa for LC die profile, 68.8615 MPa to 67.6354 MPa for the cosine die profile, and 68.6396 MPa to 67.4006 MPa for streamline die profile. Lesser product diameter creates more metal flow so more maximum stress when deformation happens. For a large volume of production in industries or for longer products, it is highly essential to improve lesser product diameter. The effect of product diameter has the most significance on the power requirement, so the relation of maximum effective stress with product diameter has been investigated.

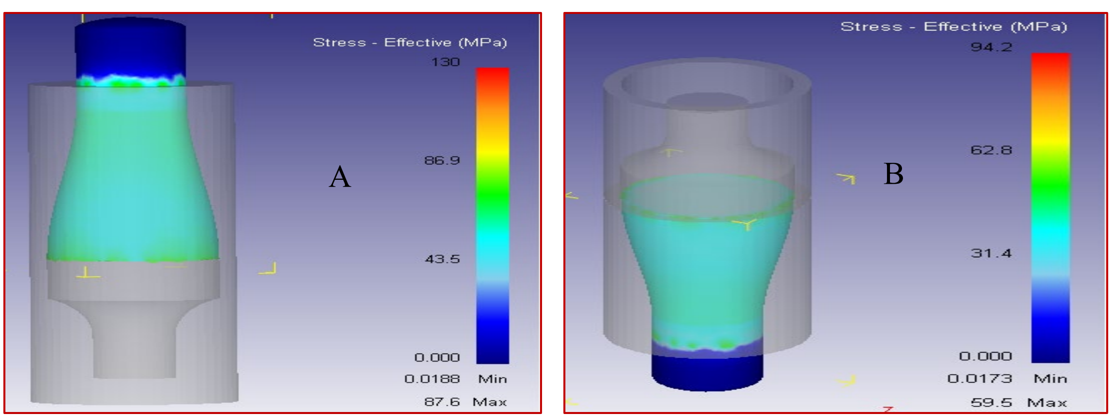

Figure 4. 18 shows the effective stress versus time graph of product diameters 7mm (A) and 13mm (B)

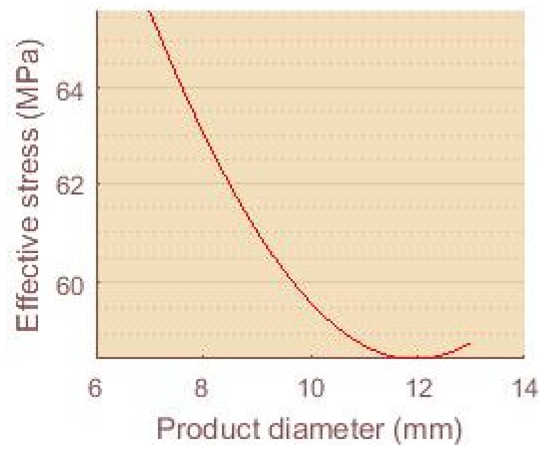

Figure 4. 19 Effective stress versus die length graph

Effect of temperature on effective stress

Temperature decreases from 900℃ and 800℃ the total effective stress increases from 57.7221 MPa to 80.4707 MPa for LC die profile, 57.638 MPa to 80.1709 MPa for the cosine die profile, and 58.0554 MPa to 81.0626 MPa for streamline die profile. The flow stress is reduced if the temperature is increased and deformation is, therefore, easier, but at the same time, the maximum extrusion speed is reduced because the localized temperature can lead to the incipient melting temperature. The increase in temperature reduces the stress necessary to deform the billet. Another important effect observed is that, as the temperature of the billet is increased, the maximum effective stress decreases. This will be of interest in the industrial application of extrusion processes because this has a direct influence on the quality of the extrudate.

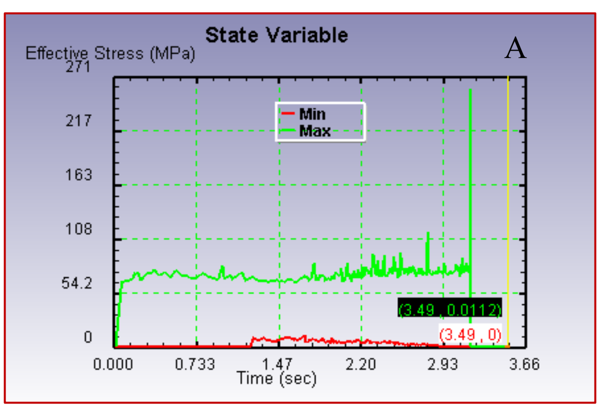

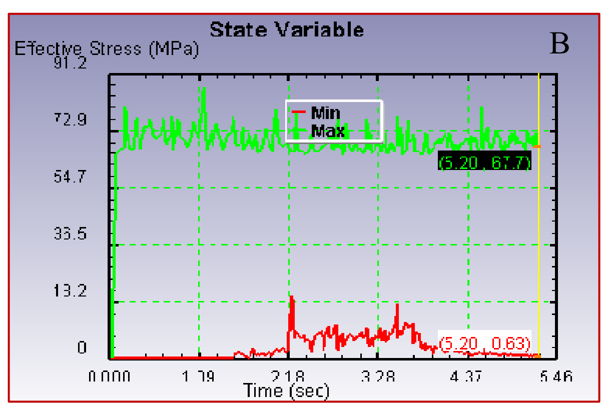

Figure 4. 20 shows the effective stress versus time graph of temperature 900℃ (A) and 800℃ (B)

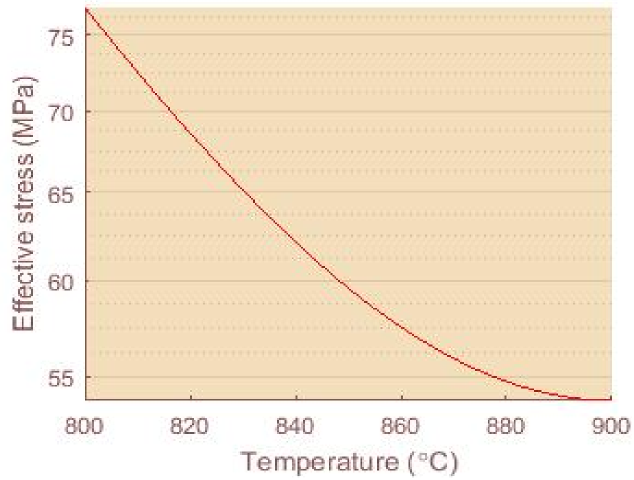

Figure 4. 21 Effective stress versus temperature graph

- Main plots are drawn for effective stress output response; it is understood in the figure below that effective stress increases with the increase in ram speed, and die length whereas decreases with increasing product diameter and temperature.

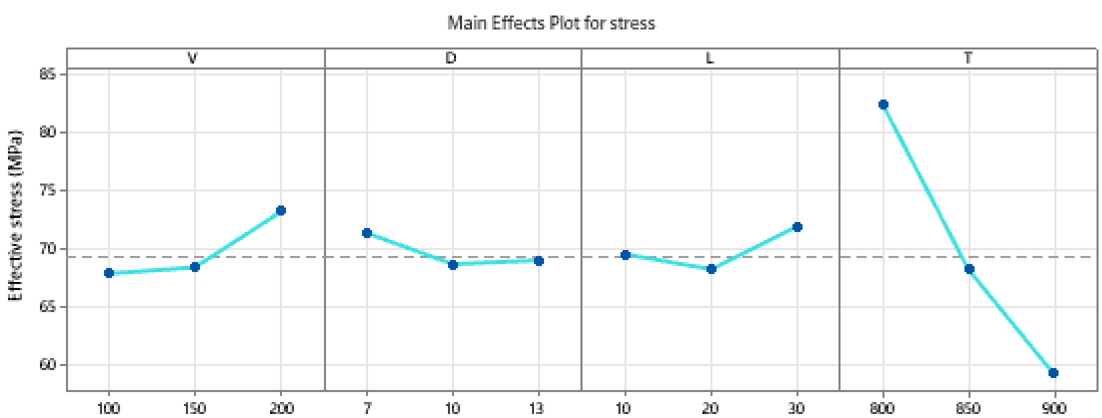

Figure 4. 22 Main plots drawn for effective stress

Effect of extrusion parameter on damage

There are other aspects concerning the quality of the final part obtained that can also be analyzed by Finite Element analysis. It is the case of the residual stresses and the damage induced in the workpiece as a consequence of the forming process. High values of damage could lead to fracture of the part during the component service, so the maximum damage such as chevron cracks can appear in extrusion under specific forming conditions) has been studied in all configurations. Damage is associated with stress states, mainly because of the hydrostatic stress as it's explained in the hydrostatic stress criterion (HSC) that says "whenever hydrostatic stress at a point on the Centre line in the deformation zone becomes zero and it is compressive elsewhere, there is a fracture initiation leading to central burst" Reddy et al., [1996].

Effect of product diameter on damage

The product diameter had a big influence on the damage factor. Product diameter decreases from 13 mm and 7 mm the total damage increases from 0.87631 to 0.97102 for LC die profile, 0.78987 to 0.97481 for the cosine die profile, and 0.7307 to 1.11732 for the streamline die profile. In general, increasing the product diameter decreased the damage. The reason behind this can be explained by the dead zone formation for low values of the product diameter. The reduction in thickness causes the billet to receive more damage during the process. In general, for low values of product diameter, the damage was highest. Figure 4.23 shows the damage versus time graph of product diameter 13 mm (A) and 7 mm (B) at a constant parameter of die length 10mm, temperature 850°C, and ram speed of 150mm/min.

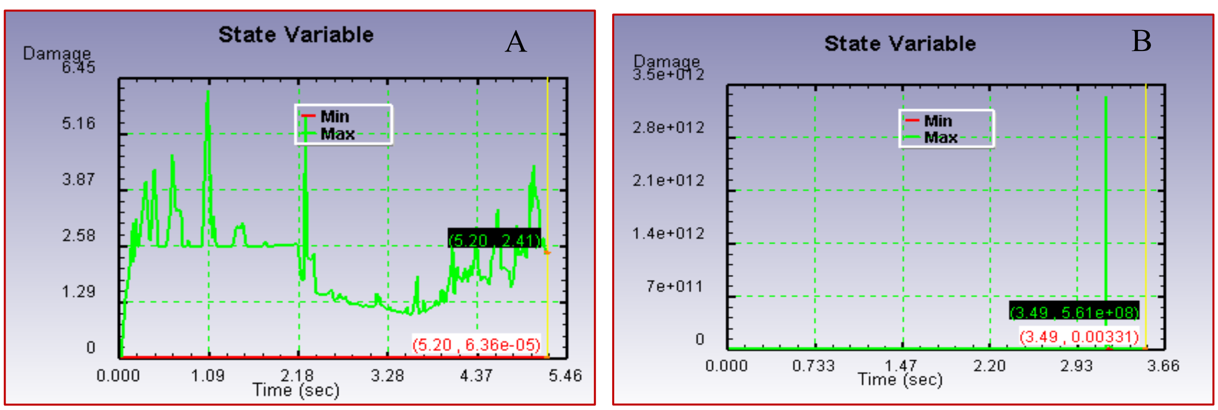

Figure 4. 23 shows the damage versus time graph of product diameters 13 mm (A) and 7 mm (B)

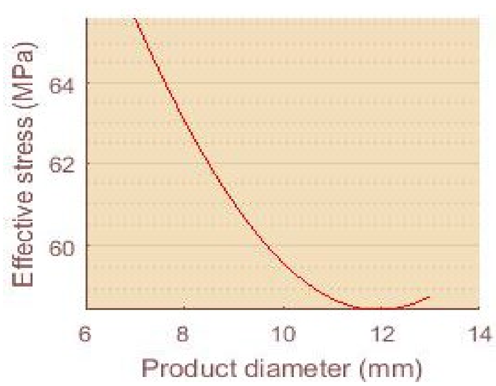

Figure 4. 24 Damage versus product diameter graph

Effect of temperature on damage

Temperature decreases from 900 °C and 800 °C the damage increases from 0.51599 to 1.582 for LC die profile, 0.48848 to 1.45491 for the cosine die profile, and 0.55407 to 1.67061 for the streamline die profile. This behavior is caused by the increase in temperature, as the damage factor is calculated by measuring stress and the stress decreased with the increase in the temperature according to the flow stress curves. Figure 4.25 shows the damage versus time graph of temperature 800°C (A) and 900°C (B) at a constant parameter of die length of 20mm, ram speed 100mm/min, and product diameter of 10mm.

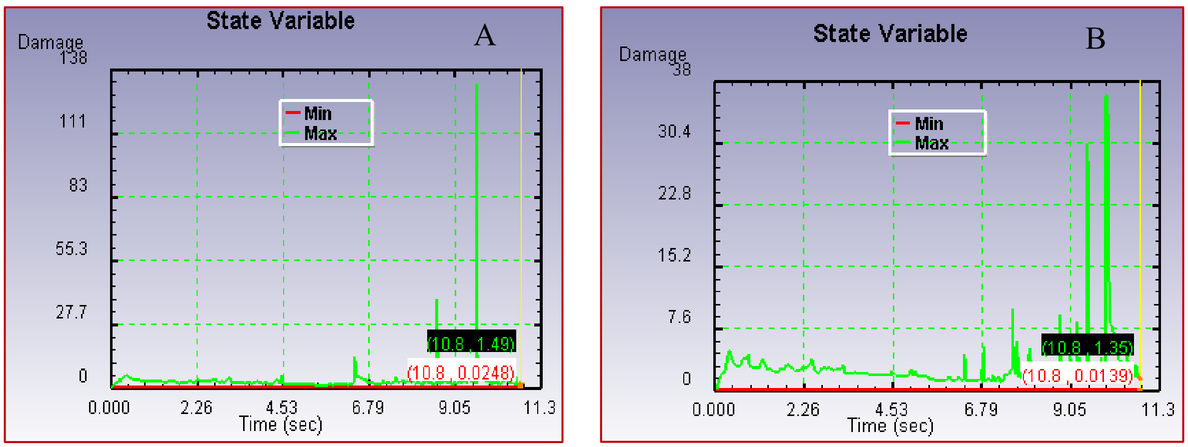

Figure 4. 25 shows that damage versus time graph of temperature 800°C (A) and 900°C (B)

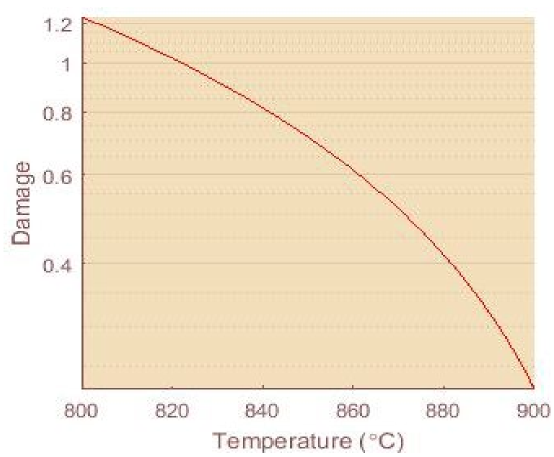

Figure 4. 26 Damage versus temperature graph

Effect of die length on damage

The Die length had an influence on the damage factor. Die length increases from 10 mm and 30 mm damage increases from 0.96805 to 1.97352 for LC die profile, 1.10632 to 1.97045 for the cosine die profile, and 1.01067 to 1.84442 for the streamline die profile. In general, increasing the Die length increased the damage. Because of friction Figure, 4.27 shows the damage versus time graph of die length 10mm (A) and 30mm (B) at the constant parameter of ram speed 150mm/min, temperature 800°C, and product diameter of 10mm.

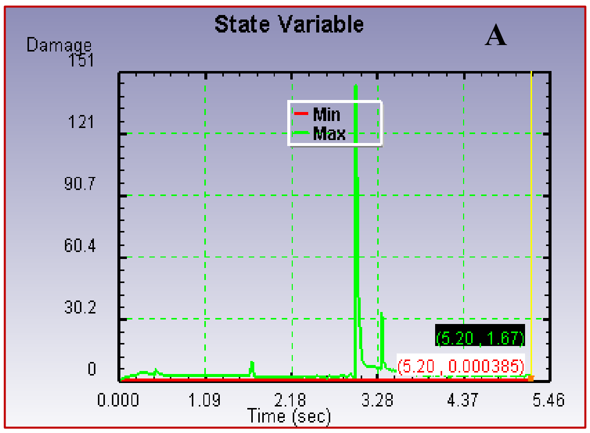

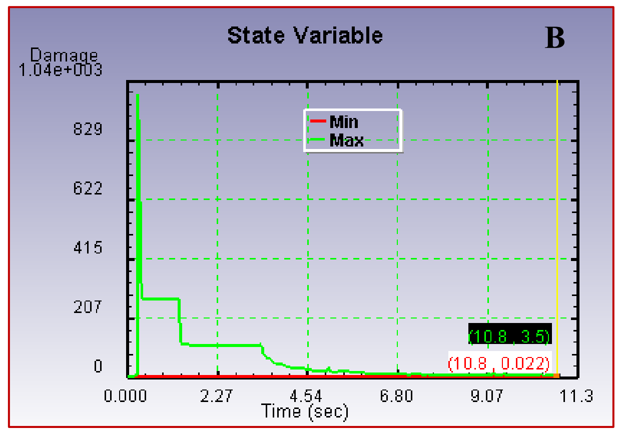

Figure 4. 27 shows the damage versus time graph of die lengths 10mm (A) and 30mm (B)

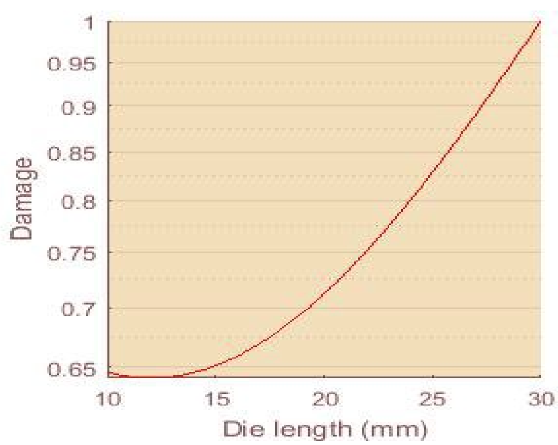

Figure 4. 28 Damage versus die length graph

Effect of ram speed on damage

In general, if a copper zirconium alloy is prone to excess speed, overheating of the exit temperature and other surface faults were observed also reduce the tool life. Damage values differ when we see the main effect plot lesser speed has less damage. Billet flow stress behavior at different average strain rates is used as simulation inputs for strain rate effect on die life. Ram speed increases from 100mm/min and 200mm/min damage increases from 0.83397 to 0.96805 for LC die profile, 1.00433 to 1.10632 for the cosine die profile, and 1.01067 to 1.06782 for the streamline die profile. Low ram speed increases the time of contact and thus leads to temperature variation along the cross-section of the extruded profile. Therefore, optimum ram speed is to be achieved. Increasing the ram speed increases strain rate which means flow stress increases which is having larger damage. Figure 4.29 shows the damage versus time graph of ram speed 200mm/min (A) and 100mm/min (B) at the constant parameter of die length 10mm, temperature 850°C, and product diameter of 10mm.

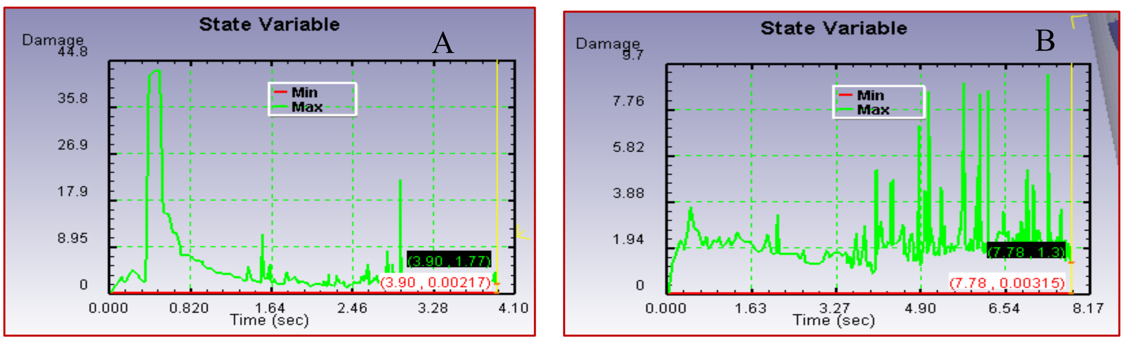

Figure 4. 29 shows the damage versus time graph of ram speed 200mm/min (A) and 100mm/min (B)

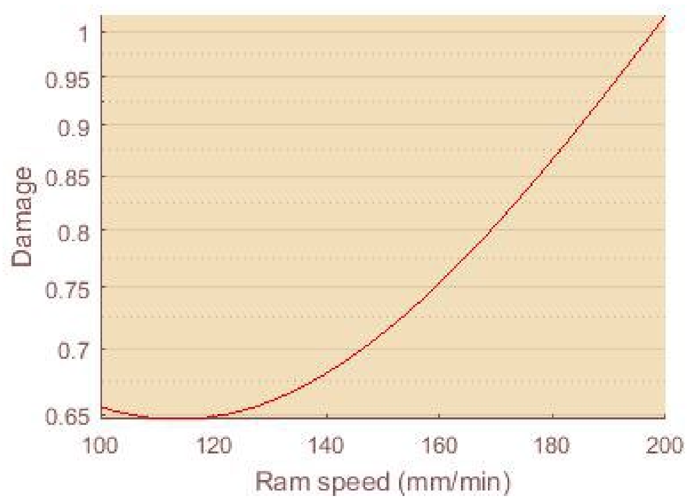

Figure 4. 30 Damage versus ram speed graph

Main plots are drawn for each output response, it is understood in the figure below that

- Damage increases with the increase in ram speed, and die length whereas decreases with increasing product diameter and temperature. And product diameter and temperature are the most affecting parameters.

Figure 4. 31 Main plots are drawn for damage output response for die profile

Surface Plots for Output Responses Surface

Surface Plots of load

From Figure 4.32 A, it is understood that extrusion force is minimum at a ram speed of 147.1mm/min and temperature of 895.9°C.

From Figure 4.32 B, it is understood that extrusion force is minimum at a die length of 10.7mm and temperature of 883.3°C.

From Figure 4.32 C, it is understood that extrusion force is minimum at a product diameter of 12.8mm and temperature of 897.8°C.

From Figure 4.32 D, it is understood that extrusion force is minimum at a die length of 10.7mm and product diameter of 12.9mm.

From Figure 4.32 E, it is understood that extrusion force is minimum at a ram speed of 145.4mm/min and product diameter of 12.8mm.

From Figure 4.32 F, it is understood that extrusion force is minimum at a die length of 10.4mm and ram speed of 147.5mm/min.

From Figure 4.32 A to F, it is clear that for minimum extrusion force the optimal input values, ram speed of 146.67mm/min, die length of 10.6mm, product diameter of 12.8mm, and temperature of 892.3°C.

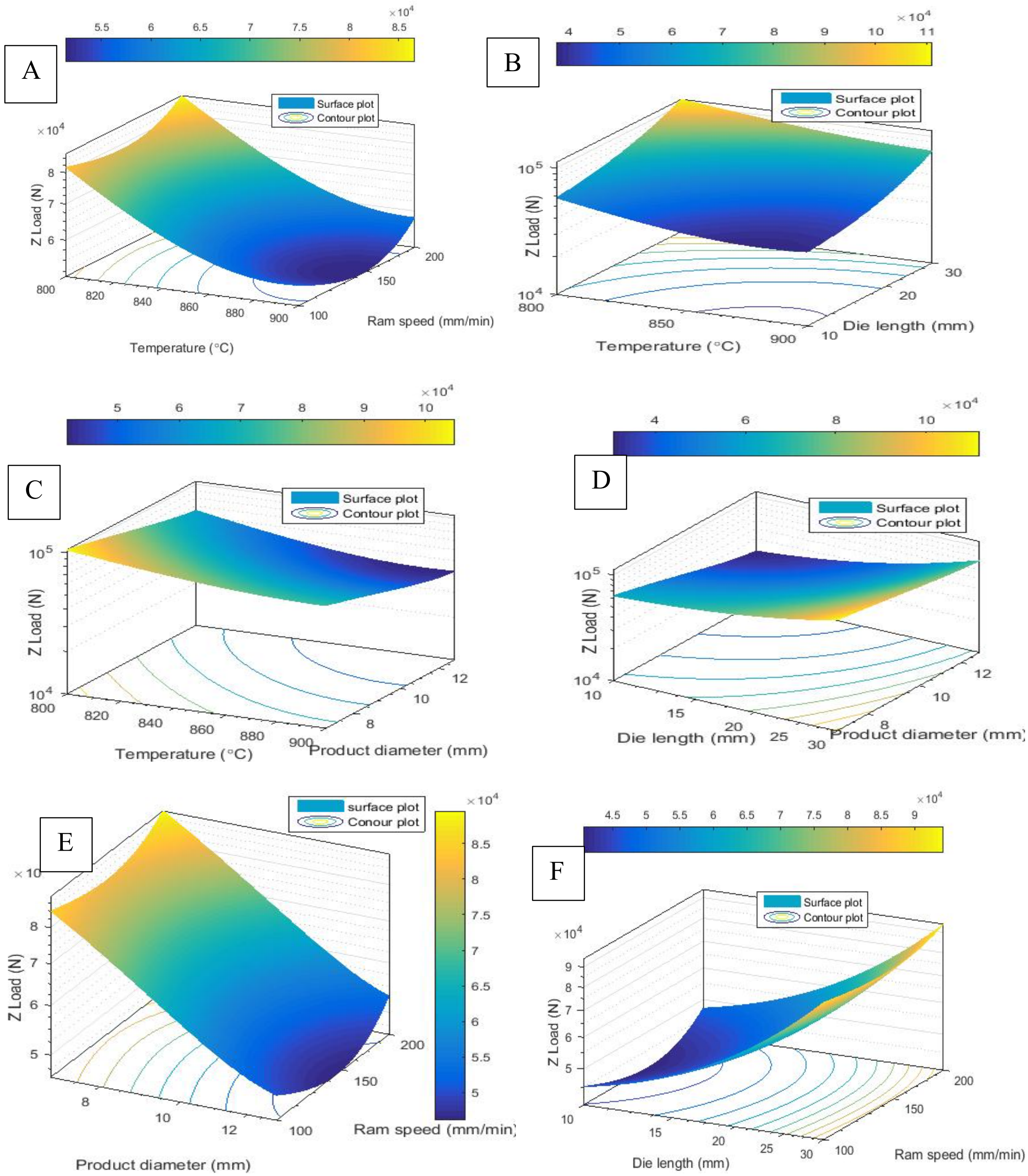

Figure 4. 32 Surface Plots of Zload for each interaction of parameter (A-F)

Surface Plots of effective stress distribution

From Figure 3.33 A, it is understood that effective stress distribution is minimum at a ram speed of 138.4mm/min and product diameter of 11.8mm.

From Figure 3.33 B, it is understood that effective stress distribution is minimum at a ram speed of 138.6mm/min and die length of 19.1mm.

From Figure 3.33 C, it is understood that effective stress distribution is minimum at a die length of 19.1mm and temperature of 898°C.

From Figure 3.33 D, it is understood that effective stress distribution is minimum at the temperature of 898.3°C and ram speed of 144.5mm/min.

From Figure 3.33 E, it is understood that effective stress distribution is minimum at a product diameter of 12.1mm and die length of 18.6mm.

From Figure 3.33 F, it is understood that effective stress distribution is minimum at product diameter of 13mm and temperature of 897.4°C.

From Figures 3.33 A to F, it is clear that for minimum effective stress distribution the optimal input values, temperature of 897.9°C, product diameter of 12.3mm, die length of 18.9mm and ram speed of 140.5mm/min.

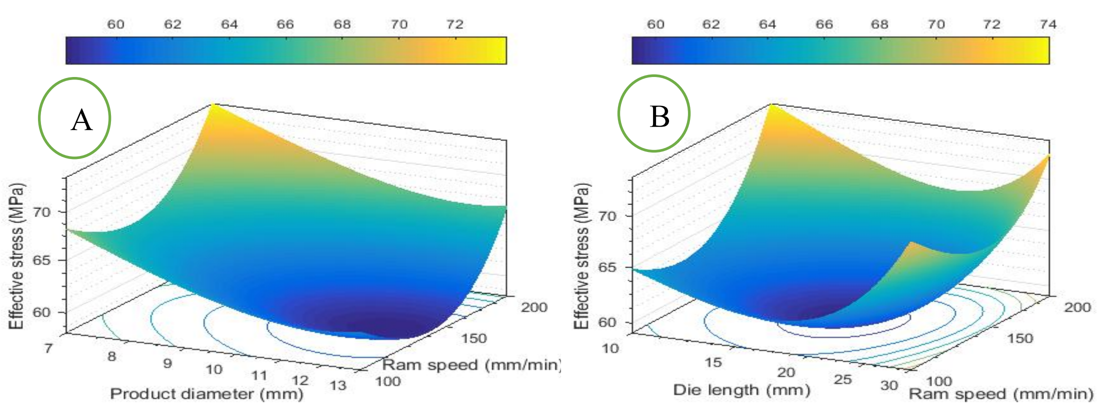

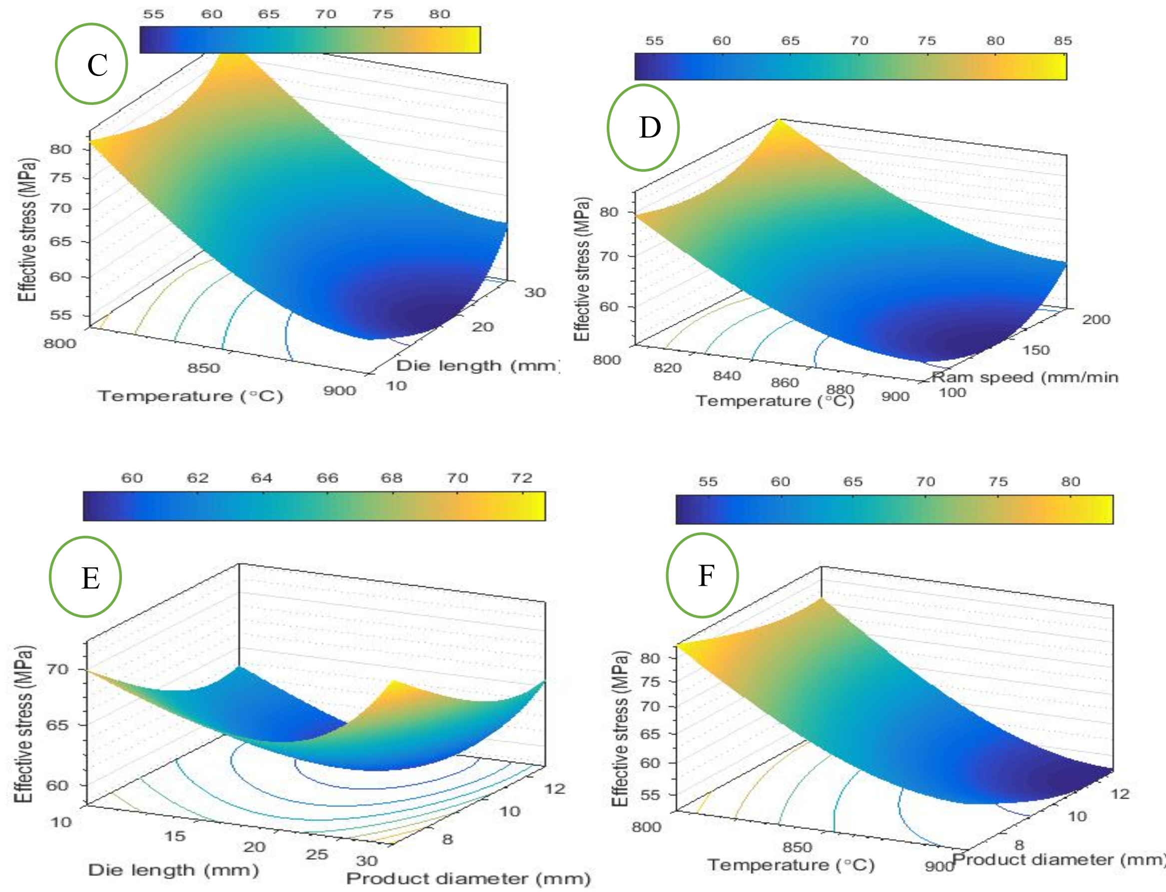

Figure 4. 33 Surface Plots of effective stress for each interaction of parameter (A-F)

Surface Plots of damage

From Figure 4.34A, it is understood that damage is minimum at a ram speed of 127.8 mm/min and a product diameter of 12.9mm.

From Figure 4.34B, it is understood that damage is minimum at a ram speed of 112.6 mm/min and temperature of 899.6°C.

From Figure 4.34C, it is understood that damage is minimum at a temperature of 896.7°C and a die length of 16.5mm.

From Figure 4.34D, it is understood that damage is minimum at a die length of 13.9mm and ram speed of 136.7 mm/min.

From Figure 4.34E, it is understood that damage is minimum at a product diameter of 12.6mm and a temperature of 900°C.

From Figure 4.34F, it is understood that damage is minimum at a product diameter of 12.9mm and die length of 12.2mm.

From Figures. 4.34A to F, it is clear that From Figure 14c, it is understood that minimum damage to the optimal input values, die length of 14.2mm, the temperature of 898.7°C, ram speed of 125.7 mm/min, and product diameter of 12.6mm.

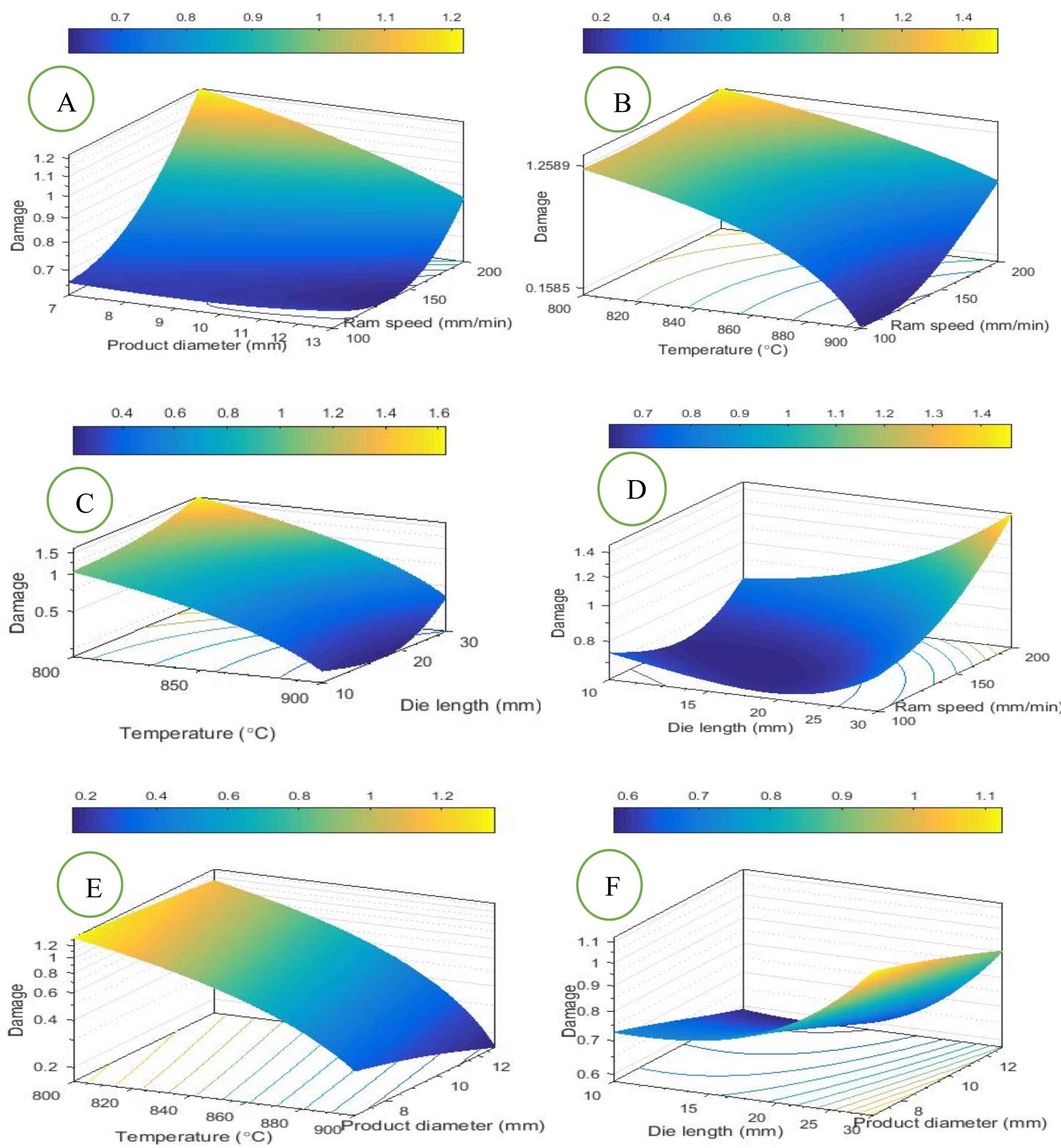

Figure 4. 34 Surface Plots of damage for each interaction of parameter (A-F)

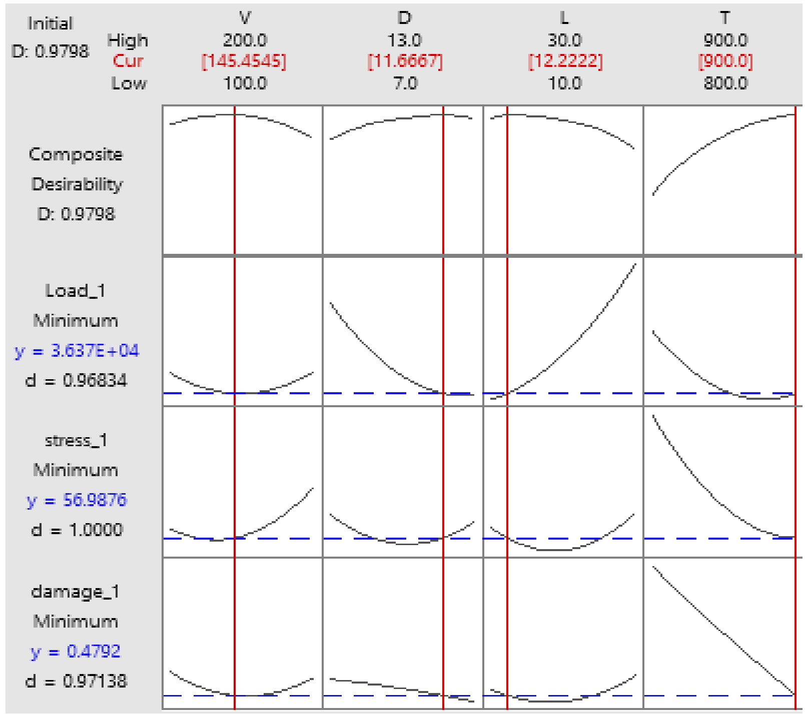

Figure 4. 35 Response Surface Optimizer Figure Cosine profile of die

From Figure 4.35, it is understood that the optimal input parameters combination of Product diameter 12 mm, die length 12 mm, Ram speed 145 mm/minute, Temperature 900°C the output responses obtained are Force required 36370 N, Effective stress 56.98 MPa, and Damage 0.4792.

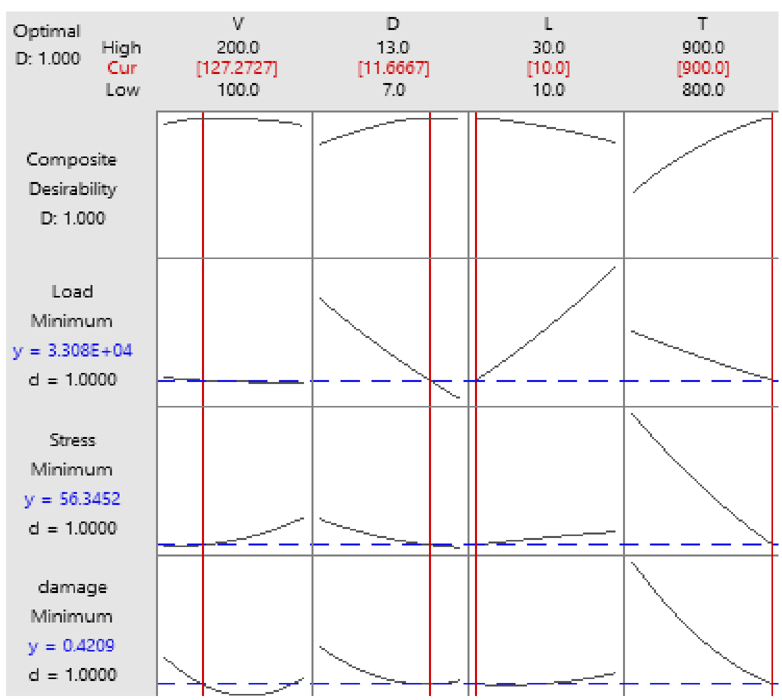

Figure 4. 36 Response Surface Optimizer Figure Streamline profile of die

From Figure 4.36, it is understood that the optimal input parameters combination of Product diameter 12 mm, die length 10 mm, Ram speed 127 mm/minute, Temperature 900°C the output responses obtained are Force required 33080 N, Effective stress 56.34 MPa and Damage 0.4209.

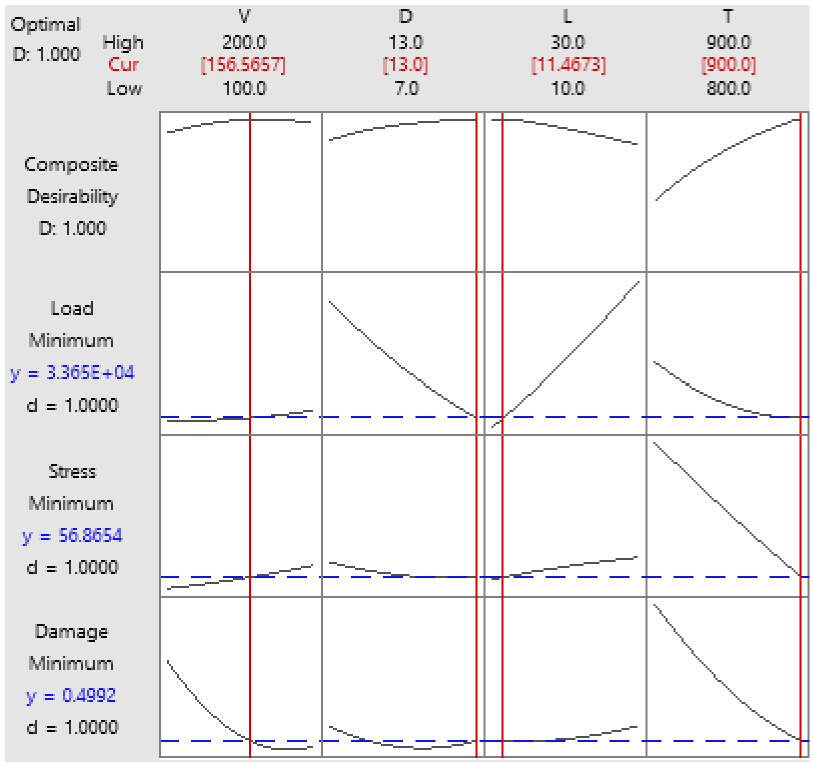

Figure 4. 37 Response Surface Optimizer Figure LC profile of die

From Figure 4.37, it is understood that the optimal input parameters combination of Product diameter 13 mm, die length 11 mm, Ram speed 156 mm/minute, Temperature 900°C the output responses obtained are Force required 33650 N, Effective stress 56.86 MPa, and Damage 0.499.

The same parameter effect was obtained from different papers such as: -

Venkatesh & Venkatesan, [2015]b; Workie & Tesfaye, [2021] L9 OA were selected using Taguchi's method of experimental design for three process parameters like ram speed, initial billet temperature, and friction between the die billet region with three levels as low, medium, and high, respectively. At elevated temperatures, the molecular bonding between inter molecules becomes distorted thereby allowing faster deformation or higher strain gradient by consuming lesser extrusion force than at cold conditions.

And higher ram speed would impart a higher strain rate followed by higher flow stress which naturally increases the load required to extrude.

H. Huang et al., [2021] show the most relevant manufacturing parameter to reduce the damage factor in the billet is the die semi-angle (in this case product diameter) as well as to obtain minimum values for the extrusion force which are very useful to reduce the power requirement of the machinery to invest in.

In general, the results obtained in this paper are consistent with experimental findings and previous numerical studies reported in the literature above.

4.3 Experimental investigation

To study the changes in microstructural properties copper zirconium round bar of 16mm diameter was extruded to a cosine and linear converging profile using the optimized parameter. For experimentation, the tooling setup is manufactured indigenously. For sample preparation, two experimental runs from simulation and RSM results have been selected. i.e., the list optimum combination for the LC die is a ram speed of 153mm/min, product diameter of 14mm, die length of 13mm, and preheating temperature of 900℃ and cosine die is ram speed of 132mm/min, product diameter of 12mm, die length of 10mm and preheating temperature of 900℃. After the arrangement of extrusion components in a 150-ton hydraulic press the sample preparation is performed. And during sample preparation, the ram speed was fixed to a constant level of 2.5mm/s.

The setup and materials are designed and decided for the hot extrusion process. The solid models are designed and generated with the help of SolidWorks® software and the components are manufactured by following the desired procedures.

The billet length was maintained at 30 mm to avoid unnecessary frictional work caused between container billet interfaces. The diameter of the billet is maintained a bit smaller than the internal diameter of the container by considering the thermal expansion into account. The lower jaw of the hydraulic press is stable and the upper jaw is provided a constant ram velocity. The experimental setup utilized for this investigation as shown in Figure 3.10 is the assembly of a punch, dummy block, container, die, and holder. The detailed list of the components is presented in Table 4.12.

Table 4.12 The detailed list of the components

S. №	Name of the part	Material	Remark	Manufacturing process
1	Holder	H13		Turning, drilling, polishing
2	Ram	H13		Turning, tapping, polishing
3	Container	H13		Turning, drilling, polishing
4	Die	H13		CNC milling, drilling, polishing
5	Dummy block	H13		Turning and polishing

4.3.1. Microstructure observation

The optical pictures of the microstructures of commercially available LC and cosine samples following chemical etching are shown in Figure. Furthermore, no copper-zirconium intermetallic complex particles are visible under optical after or before extrusion, which may be attributed to the tiny size of these particles. Figure 4.38 shows optical pictures of the microstructures of commercially available, LC, and cosine samples. When comparing commercial and LC samples, it can be noticed that the microstructures are markedly different, indicating that the microstructure of cosine has a tiny grain size. The commercial sample has a considerable quantity of elongated grains. Furthermore, the grain size is not consistent, particularly in commercial samples.

Figure 4.38 (a), (b), and (c) illustrate the microstructure of raw material 16 mm in diameter and deformed with LC and cosine die profile specimens 10 mm in diameter. As shown in figure 4.38 (a), the surface of a raw material with a diameter of 16 mm is heavily corroded as a result of the etching chemical (HNO3) used during the etching process.

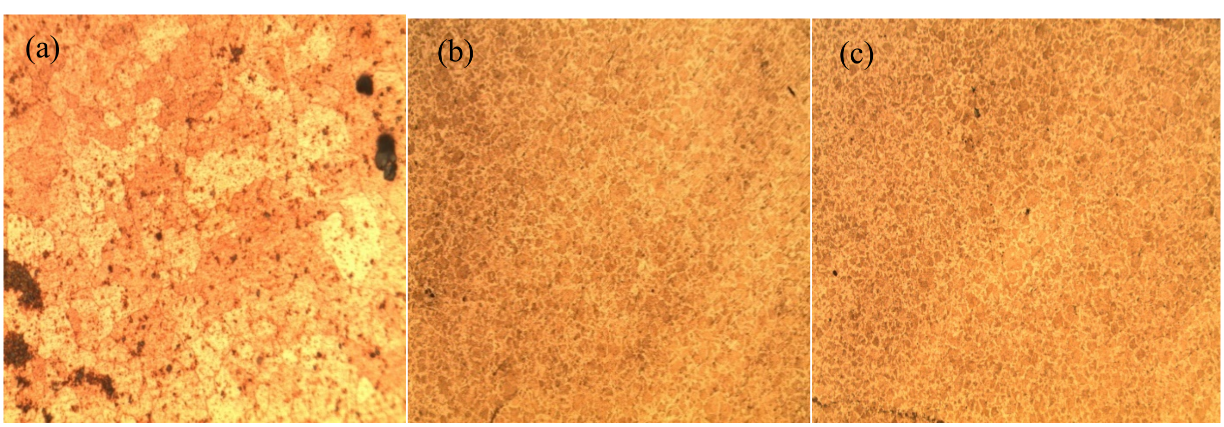

Figure 4. 38 Microstructural analyses of C15000 material; a) 16 mm diameter (raw material), and 13mm diameter deformed product of b) LC and c) cosine die profile

Figure 4.39 depicts that the grains are extremely small after deformation.

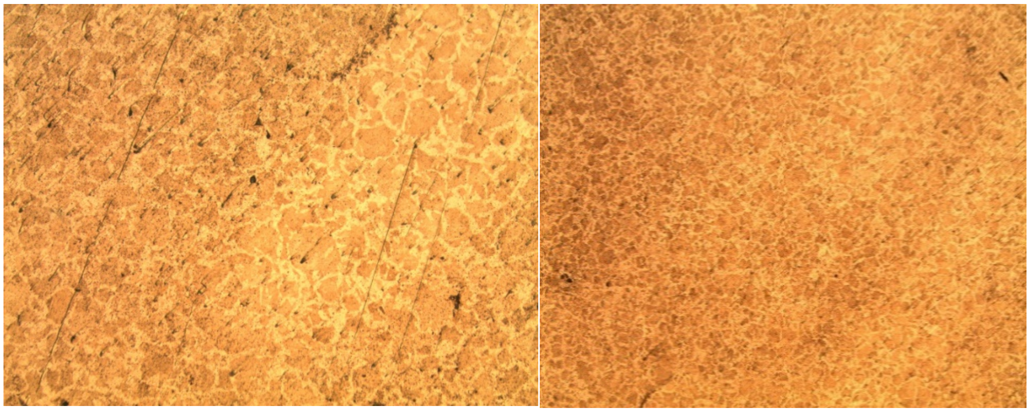

Figure 4. 39 Microstructural analysis of C15000 deformed specimens a) 16mm diameter of commercial raw material and b) 13mm diameter of deformed specimens

When the microstructures of commercial raw material 16 mm and 13mm of deformed product for LC and cosine die are compared to the microstructures of 16 mm raw material, the microstructures of the extruded products are refined and evenly distributed in the deformed products, which are beneficial for improving the product's Hardness and compressive strength. Furthermore, a tendency toward a more homogenous microstructure was seen when the cosine die profile was extruded.

4.3.2. Mechanical testing

4.3.2.1. Hardness test

At room temperature, a hardness test was performed to determine the resistance of C15000 commercial tempers material in the form of 16-mm rods extruded from it using various die profiles at 900°C.

Vickers hardness tests are performed using a diamond indenter (Wilson 401MVA) in the shape of right pyramids with a square base and an angle of 136 degrees between opposing sides exposed to a force of 10kgf and the whole load is applied for an average period of 10 to 15 seconds. As shown in table 4.13, the surface hardness of commercialized Cu-Zr and deformed Cu-Zr materials in both linear convergent and cosine die profiles were investigated three times, and average Vickers Hardness values were collected to explain the changes that were created after the operations.

Table 4.13 surface hardness of commercially Cu-Zr and deformed product of Cu-Zr materials in both linear convergent and cosine die profile

Hardness Test Results					
Material types	Material	Test 1	Test 2	Test 3	Average
Prepared specimens (Deformed products)	Commercially	139.8	132.4	129.6	133.9VH10
	LC	158.6	161.5	164.6	161.6VH10
	Cosine die	153.7	158.6	176.2	162.8VH10

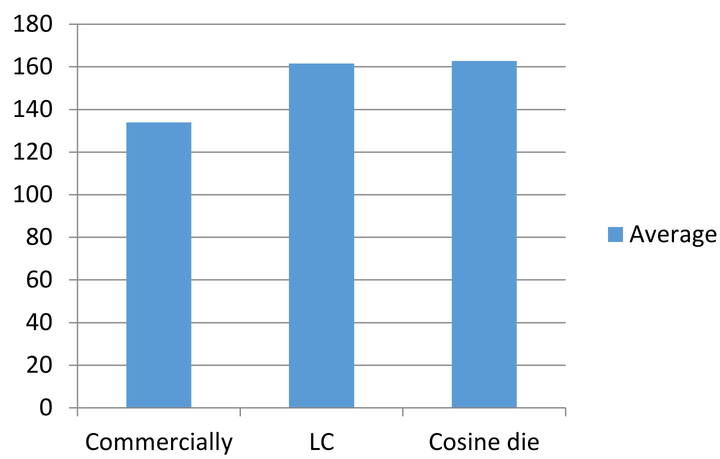

Figure 4.40 The graphical illustration of Vickers hardness test results of raw material and deformed products

As illustrated in figure 4.40, the Vickers hardness test result demonstrates that the deformed product has a higher hardness value and cosine die has the highest hardness test result, and the surface hardness of the deformed product has been increased when compared to commercially available material and when the hardness improvement was shown in the figure above. The commercially accessible specimen has a hardness of 133.9HV. As the specimen is extruded in linear convergent and cosine die profiles, the hardness increases to 161.6HV and 162.8HV, respectively, and the grain refinement and dislocation strengthening are produced.

4.3.2.1. Compressive test

After a compressive test at room temperature, the compression stress-strain curves of cosine and linear convergent die extruded and commercially available Cu-Zr alloy are presented.

The linear convergent die extruded sample has somewhat lower compression strength than the cosine dies extruded sample but a lot greater compression strength than the commercially available sample. Furthermore, the cosine dies profile has higher stress than the linear convergent die. It should be observed that fracture failure does not occur during compression because of the excellent ductility, even when the strain approaches 30%, demonstrating that both commercially and extruded Cu-Zr alloys have acceptable properties and good processability. After compression stress-strain curves of cosine and linear convergent die extruded and commercially available Cu-Zr alloy are shown.

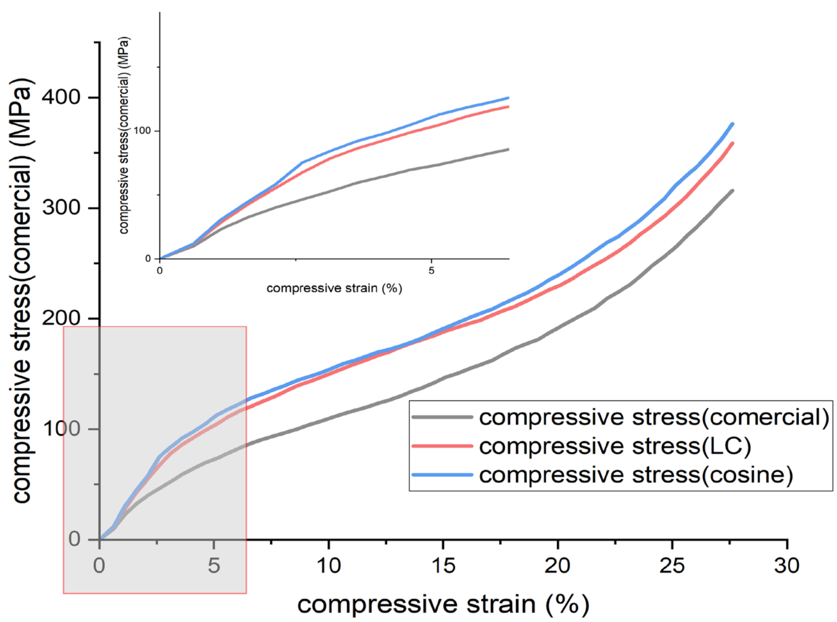

Figure 4. 41 shows three deformed cross-sections of Cu-Zr alloy under different die profiles and before and after the extrusion process

CONCLUSIONS AND RECOMMENDATIONS

5.1. Conclusions

This study analyzes the deformation behavior during multi-profile die extrusion for copper zirconium alloy through different process parameters. The effect of process parameters on damage, extrusion load, and effective stress was accomplished by using DEFORMTM-3D simulation software basis on FEM. Response surface methodology (a multi-response optimization) was employed for the optimization of process parameters for damage, extrusion load, and Effective stress. DEFORMTM-3D was known to be an effective tool for studying the consequences of design and the Design of Experiments is adopted and the Response Surface Method is used in designing the experiments. 27 experiments are performed using box-Behnken design and process parameters for variant responses can be efficiently recognized. The experimental investigation of the optimum parameter was also performed in this study and the conclusions are presented as follows.

- The force required for extrusion increases with the increase in ram speed, and die length whereas decreases with increasing product diameter and temperature.
- Effective stress increases with the increase in ram speed, and die length whereas decreases with increasing product diameter and temperature.
- Damage increases with the increase in ram speed, and die length whereas decreases with increasing product diameter and temperature.
- The optimum process parameters obtained by the method of RSM optimize extrusion load, effective stress, and damage simultaneously for all three profiles of die extrusion. And was found the redundant work is less so comparatively less energy consumption and product defects in the process in the case of extrusion through cosine profiled die.
- From the ANOVA results, the billet temperature is the most important contributing factor, followed by ram speed, die length, and product diameter, and finally the interaction effect of ram speed and product diameter in damage.
- The billet temperature creates the prime impact on the total sum of squares followed by the square of billet temperature, die length, ram speed, product diameter, and finally ram speed in effective stress.

- The die length creates the prime impact on the total sum of squares followed by product diameter, billet temperature, and finally square of billet temperature and square product diameter. Therefore, for product quality enhancement and capability of product efficiency the geometrical layout of holes during profile die extrusion should be selected carefully.
- For the cosine die profile it is understood that the optimal input parameters combination of Product diameter 13.1mm, die length 10mm, Ram speed 117.2mm/minute, Temperature 900℃ the output responses obtained are Force required 31370 N, Effective stress 55.7MPa, and Damage 0.425.
- For streamline die profile the optimal input parameters combination of Product diameter 14.6mm, die length 13.2mm, Ram speed 153.53mm/minute, Temperature 900℃ the output responses obtained are Force required 33860 N, Effective stress 55.7MPa and Damage 0.4435.
- For linear convergent die profile, the optimal input parameters combination of Product diameter 12.18mm, die length 10.2mm, Ram speed 132.3mm/minute, Temperature 900℃ the output responses obtained are Force required 34940 N, Effective stress 55.2MPa, and Damage 0.498.
- The linear convergent die extruded sample has somewhat lower compression strength than the cosine dies extruded sample but a lot greater compression strength than the commercially available sample.
- The Vickers hardness test result demonstrates that the deformed product has a higher hardness value and cosine die has the highest hardness test result, and the surface hardness of the deformed product has been increased when compared to commercially available material.
- When the microstructures of commercial raw material 16 mm and 13mm of deformed product for LC and cosine die are compared to the microstructures of 16 mm raw material, the microstructures of the extruded products are refined and evenly distributed in the deformed products.

The optimum process enhancement for this study has been observed through the multi-profile die extrusion process. Therefore, manufacturing firms or any industries that intend to work in the extrusion of copper material will enhance their productivity and product quality by using the multi-profile die extrusion process.

5.2. Recommendations

Copper alloy extrusion products have many interesting areas where electrical and optical applications are used. copper zirconium alloy material is one of the engineering materials used for electrical uses. The result of this study stated that the extrusion process parameters trough multi-profile die has a significant influence on the quality and productivity of extrusion products.

Some of the future scopes and suggestions are;

- In this thesis, the analysis was performed for the simple bar extrusion. For similar investigations, the complex shapes can be focused.
- The die profile design for the simple bar extrusion process was successful. The design methodology can be extended for the complex shape extrusion.
- Finite element analysis was performed to investigate the effect of various state variables, but the analysis can be increased to the microstructural changes due to the variables.
- For improving the product quality, different kinds of twist extrusions can be performed to have a significant change in the microstructural level.
- Multi-profile die extrusion process for different copper alloy materials can be conducted.

6. REFERENCE

Ab Rahim, S. N., Lajis, M. A., & Ariffin, S. (2016). Effect of extrusion speed and temperature on hot extrusion process of 6061 aluminum alloy chip. ARPN Journal of Engineering and Applied Sciences, *11*(4), 2272–2277.

Avitzur, B., Narayan, C., & Chou, Y. T. (1982). Upper-bound solutions for flow through conical converging dies. International Journal of Machine Tool Design and Research, *22*(3), 197–214. 10.1016/0020-7357(82)90026-9

AZO materials (September 13, 2012) Zirconium Copper UNS C15000 website; https://www.azom.com/article.aspx?ArticleID=6324

AZO materials (September 13, 2012) H13 Tool Steel - Chromium Hot-Work Steels website; https://www.azom.com/article.aspx?ArticleID=6324

Banerjee, M., Verma, T. N., & Nashine, P. (2018). Experimental and numerical analysis of extrusion process for AA 7178 alloy with varying process parameters. Materials Today: Proceedings, *5*(2), 6839–6847. 10.1016/j.matpr.2017.11.344

Becker, F. G., Cleary, M., Team, R. M., Holtermann, H., The, D., Agenda, N., Science, P., Sk, S. K., Hinnebusch, R., Hinnebusch A, R., Rabinovich, I., Olmert, Y., Uld, D. Q. G. L. Q., Ri, W. K. H. U., Lq, V., Frxqwu, W. K. H., Zklfk, E., Edvhg, L. V, Wkh, R. Q Title. *In Syria Studies* (Vol. 7, Issue 1).

Bhavani, B. (2019). Optimization of Die Extrusion Parameters By Using Fem. 9(6), 1705–1717.

Buschhausen, A., Weinmann, K., Lee, J. Y., & Altan, T. (1992). Evaluation of lubrication and friction in cold forging using a double backward-extrusion process. Journal of Materials Processing Tech., *33*(1–2), 95–108. 10.1016/0924-0136(92)90313-H

Canadinc, D., Niendorf, T., & Maier, H. J. (2011). A comprehensive evaluation of parameters governing the cyclic stability of ultrafine-grained FCC alloys. Materials Science and Engineering A, *528*(21), 6345–6355. 10.1016/j.msea.2011.04.051

Chen, C. T., & Ling, F. F. (1968). Upper bound axisymmetric extrusion problems. *10*, 863–879.

Chen, D. C., Syu, S. K., Wu, C. H., & Lin, S. K. (2007). Investigation into cold extrusion of aluminum billets using the three-dimensional finite element method. Journal of Materials Processing Technology, *192–193*, 188–193. 10.1016/j.jmatprotec.2007.04.067

Chen, F. K., Chuang, W. C., & Torng, S. (2008). Finite element analysis of multi-hole extrusion of aluminum-alloy tubes. Journal of Materials Processing Technology, *201*(1–3), 150–155. 10.1016/j.jmatprotec.2007.11.292

Chen, L., Zhao, G., Yu, J., & Zhang, W. (2015). Constitutive analysis of homogenized 7005 aluminum alloy at evaluated temperature for the extrusion process. Materials and Design, *66*(PA), 129–136. 10.1016/j.matdes.2014.10.045

Chen, Z. Y., Xu, S. Q., & Dong, X. H. (2008). Deformation behavior of AA6063 aluminum alloy after removing friction effect under hot working conditions. Acta Metallurgica Sinica (English Letters), *21*(6), 451–458. 10.1016/S1006-7191(09)60008-9

Conte, S. D. (1966). Numerical analysis. Communications of the ACM, *9*(7), 475. 10.1145/365719.366369

Correia, J. B., Davies, H. A., & Sellars, C. M. (1997). Strengthening in rapidly solidified age-hardened Cu-Cr and Cu-Cr-Zr alloys. Acta Materialia, *45*(1), 177–190. 10.1016/S1359-6454(96)00142-5

Das, R., Sarmah, A., Lakshmi, D. V. N., & Sood, A. (2014). A finite element analysis on the effect of the location of holes die pockets, and extrusion speed in a multi-hole extrusion process. Procedia Engineering, *97*, 1247–1253. 10.1016/j.proeng.2014.12.403

DeGroh, H. C., Ellis, D. L., & Loewenthal, W. S. (2008). Comparison of GRCop-84 to other Cu alloys with high thermal conductivities. Journal of Materials Engineering and Performance, *17*(4), 594–606. 10.1007/s11665-007-9175-3

Deguchi, M., Yamamoto, K., Tobe, H., & Sato, E. (2018). Transient creep behavior and dislocation cell structure development during creep-fatigue deformation of fully annealed Cu–Cr–Zr alloy. International Journal of Fatigue, *116*, 156–162. 10.1016/j.ijfatigue.2018.06.027

Dewang, Y., & Sharma, V. (2021). Effect of process parameters on thermo-mechanical behavior of extrusion of aluminum alloy. Iranian Journal of Materials Science and Engineering, *18*(1), 21–31. 10.22068/ijmse.18.1.3

Engelhardt, M., Kurmajev, S., Maier, J., Becker, C., & Hora, P. (2019). The application of FEA for optimization of die design. Materials Today: Proceedings, 10, 226–233. 10.1016/j.matpr.2018.10.400

Fang, H. C., Chao, H., & Chen, K. H. (2015). Effect of recrystallization on intergranular fracture and corrosion of Al-Zn-Mg-Cu-Zr alloy. Journal of Alloys and Compounds, *622*, 166–173. 10.1016/j.jallcom.2014.10.044

Farzad, H., & Ebrahimi, R. (2017). Die profile optimization of rectangular cross-section extrusion in plane strain condition using upper bound analysis method and simulated annealing algorithm. Journal of Manufacturing Science and Engineering, Transactions of the ASME, *139*(2), 1–11. 10.1115/1.4034336

Feng, H., Jiang, H., Yan, D., & Rong, L. (2013). Effect of continuous extrusion on the microstructure and mechanical properties of a CuCrZr alloy. Materials Science and Engineering A, *582*, 219–224. 10.1016/j.msea.2013.06.031

Gao, L., Yang, X., Zhang, X., Zhang, Y., Sun, H., & Li, N. (2019). Aging behavior and phase transformation of the Cu-0.2 wt%Zr-0.15 wt%Y alloy. Vacuum, *159*, 367–373. 10.1016/j.vacuum.2018.10.054

Ghaemi, F., Ebrahimi, R., & Hosseinifar, R. (2013). Using an Improved Slab Method Analysis. *37*, 189–202.

Gunasekera, J. S., & Hoshino, S. (1985). Analysis of extrusion of polygonal sections through streamlined dies. Journal of Manufacturing Science and Engineering, Transactions of the ASME, *107*(3), 229–233. 10.1115/1.3185991

Guo, N., Li, D., Yu, H., Xin, R., Zhang, Z., Li, X., Liu, C., Song, B., & Chai, L. (2017). Annealing behavior of gradient structured copper and its effect on mechanical properties. Materials Science and Engineering A, *702*(July), 331–342. 10.1016/j.msea.2017.07.023

Harničárová, M., Valíček, J., Kušnerová, M., Kopal, I., Lupták, M., Mikuš, R., Pavelek, Z., Fabián, M., & Šepelák, V. (2022). Structural and Mechanical Changes of AlMgSi0.5 Alloy during Extrusion by ECAP Method. Materials, *15*(6). 10.3390/ma15062020

Hatakeyama, M., Toyama, T., Nagai, Y., Hasegawa, M., Eldrup, M., & Singh, B. N. (2008). Nanostructural evolution of Cr-rich precipitates in a Cu-Cr-Zr alloy during heat treatment studied by 3-dimensional atom probe. Materials Transactions, *49*(3), 518–521. 10.2320/water trans.MBW200736

Hotea, V., & Juhasz, J. (2020). Analysis of the extrusion process parameters of high-strength aluminum alloys used in the aerospace industry. IOP Conference Series: Materials Science and Engineering, *749*(1), 3–9. 10.1088/1757-899X/749/1/012035

Huang, A. H., Wang, Y. F., Wang, M. S., Song, L. Y., Li, Y. S., Gao, L., Huang, C. X., & Zhu, Y. T. (2019). Optimizing the strength, ductility, and electrical conductivity of a Cu-Cr-Zr alloy by rotary swaging and aging treatment. Materials Science and Engineering A, *746*(September 2018), 211–216. 10.1016/j.msea.2019.01.002

Huang, H., Zhong, J., Min, F., Zhu, G., Yue, B., Shao, Y., & Tang, T. (2021). Analysis of AZ31B – Ti6Al4V bimetallic extrusion by numerical simulation and Taguchi method Analysis of AZ31B – Ti6Al4V bimetallic extrusion by numerical simulation and Taguchi method. 10.1088/1757-899X/1193/1/012080

Jajimoggala, S., Dhananjay, R., Lakshmi, V. V. K., & Shabana. (2019). Multi-response optimization of hot extrusion process parameters using FEM and Grey relation-based Taguchi method. Materials Today: Proceedings, *18*, 389–401. 10.1016/j.matpr.2019.06.316

Jurković, Z., Brezočnik, M., Grizelj, B., & Mandic, V. (2009). Optimization of extrusion process by genetic algorithms and conventional techniques. Tehnicki Vjesnik, *16*(4), 27–33.

K, R., K, S., Ramya, K., Sreedevi, K., Engineering, M., Ramya, K., Sreedevi, K., Engineering, M., Ramya, K., Sreedevi, K., Engineering, M., Ramya, K., & Sreedevi, K. (2016). Modeling and Optimization of Extrusion Process Parameters of AA6061 using Taguchi Method. Engineering, Mechanical, 1753–1756.

Karami, P., & Abrinia, K. (2014). An analytical formulation as an alternative to FEM software giving strain and stress distributions for the three-dimensional solution of extrusion problems. International Journal of Advanced Manufacturing Technology, 71(1–4), 653–665. 10.1007/s00170-013-5500-1

Keife, H. (1993). Extrusion through two die openings: A 2D upper-bound analysis checked by plasticine experiments. Journal of Materials Processing Tech., *37*(1–4), 189–202. 10.1016/0924-0136(93)90090-S

Ketabchi, M., Mohammadi, H., & Izadi, M. (2012). Finite-Element Simulation and Experimental Investigation of Isothermal Backward Extrusion of 7075 Al Alloy. Arabian Journal for Science and Engineering, *37*(8), 2287–2296. 10.1007/s13369-012-0320-4

Lechner, S., Rœmisch, U., Nitschke, R., Gensch, F., & Mueller, S. (2021). Optimization of the Indirect Extrusion Process of Copper-Clad Aluminum Rods by Methods of Statistical Experimental Designs and Numerical Analyses. Frontiers in Materials, *8*(May), 1–11. 10.3389/fmats.2021.663306

Lee, Y. S., Kim, W. K., Jo, D. A., Lim, C. Y., & Kim, H. W. (2014). Recrystallization behavior of the cold rolled Al-Zn-Mg-Cu fabricated by twin roll casting. Transactions of Nonferrous Metals Society of China (English Edition), *24*(7), 2226–2231. 10.1016/S1003-6326(14)63337-9

Liu, P., Tong, L., Wang, J., Shi, L., & Tang, H. (2012). Challenges and developments of copper wire bonding technology. Microelectronics Reliability, *52*(6), 1092–1098. 10.1016/j.microrel.2011.12.013

Liu, Z., Zhou, J., Feng, W., & Chen, Y. (2021). Modeling, analysis, and multi-objective optimization of the cold extrusion process of clutch outer gear hub using response surface method and meta-heuristic approaches. International Journal of Advanced Manufacturing Technology, *116*(1–2), 229–239. 10.1007/s00170-021-07451-2

Ma, X., De Rooij, M. B., & Schipper, D. J. (2010). Modeling of contact and friction in aluminum extrusion. Tribology International, *43*(5–6), 1138–1144. 10.1016/j.triboint.2009.12.033

Marmy, P., & Gillia, O. (2010). Investigations of the effect of creep-fatigue interaction in a Cu-Cr-Zr alloy. Procedia Engineering, *2*(1), 407–416. 10.1016/j.proeng.2010.03.045

Meng-jun, W., Zhao, H. E., & Xing-xing, W. U. (2010). Deformation simulation of low-temperature high-speed extrusion for 6063 Al alloy. 881–887. 10.1007/s11771

Moore, P., & Booth, G. (2015). Mechanical testing of welds. The Welding Engineers Guide to

Fracture and Fatigue, 113–141. 10.1533/9781782423911.2.113

Morozova, A., Borodin, E., Bratov, V., Zherebtsov, S., Belyakov, A., & Kaibyshev, R. (2017). Grain refinement kinetics in a low alloyed Cu-Cr-Zr alloy subjected to large strain deformation. Materials, *10*(12), 1394. 10.3390/ma10121394

Namburi, K. P. V., Kothasiri, A. F., & Yerubandi, V. S. M. (2020). Modeling and simulation of Aluminum 1100 alloy in an extrusion process. Materials Today: Proceedings, *23*(xxxx), 518–522. 10.1016/j.matpr.2019.05.398

Novotny, P. M., & Banerjee, M. K. (2016). Tool and Die Steels. Reference Module in Materials Science and Materials Engineering, July 2015, 1–8. 10.1016/b978-0-12-803581-8.02534-0

Olivero, R. A., Nocerino, J. M., & Deming, S. N. (1995). Experimental Design and Optimization. Handbook of Environmental Chemistry, *2*, 73–122. 10.1007/978-3-540-49148-4_3

Ong, P., Chin, D. D. V. S., Ho, C. S., & Ng, C. H. (2018). Modeling and optimization of cold extrusion process by using response surface methodology and metaheuristic approaches. Neural Computing and Applications, *29*(11), 1077–1087. 10.1007/s00521-016-2626-8

Orangi, S., Abrinia, K., & Bihamta, R. (2011). Process parameter investigations of backward extrusion for various aluminum-shaped section tubes using FEM analysis. Journal of Materials Engineering and Performance, *20*(1), 40–47. 10.1007/s11665-010-9655-8

Oyinbo, S., Ikumapayi, O., Ajiboye, J., & Afolalu, S. (2015). Numerical Simulation of Axisymmetric and Asymmetric Extrusion Process Using Finite Element Method. International Journal of Scientific & Engineering Research, *6*(6), 1246.

Peng, L., Xie, H., Huang, G., Xu, G., Yin, X., Feng, X., Mi, X., & Yang, Z. (2017). The phase transformation and strengthening of a Cu-0.71 wt% Cr alloy. Journal of Alloys and Compounds, *708*, 1096–1102. 10.1016/j.jallcom.2017.03.069

Rahul, R. Y., Dewang, Y., & Raghuvanshi2, J. (2018). A study on the metal extrusion process. Advanced Materials Research, *2*(6), 124–130.

Rajabzadeh Gatabi, M., Afrasiab, H., & Moazemi Goudarzi, A. (2020). Numerical and experimental study of the effect of the process parameters on the void evolution in the cold extrusion of rods. Scientia Iranica, *27*(1), 287–294. 10.24200/sci.2018.50154.1540

Ranjan Yadav, R., Dewang, Y., Raghuwanshi, J., & Sharma, V. (2020). Finite element analysis of extrusion process using aluminum alloy. Materials Today: Proceedings, *24*, 500–509. 10.1016/j.matpr.2020.04.302

Ranjbari, G., Doniavi, A., Shahbaz, M., & Ebrahimi, R. (2021). Effect of Processing Parameters on the Strain Inhomogeneity and Processing Load in Vortex Extrusion of Al–Mg–Si Alloy. Metals and Materials International, *27*(4), 683–690. 10.1007/s12540-020-00761-2

Rao, T. B., & Krishna, A. G. (2012). Design and Optimization Of Extrusion Process Using FEA And Taguchi Method. International Journal of Engineering Research & Technology (IJERT), *1*(8), 1–5.

Reddy, N. V., Dixit, P. M., & Lal, G. K. (1996). Die design for axisymmetric extrusion. 6.

Sadollah, A., & Bahreininejad, A. (2012). Optimization of die design using metaheuristic methods in the cold forward extrusion process. Neural Computing and Applications, *21*(8), 2071–2076. 10.1007/s00521-011-0630-6

Sahu, R. K., Das, R., & Routara, B. C. (2018). Effect of die pockets on the extruded products in Multi-hole Extrusion Process: A finite element simulation study. IOP Conference Series: Materials Science and Engineering, *455*(1). 10.1088/1757-899X/455/1/012020

Sarabia, L. A., & Ortiz, M. C. (2009). Response Surface Methodology. Comprehensive Chemometrics, *1*, 345–390. 10.1016/B978-044452701-1.00083-1

SARIN VK, & GRANT NJ. (1972). Cu- Zr and Cu- Zr- Cr alloys are produced from rapidly quenched powders. Met Trans, *3*(4), 875–878. 10.1007/bf02647661

Sathishkumar, D., Sivakumar, P., Sundaram, K. S., & Anand, S. (2017). Finite element analysis and experimental study on the effect of extrusion ratio during the hot extrusion process of aluminum matrix composites. Defense Science Journal, *67*(4), 428–436. 10.14429/dsj.67.11535

Shakhova, I., Yanushkevich, Z., Fedorova, I., Belyakov, A., & Kaibyshev, R. (2014). Grain refinement in a Cu-Cr-Zr alloy during multidirectional forging. Materials Science and Engineering A, *606*, 380–389. 10.1016/j.msea.2014.03.116

Sharififar, M., & Akbari Mousavi, S. A. A. (2015). Simulation and optimization of the hot extrusion process to produce rectangular waveguides. International Journal of Advanced Manufacturing Technology, *79*(9–12), 1961–1973. 10.1007/s00170-015-6950-4

Shen, G., Vedhanayagam, A., Kropp, E., & Altan, T. (1992). A method for evaluating friction using a backward extrusion-type forging. Journal of Materials Processing Tech., *33*(1–2), 109–123. 10.1016/0924-0136(92)90314-I

Shiro Kobayashi, Soo-Ik Oh, T. A. (1989). Shiro Kobayashi, Soo-Ik Oh, Taylan Altan-Metal Forming and the Finite-Element Method (Oxford Series on Advanced Manufacturing) (1989).pdf.

Shukur, J. J., & Jaber, A. S. (2020). Experimental and finite element analysis study of die geometrical affect the forming load during the extrusion process. IOP Conference Series: Materials Science and Engineering, *881*(1). 10.1088/1757-899X/881/1/012045

Shuqin, F. (2020). Internal Thread Cold Extrusion Process. 1–13.

Singh, J., Jerman, G., Poorman, R., Bhat, B. N., & Kuruvilla, A. K. (1997). Mechanical properties and microstructural stability of wrought, laser, and electron beam glazed NARloy-Z alloy at elevated temperatures. Journal of Materials Science, *32*(14), 3891–3903. 10.1023/A:1018604513547

Syahrullail, S., Azwadi, C. S. N., & Najib, Y. M. (2013). The Influences of the Die Half Angle of Taper Die During Cold Extrusion Process. Arabian Journal for Science and Engineering, *38*(5), 1201–1207. 10.1007/s13369-012-0531-8

Tian, W., Bi, L., Ma, F., & Du, J. (2018). Effect of Zr on as-cast microstructure and properties of Cu-Cr alloy. Vacuum, *149*, 238–247. 10.1016/j.vacuum.2017.12.011

Tu, J. P., Qi, W. X., Yang, Y. Z., Liu, F., Zhang, J. T., Gan, G. Y., Wang, N. Y., Zhang, X. B., & Liu, M. S. (2001). Effect of aging treatment on the electrical sliding wear behavior of Cu-Cr-Zr alloy. Wear, *249*(10–11), 1021–1027. 10.1016/S0043-1648(01)00843-2

Venkatesan, R., & Venaktesh, C. (2014). Analytical, numerical, and experimental approach for design and development of optimal die profile for the cold extrusion of B4C DRMM Al 6061 composite billet into a hexagonal section. Journal of Mechanical Science and Technology, *28*(12), 5117–5127. 10.1007/s12206-014-1134-y

Venkatesh, C., & Venkatesan, R. (2015a). Design and analysis of optimal die profile for the extrusion of round SiC DRMM Al 6061 composite billet into the hexagonal section. Journal of the Brazilian Society of Mechanical Sciences and Engineering, *37*(6), 1687–1700. 10.1007/s40430-014-0268-2

Venkatesh, C., & Venkatesan, R. (2015b). Optimization of process parameters of hot extrusion of SiC/Al 6061 composite using Taguchi's technique and upper bound technique. Materials and Manufacturing Processes, *30*(1), 85–92. 10.1080/10426914.2014.962658

Wagstaff, S. (2020). Fundamentals 2020.

Wang, H., Gong, L., Liao, J., Chen, H., Xie, W., & Yang, B. (2018). Retaining meta-stable fcc-Cr phase by restraining nucleation of equilibrium bcc-Cr phase in CuCrZrTi alloys during aging. Journal of Alloys and Compounds, *749*, 140–145. 10.1016/j.jallcom.2018.03.238

Wang, L., Zhou, J., Duszczyk, J., & Katgerman, L. (2012). Friction in aluminum extrusion - Part 1: A review of friction testing techniques for aluminum extrusion. Tribology International, *56*, 89–98. 10.1016/j.triboint.2012.01.012

Wang, S.-C., Zhang, X.-H., Hu, X.-L., Cai, Z.-G., & Peng, B. (2017). Study on the hot extrusion forming process of AZ31 magnesium alloy cylindrical shell. 249–258. 10.1142/9789813220393_0031

Wongsa-Ngam, J., Kawasaki, M., & Langdon, T. G. (2012). Achieving homogeneity in a Cu-Zr alloy processed by high-pressure torsion. Journal of Materials Science, *47*(22), 7782–7788. 10.1007/s10853-012-6587-8

Workie, F., & Tesfaye, A. (2021). Analytical and Numerical Analysis of Extrusion Force, Stress and Strain Development During Extrusion Al6063-SiC Composite. *5*(1), 1–16. 10.11648/j.cm.20200501.11

Wu, Y., Huang, S., Chen, Q., Feng, B., Shu, D., & Huang, Z. (2019). Microstructure and

Mechanical Properties of Copper Billets Fabricated by the Repetitive Extrusion and Free Forging Process. Journal of Materials Engineering and Performance, *28*(4), 2063–2070. 10.1007/s11665-019-03898-3

Xu, C. Z., Wang, Q. J., Zheng, M. S., Zhu, J. W., Li, J. D., Huang, M. Q., Jia, Q. M., & Du, Z. Z. (2007). Microstructure and properties of ultra-fine grain Cu-Cr alloy prepared by equal-channel angular pressing. Materials Science and Engineering A, *459*(1–2), 303–308. 10.1016/j.msea.2007.01.105

Yang, L., Li, S., Li, Y., Yang, M., & Yuan, Q. (2019). Experimental Investigations for Optimizing the Extrusion Parameters on FDM PLA Printed Parts. Journal of Materials Engineering and Performance, *28*(1), 169–182. 10.1007/s11665-018-3784-x

Yang, T. S., Hsu, Y. C., Lin, H. S., & Chang, S. Y. (2008). A finite element analysis for the initial blank's shape design of sheet metal in the deep drawing process. Key Engineering Materials, *364-366 II*, 980–985. 10.4028/www.scientific.net/kem.364-366.980

Zhang, C., Zhao, G., Chen, H., Guan, Y., & Li, H. (2012). Optimization of an aluminum profile extrusion process based on Taguchi's method with S/N analysis. International Journal of Advanced Manufacturing Technology, *60*(5–8), 589–599. 10.1007/s00170-011-3622-x

Zhang, Q., Felder, E., & Bruschi, S. (2009). Evaluation of friction condition in cold forging by using T-shape compression test. Journal of Materials Processing Technology, *209*(17), 5720–5729. 10.1016/j.jmatprotec.2009.06.002

Zhang, Y. N., Zheng, M. S., & Zhu, J. W. (2011). Effect of Cr and Zr addition on the corrosion behavior of copper in the chloride solution. Advanced Materials Research, *194–196*, 1253–1256. 10.4028/www.scientific.net/AMR.194-196.1253

Zhang, Y., Sun, H., Volinsky, A. A., Wang, B., Tian, B., Chai, Z., Liu, Y., & Song, K. (2017). Small Y Addition Effects on Hot Deformation Behavior of Copper-Matrix Alloys. Advanced Engineering Materials, *19*(12), 1–10. 10.1002/adem.201700197

Zhang, Y., Volinsky, A. A., Tran, H. T., Chai, Z., Liu, P., & Tian, B. (2015). Effects of Ce Addition on High-Temperature Deformation Behavior of Cu-Cr-Zr Alloys. Journal of Materials Engineering and Performance, *24*(10), 3783–3788. 10.1007/s11665-015-1693-9

Zhao, Y. H., Liao, X. Z., Cheng, S., Ma, E., & Zhu, Y. T. (2006). Simultaneously increasing the ductility and strength of nanostructured alloys. Advanced Materials, *18*(17), 2280–2283. 10.1002/adma.200600310

Zhao, Y., Pang, T., He, J., Tao, X., Chen, H., Ouyang, Y., & Du, Y. (2018). Interdiffusion behaviors and mechanical properties of Cu-Zr system. Calphad: Computer Coupling of Phase Diagrams and Thermochemistry, *61*(February), 92–97. 10.1016/j.calphad.2018.02.008

Zhilyaev, A. P., Shakhova, I., Morozova, A., Belyakov, A., & Kaibyshev, R. (2016). Grain refinement kinetics and strengthening mechanisms in Cu-0.3Cr-0.5Zr alloy subjected to intense plastic deformation. Materials Science and Engineering A, *654*, 131–142. 10.1016/j.msea.2015.12.038

Zhou, J., Li, L., & Duszczyk, J. (2003). 3D FEM simulation of the whole cycle of aluminum extrusion throughout the transient state and the steady state using the updated Lagrangian approach. Journal of Materials Processing Technology, *134*(3), 383–397. 10.1016/S0924-0136(02)01128-7

Appendix

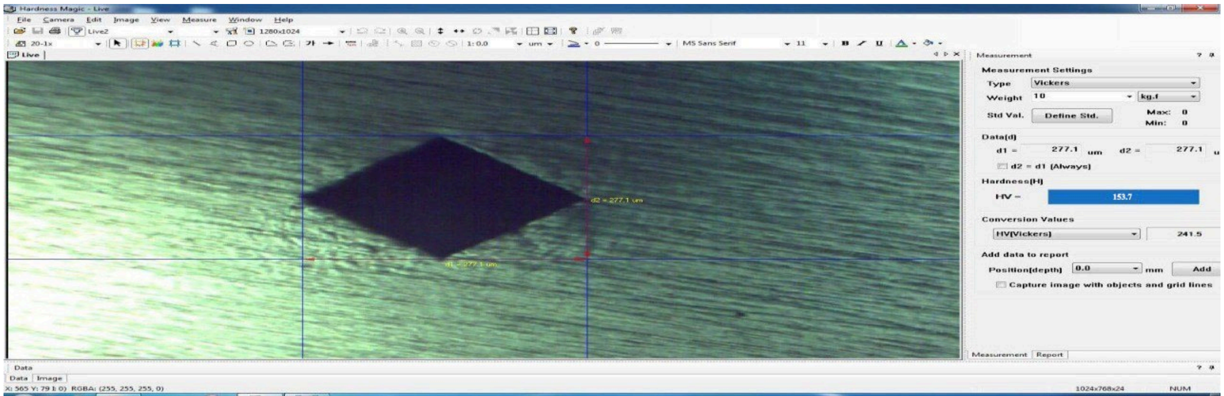

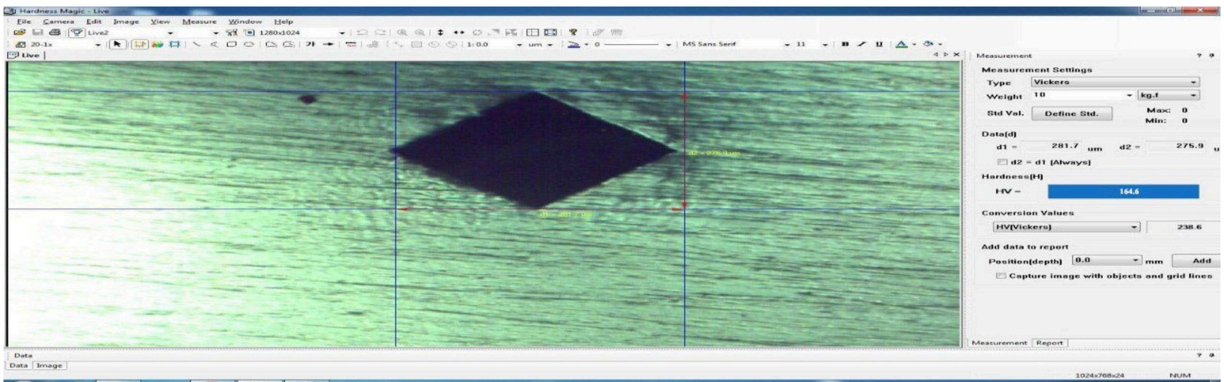

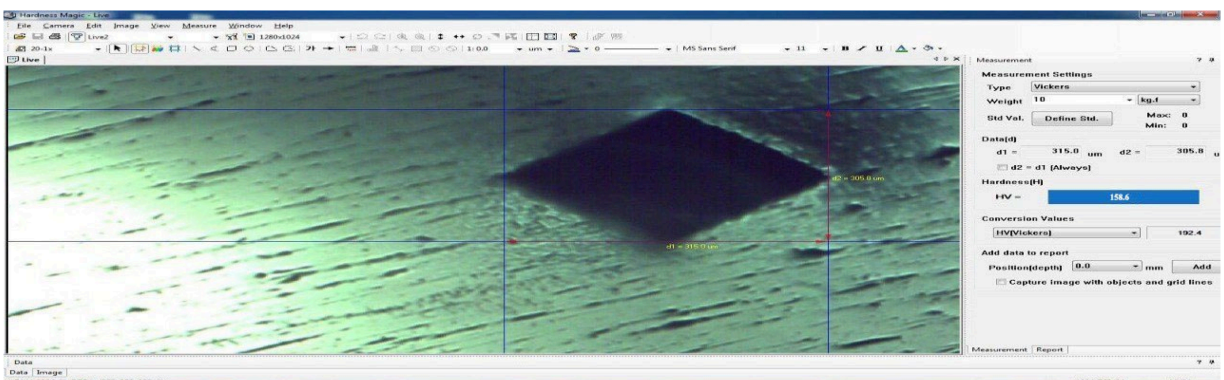

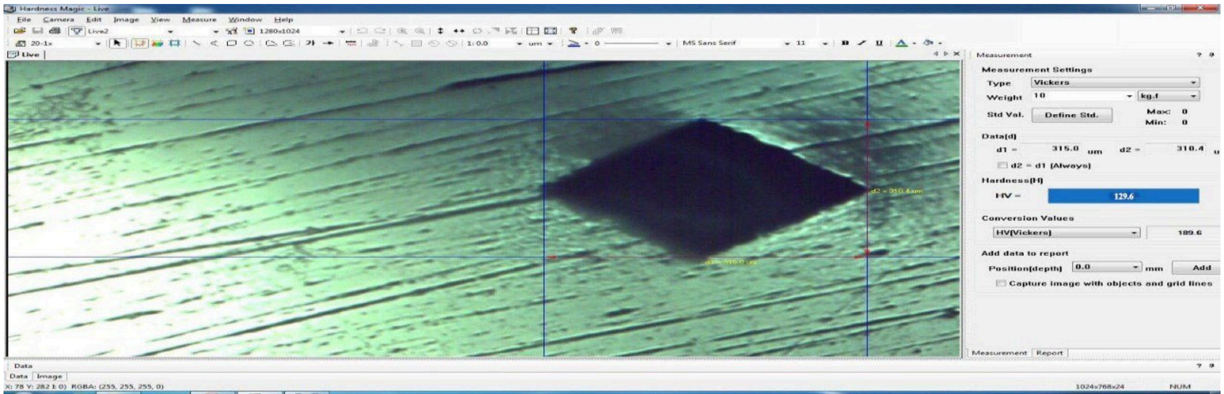

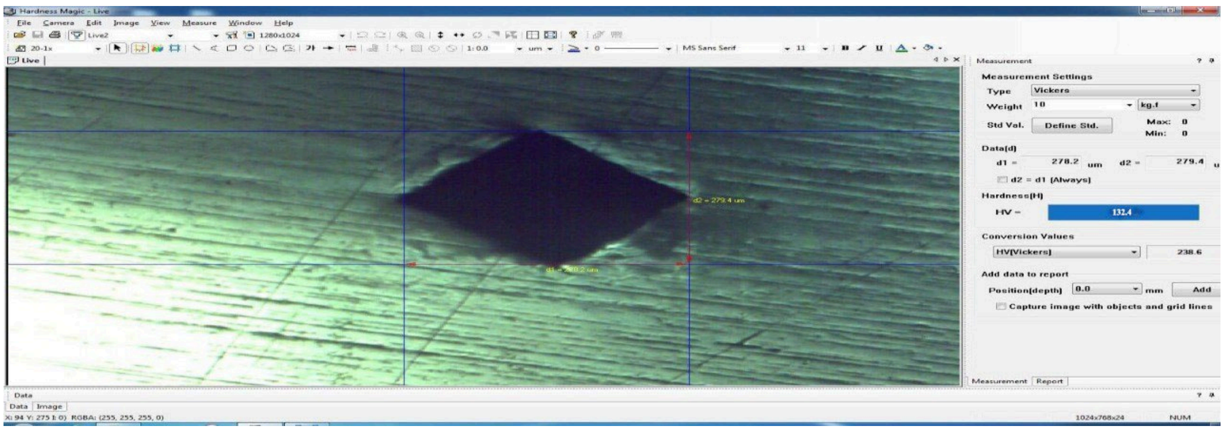

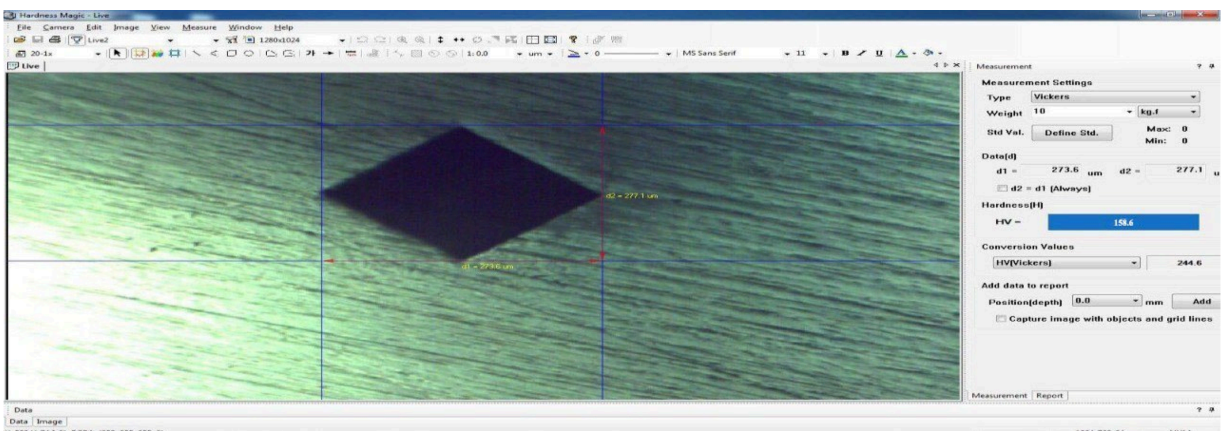

Hardness test result all three sample

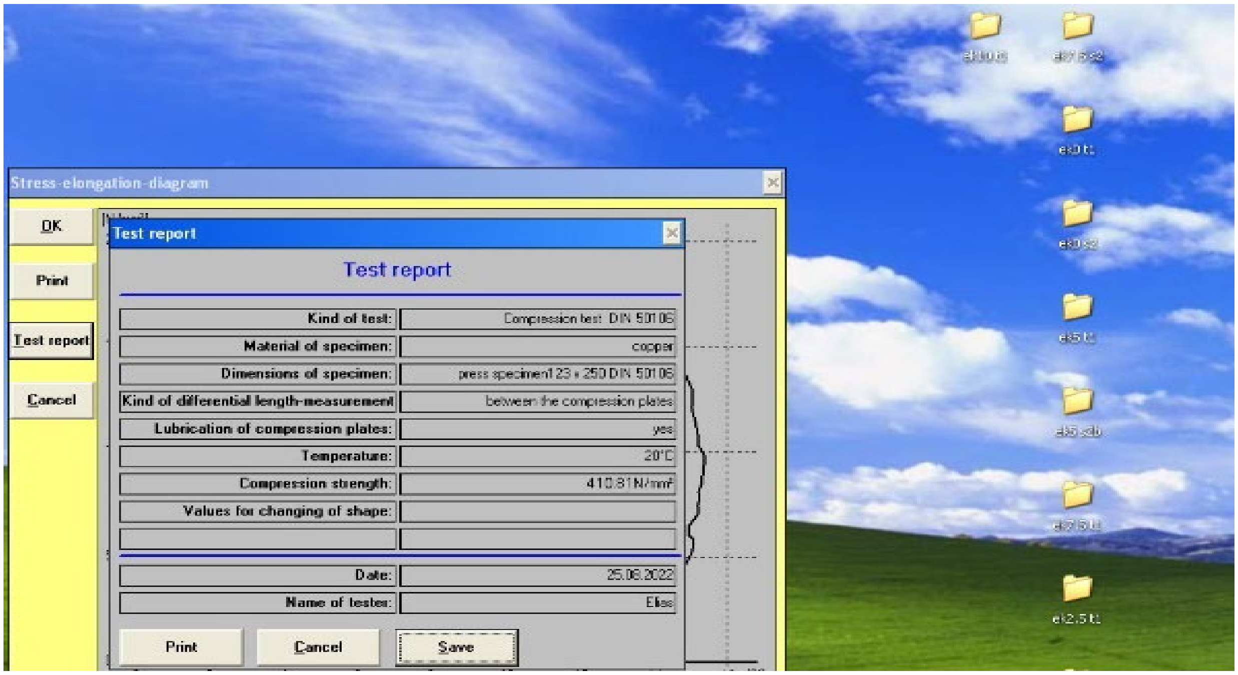

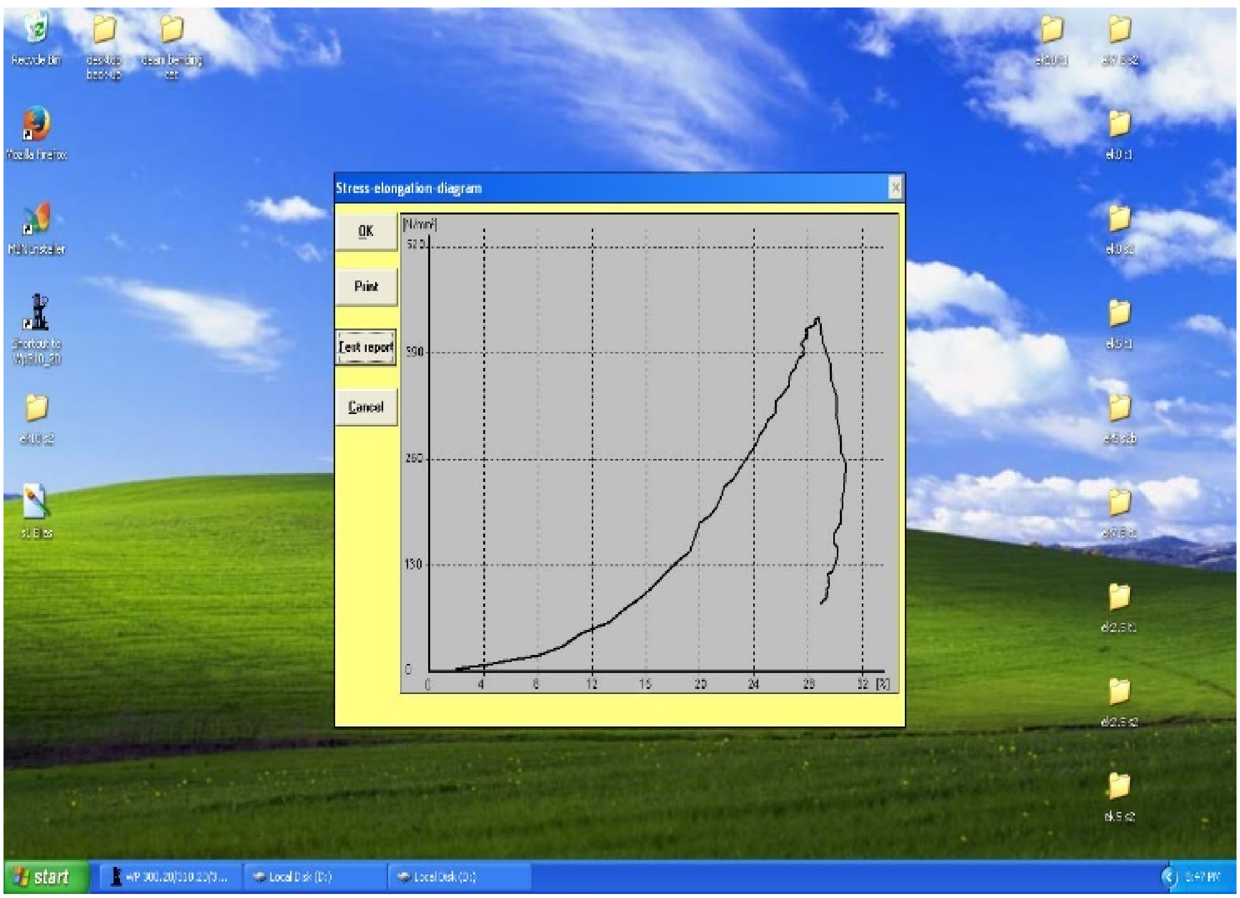

Compressive strength of cosine profile extruded material

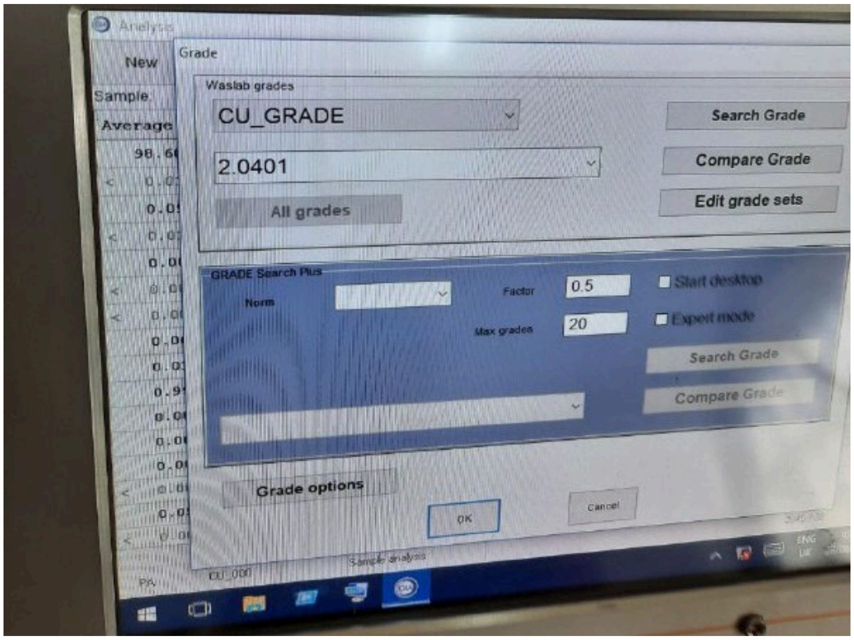
New
Sample
Average
Grade
Waslab grades
CU_GRADE
2.0401
All grades
Search Grade
Compare Grade
Edit grade sets
GRADE Search Plus
Norm
Factor
0.5
Max grades
20
Start desktop
Expert mode
Search Grade
Compare Grade
Grade options
OK
Cancel

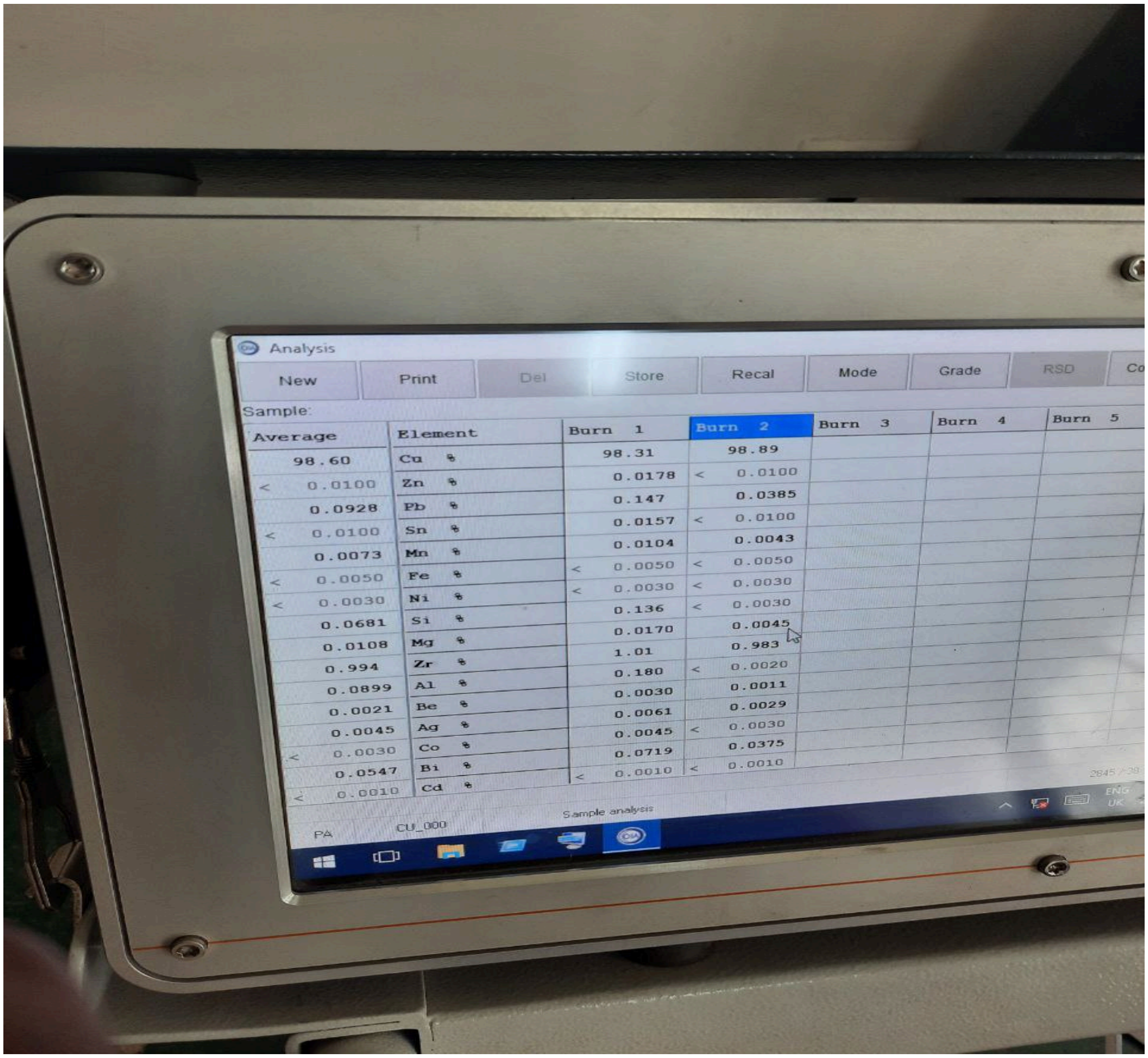

Spectroscopy result of Copper zirconium material